

# Computational analysis of reef structure and benthic composition

**Jessica Wright**

A thesis submitted for the degree of  
*Doctor of Philosophy*

School of Computer Science and Electronic Engineering  
and School of Life Sciences

University of Essex  
November 2023



# Acknowledgements

I would firstly like to thank my supervisors, particularly Jon Chamberlain for his tireless efforts to encourage and push me academically and force me to socialise as much as he could manage. I would not have considered applying for this studentship without his willingness to help a clueless MSc student and share beers on a tropical beach.

My trip to Pulau Hoga in 2017 provided vital data after the COVID-19 pandemic restricted field work. The staff and RAs were essential to my diving and data collection, and I owe a special thank you for the sanity-keeping efforts of Amelia White and Leslie Galstaun. More thanks go to the Cromer team, who were amazing collaborators, particularly when a broken leg put me out of diving. The entire rotating team of ImageCLEFcoral, particularly Louis Clift and Lia Palosanu, cannot be thanked enough. Patiently explaining image annotation to a biologist was not easy and you deserve a medal or 5. The ImageCLEFcoral project would not have been possible without the Marine Biology MSc interns, who kept their enthusiasm even through 20 hours of manual annotation.

To the friends who have put up with me turning into a hermit and soliloquising on topography, I cannot thank nor apologise enough. I have to highlight Will Spanner, Leslie Galstaun and Emma Ward for the pushes we gave each other throughout our research and for the conversations where no one understood the others' work but we were all very positive about it. To EUSAC, thank you for managing to swing me 17 fun dives in 4 years. Yes I counted. To Sorcha Shanley, Callum Etridge, and Emily Delva, thanks for all the pints - enough said.

Finally, the most important thank you goes to my family, who have put up with me constantly going back to university, reminded me to stop working and have dinner (or to stop playing video games and actually write my thesis), and listened to my rants on structural complexity, coral reefs and why I definitely need one more set of fins. You are the absolute best.

This PhD was fully funded by a University of Essex PhD Scholarship.

# Abstract

Structural complexity is vital to coral reef systems and is threatened by direct and indirect anthropogenic acts, resulting in a global decline of reef health. As such, these systems are regularly assessed and monitored. The use of computational techniques in surveys is becoming more commonplace, but is an intensive process and often only covers small areas of a reef. Non-coral reef systems are rarely considered in terms of their structural complexity and do not have standardised metrics or methodologies, nor are structural links to health known. They are monitored in terms of biodiversity, but often structure and benthos are excluded from these assessments. To improve the capabilities of computational analysis of benthic environments, this thesis first developed and tested a multi-camera array for surveying of coral reefs, then utilised an array in a survey of a distinct rocky reef environment. The surveying method demonstrated a rapid approach to data collection that successfully generated 3D modelled environments that enabled successful data extraction. The complexity metrics used, however, appeared to be disconnected from *in-situ* observations of the rocky reef environment. From this, a novel assessment of relief and the use of tailored fractal dimension was developed to contextualise rocky reef complexity and link it to commercially relevant associated species. From this, links between structural complexity and associated species were found, and relief proved to be a distinct form of complexity on the rocky reef. Additionally, the development of the ImageCLEFcoral task is outlined: a global benchmarking competition which aimed to further the capabilities of automatic annotation of coral reef substrates. A series of submitted runs were produced for the 2021 edition of the task and are also presented here. Though the annotation approaches are not yet successful enough for practical use, the annual task has continued to develop and will likely improve year on year. When fully utilised, computational analysis would enable researchers to focus on furthering knowledge rather than surveying restrictions and repetitive data extraction. While the approaches presented here do require *in-situ* data collection and researcher interaction, the benefits lend themselves to widely expanded analysis capabilities and shareable data stores. Multi-camera arrays allow for data collection to span larger areas in less time, while automatic annotation increases the data volume without manual intervention. When used appropriately, research can become more efficient, cost-effective, replicable, and accurate.

# Contents

<b>1</b>	<b>Introduction</b>	<b>1</b>
1.1	The value of coral reefs . . . . .	1
1.2	Rocky reefs as important habitats . . . . .	3
1.3	Environmental monitoring of marine reef ecosystems . . . . .	5
1.4	Research objectives . . . . .	8
1.5	Research contributions . . . . .	10
1.6	Research publications and presentations . . . . .	11
<b>2</b>	<b>Literature review</b>	<b>14</b>
2.1	The importance of structural complexity in reef systems . . . . .	14
2.1.1	Coral reef structure, health, and biodiversity . . . . .	14
2.1.2	Coral reef complexity decline in the Anthropocene . . . . .	16
2.1.3	The structure of non-coral reefs . . . . .	19
2.2	Reconstructing marine environments . . . . .	20
2.2.1	The history of photogrammetry . . . . .	21
2.2.2	3D modelling of underwater systems . . . . .	23
2.2.3	Processing 3D models in Agisoft Metashape . . . . .	25
2.3	Measuring structural complexity in marine habitats . . . . .	26
2.3.1	Reef complexity with analogue metrics . . . . .	27
2.3.2	Computational methods to extract complexity . . . . .	27
2.3.3	Complexity metrics in marine monitoring . . . . .	29
2.4	Automatic image annotation . . . . .	37
2.4.1	Methods for automatic image annotation . . . . .	38
2.4.2	Coral reef image annotation . . . . .	41
2.5	Summary . . . . .	43
<b>3</b>	<b>3D models in coral reef monitoring</b>	<b>44</b>
3.1	Introduction . . . . .	44
3.2	Methodology . . . . .	45
3.2.1	Reef model sites . . . . .	45
3.2.2	Single camera data capture . . . . .	46
3.2.3	Single-camera 3D model build quality . . . . .	48
3.2.4	Multi-camera arrays . . . . .	49
3.2.5	Action camera field of view . . . . .	51
3.2.6	Single versus multi-camera complexity . . . . .	52
3.2.7	Data analysis . . . . .	52
3.3	Results . . . . .	52
3.3.1	Build quality testing . . . . .	52
3.3.2	Action camera field of view . . . . .	54
3.3.3	Single versus multi-camera complexity . . . . .	55
3.4	Discussion . . . . .	55
3.4.1	3D model build quality . . . . .	55

3.4.2	Action camera field of view . . . . .	57
3.4.3	Single versus multi-camera complexity . . . . .	57
3.5	Summary . . . . .	57
<b>4</b>	<b>Assessing structural damage on a chalk reef system</b>	<b>59</b>
4.1	Introduction . . . . .	59
4.2	Methodology . . . . .	60
4.2.1	Study sites . . . . .	60
4.2.2	Chalk reef imaging . . . . .	62
4.2.3	Substrate damage assessment . . . . .	63
4.2.4	Crustacean assessment . . . . .	64
4.2.5	Data analysis . . . . .	64
4.3	Results . . . . .	67
4.3.1	Complexity metric variation between chalk reef sites . . . . .	67
4.3.2	Damage annotator agreement . . . . .	67
4.3.3	Complexity and observed human impacts . . . . .	69
4.3.4	Complexity and species abundance . . . . .	70
4.4	Discussion . . . . .	70
4.4.1	Human-attributed impact to the chalk bed . . . . .	70
4.4.2	Annotation of damage . . . . .	72
4.4.3	Commercial crustacean preferences in habitat complexity . . . . .	74
4.4.4	Survey limitations . . . . .	75
4.5	Summary . . . . .	76
<b>5</b>	<b>Adapting complexity to a rocky chalk reef</b>	<b>77</b>
5.1	Introduction . . . . .	77
5.2	Methodology . . . . .	78
5.2.1	Model analysis . . . . .	78
5.2.2	Ecosystem data . . . . .	79
5.2.3	Statistical analysis . . . . .	80
5.3	Results . . . . .	80
5.3.1	Relief and metrics of complexity in coral and chalk reefs . . . . .	80
5.3.2	Relief and species abundance on chalk reefs . . . . .	80
5.3.3	Relief and observed human impacts on chalk reefs . . . . .	81
5.4	Discussion . . . . .	82
5.4.1	Complexity and relief on chalk and coral reefs . . . . .	82
5.4.2	<i>C. pagurus</i> preferences in habitat complexity . . . . .	84
5.4.3	Monitoring human impacts on chalk reefs . . . . .	85
5.4.4	Limitations of the survey . . . . .	86
5.5	Summary . . . . .	87
<b>6</b>	<b>Automatic annotation of reef substrates</b>	<b>88</b>
6.1	Introduction . . . . .	88
6.2	ImageCLEFcoral tasks . . . . .	89
6.3	Coral reef image datasets . . . . .	90
6.3.1	Habitat feature classification . . . . .	91
6.3.2	Image annotation and validation . . . . .	93
6.3.3	Training image analysis . . . . .	95
6.4	ImageCLEFcoral submissions . . . . .	97
6.5	Results . . . . .	98
6.5.1	Subtask 1 - annotation and localisation . . . . .	98
6.5.2	Subtask 2 - pixelwise parsing . . . . .	102

6.6	Discussion . . . . .	104
6.6.1	Challenges of ImageCLEFcoral . . . . .	105
6.7	Summary . . . . .	106
<b>7</b>	<b>Using global data for automatic annotation</b>	<b>108</b>
7.1	Introduction . . . . .	108
7.2	Methodology . . . . .	109
7.2.1	Supplementing the ImageCLEF dataset . . . . .	109
7.2.2	Submitted runs . . . . .	112
7.3	Results . . . . .	113
7.4	Discussion . . . . .	115
7.4.1	Limitations of the model . . . . .	116
7.4.2	Improving the approach . . . . .	116
7.5	Summary . . . . .	117
<b>8</b>	<b>Discussion</b>	<b>119</b>
8.1	Key findings . . . . .	119
8.1.1	Multi-camera arrays for coral reef surveying . . . . .	119
8.1.2	Expanding the cases for computational complexity measurements . . . . .	123
8.1.3	Automatic analysis of coral reef imagery . . . . .	125
8.2	Limitations of the work . . . . .	127
8.2.1	Data collection . . . . .	127
8.2.2	3D reconstruction . . . . .	128
8.2.3	Automatic annotation . . . . .	128
8.3	Future directions for research . . . . .	128
8.3.1	Reef-wide surveying of the Cromer Shoal Chalk Bed MCZ . . . . .	129
8.3.2	Automatically annotating other substrate features . . . . .	129
8.3.3	Computational habitat-wide assessments . . . . .	130
8.3.4	3D printing in coral reef research . . . . .	130
8.4	Concluding remarks . . . . .	131
<b>I</b>	<b>Agisoft Metashape outline</b>	<b>148</b>
I.1	Processing 3D models in Agisoft Metashape . . . . .	148
I.1.1	Step 1 - Photo alignment . . . . .	148
I.1.2	Step 2 - The dense cloud . . . . .	149
I.1.3	Step 3 - Meshing . . . . .	150
I.1.4	Step 4 - Adding texture . . . . .	150
<b>II</b>	<b>Method testing data</b>	<b>152</b>
<b>III</b>	<b>Cromer MCZ data</b>	<b>157</b>
<b>IV</b>	<b>Relief script</b>	<b>160</b>
<b>V</b>	<b>ImageCLEFcoral data</b>	<b>161</b>

# List of Tables

2.1	A brief summary of habitat complexity metrics. . . . .	38
3.1	Field of view captured for an SJCam and GoPro. . . . .	55
4.1	Damage categories observed on the Cromer Shoal Chalk Bed. . . . .	65
4.2	Damage to the Cromer Shoal Chalk Bed per type at the sampled sites. . . . .	70
4.3	Correlations between chalk bed complexity and crab abundance. . . . .	72
5.1	Correlations between crab abundance and adapted chalk complexity metrics. . . . .	82
5.2	Incidence of damage by severity level. . . . .	82
6.1	Substrate morphological categories used to classify ImageCLEFcoral images. . . . .	92
6.2	Benthic substrate distribution as a percentage of pixels in 2019. . . . .	95
6.3	Benthic substrate distribution as a percentage of pixels in 2021. . . . .	97
6.4	Teams of the ImageCLEFcoral task . . . . .	98
6.5	Results of ImageCLEFcoral 2019 subtask 1. . . . .	99
6.6	Results of ImageCLEFcoral 2020 subtask 1. . . . .	101
6.7	Results of ImageCLEFcoral 2021 subtask 1. . . . .	101
6.8	Results of ImageCLEFcoral 2019 subtask 2. . . . .	102
6.9	Results of ImageCLEFcoral 2020 subtask 2. . . . .	103
6.10	Results of ImageCLEFcoral 2021 subtask 2. . . . .	104
7.1	Results of ImageCLEFcoral 2021 subtask 2 per substrate label. . . . .	114
II.1	Linear captured distance of an SJCam. . . . .	152
II.2	Linear captured distance of a GoPro. . . . .	152
II.3	Rugosity of a Pak Kasims reef model. . . . .	153
II.4	Vector dispersion and fractal dimension of a Pak Kasims reef model. . . . .	154
II.5	Percentage of aligned photos per Metashape quality setting. . . . .	155
II.6	Dense cloud-to-cloud distances per Metashape quality setting. . . . .	156
III.1	<i>Cancer pagurus</i> and <i>Homarus gammarus</i> abundance in the Cromer MCZ. . . . .	157
III.2	Rugosity across on the Cromer Shoal Chalk Bed. . . . .	158
III.3	Vector dispersion and fractal dimension on the Cromer Shoal Chalk Bed. . . . .	159
V.1	Results of ImageCLEFcoral 2019 subtask 1 per substrate label. . . . .	162
V.2	Results of ImageCLEFcoral 2019 subtask 2 per substrate label. . . . .	163
V.3	Results of ImageCLEFcoral 2020 subtask 1 per substrate label. . . . .	164
V.4	Results of ImageCLEFcoral 2020 subtask 1 per location per substrate label. . . . .	165
V.5	Results of ImageCLEFcoral 2020 subtask 2 per substrate label. . . . .	166
V.6	Results of ImageCLEFcoral 2020 subtask 2 per location per substrate label. . . . .	167



# List of Figures

2.1	Reef interaction cycle for coral dominance. . . . .	15
2.2	Factors of tropical reef phase shifts. . . . .	19
2.3	Bathymetric maps of the North Atlantic ocean. . . . .	21
2.4	Measurement of linear rugosity. . . . .	30
2.5	Angular standard deviation of vectors and angles. . . . .	33
2.6	Measurement of verticality of a linear section of substrate. . . . .	33
2.7	A Koch snowflake example of fractal dimension. . . . .	36
2.8	Field of view of a fish when grazing. . . . .	37
2.9	An example of semantic and instance segmentation of an image. . . . .	39
2.10	The classification of an image through a convolutional neural network. . . . .	40
3.1	Quadrat positioning per coral reef site. . . . .	46
3.2	Substrate image capture patterns using a single camera. . . . .	47
3.3	Substrate area captured by a single camera. . . . .	48
3.4	Angles of a multi-camera array on a regular dodecahedron frame. . . . .	50
3.5	Mean total points and cloud-to-cloud distance per dense cloud build quality. . . . .	53
3.6	Mean cloud-to-mesh distance per face count and site. . . . .	54
3.7	A coral model at each Metashape processing stage. . . . .	54
3.8	Fractal dimension of models generated by a single or multi-camera method. . . . .	55
4.1	A typical potting shank used in crustacean fisheries. . . . .	60
4.2	A map of the Cromer Shoal Chalk Bed Marine Conservation Zone. . . . .	61
4.3	The camera array used for surveying the Cromer Shoal Chalk Bed MCZ. . . . .	63
4.4	Transect surveying layout between 2 pots on a shank line. . . . .	63
4.5	Sliding damage window positioning within a transect. . . . .	66
4.6	Cohens' Kappa agreement of damage annotations on the chalk bed. . . . .	69
4.7	Incidences of damage per site on the Cromer Shoal Chalk Bed. . . . .	71
4.8	A pot attached to a shank by a rope tether on the chalk bed. . . . .	73
5.1	Relief assessment of an area of reef. . . . .	79
5.2	Linear correlations between relief and other complexity metrics. . . . .	81
5.3	Incidences of damage per category on the Cromer Shoal Chalk Bed. . . . .	83
6.1	The custom annotation tool used for the ImageCLEFcoral task. . . . .	93
6.2	A vase sponge with annotated outline points and as a polygon. . . . .	94
6.3	A training image used to test annotator accuracy for ImageCLEF coral. . . . .	94
6.4	Analysis of ImageCLEFcoral 2020 training data. . . . .	96
7.1	Annotations within the ImageCLEFcoral 2021 and NOAA training set. . . . .	110
7.2	Enhancement of ImageCLEF2021 training images through colour balancing. . . . .	111
8.1	Single camera versus multi-camera imaging pathway. . . . .	121
8.2	Processing of a coral reef 3D model generated using a multi-camera array. . . . .	122

# 1 | Introduction

## 1.1 The value of coral reefs

Coral reef systems are vital to the health and prosperity of the oceans and the communities that rely upon them. They are some of the most biodiverse and productive naturally occurring ecosystems in the world, and provide a wide range of ecosystem functions and services [1]. Despite coral reefs covering less than 0.1 % of the ocean floor, they support around 25 % of marine fishes and a third of marine species at some point in their life cycle [2]. For those that make up the benthos, these species can be separated broadly into reef-building and non-reef-building organisms. Reef-builders are those that provide some form of structure or substrate to the reef itself, along with the natural geological structure of the seabed and the dead organisms layered below the living ones. While a considerable component of this is scleractinian coral (those that secrete carbonate with a positive carbonate budget) [3], other organisms make up a vital part of the reef structure. Soft corals, rocks, sponges, and algae all provide ranging microhabitats through complex and varied morphology [4, 5]. The diversity and abundance of these substrates allows for the healthy function of a reef system, wherein they provide services and functions to the reef and the organisms living on it [1].

The Millennium Ecosystem Assessment classifies ecosystem services in four ways: provisioning, regulating, cultural, and supporting [6]. The complex physical structure of a reef is critical to many of the ecosystem services that they provide to these communities and to the environment and can be considered a supporting service itself [7]. It underpins the entire ecosystem, maintains the vast array of life present, and bolsters many other services provided by the reef system [8].

Provisioning services of coral reefs are vital to the survival of many coastal communities. Many people who live within 30 km of a reef system reside in nations that are heavily reliant on coral reefs for food and income [9]. Fishery and material services of

coral reefs rely on 3D reef structure to sustain the marine life and promote resilience [10]. Reef fish and invertebrates across most trophic levels are valuable as a protein source for these communities and can provide considerable income, although higher trophic levels are worth more when sold [11]. Similar to fishing for food, the aquarium trade is also an economic avenue for small scale fisheries to earn money. Target species for aquaria may differ from those desired as a food source, with smaller colourful fish being more valuable [12]. Western medicine has seen corals used for anti-inflammatory and anti-carcinogenic purposes [13]. The traditional medicine trade is also somewhat reliant on coral reefs, using animals such as seahorses, sea cucumbers, and pipefish in medicinal practices [14]. Alternative medicine may also see a turn towards coral as a resource for treatments and prevention for a range of ailments, including cancers and deformities [15].

Many key services provided by coral reefs regulate nearby coastal and marine environmental factors. The physical barrier that a coral reef can provide to the land enables them to deplete 97 % of energy in tidal water that could otherwise destroy these areas [16]. 87 % of this dissipation comes from the reef crest which, along with the slope, is one of the reef areas of highest complexity [17]. The monetary value of this has been estimated at \$4 billion through the protection of over 197 million people in reef-side communities [18]. This structure similarly protects shorelines from erosion, which is a threat to many communities, particularly in smaller towns and villages [16].

Coral reefs can also provide culturally based services and benefit local economies through tourism. Eco-tourism can benefit reef systems through conservation-related activities and by bringing awareness and funding to local organisations working to protect a reef system. Often this tourism is reliant on a healthy ecosystem with prosperous, structurally complex reefs encouraging underwater recreation, while the calm waters and seafood also provided by the reefs structure and services support for land and sea activities [7]. However, unsustainable tourism has had a negative impact on reef health through direct damage by SCUBA divers, fishers and swimmers interacting with the reef and by tourist infrastructure, like hotels and stores, being improperly developed and increasing pollutants through waste and construction [9, 19].

The economic value of reef systems are closely linked to biological functions and ecosystem services that the particular reef can provide, which has led to the overexploitation of resources [9, 20, 21]. Coral reefs are expected to change drastically in coming decades

[22, 23], with 24 of 27 world heritage coral reef sites predicted to bleach twice per decade by 2040 if the atmosphere continues to warm at its current rate [24]. Repeated bleaching over time impacts reef sites, with loss of coral cover, diversity, and reproductive output being common outcomes, but specific changes vary per reef depending on coral size, location, ambient water temperature, and other stressors [25, 26].

Contrasting the amount data and predictions on the future of coral reef environments, there has been far less research into non-coral reef systems. Rocky reef environments are formed by the erosion of hard substrate through tidal and wave action and can be highly productive and diverse habitats with complex and varied structures [27]. Investigations of these ecosystems is less extensive than with coral reef systems, but they are hubs of temperate biodiversity that provide many ecosystem services to their environment [28, 29].

## 1.2 Rocky reefs as important habitats

Rocky reefs are composed of a rocky substratum with varyingly sized rock, from bedrock to boulders, and cobbles; and contain sand patches, macroalgae, sponges, sea-grasses, and other benthic structures within them [30, 31, 32]. The structure of the rocky reef itself, as with coral reefs, influences species richness, abundance, and diversity, with greater complexity being associated within each of these variables [33]. For individual fauna, this structure provides greater availability of refuge areas, feeding grounds, and mating sites [31].

Many of the provisioning ecosystem services provided by rocky reef environments are analogous to those provided by coral reefs. Rocky reefs are often structurally complex habitats that support biodiversity through benthic availability for settling organisms and refugia for mobile ones [33, 34]. In British Columbia, rugose rocky reefs had 800% more temperate reef fish biomass (of small reef fish) compared to less complex reefs [35]. Rocky reef coastlines in Britain have seen new species discoveries [36]. Some rocky reefs are able to provide services even when no longer living: rocky coralline algae reefs can continue to provision habitat, structural complexity, and refuge after death [37]. Rocky reefs can be supported and enhanced by algae, kelp, and other flora that provide additional habitat and resources to the system. Overfishing in these environments can lead to a cascading habitat shift through subsequent algal and kelp losses leading to a barren-reef phase shift

[38]. Rocky reef ecosystems can act as environmental buffers to coastlines. Coastal protection from wave action and storms is key to minimising erosion of both natural coastal environments and of man-made structures nearby [28]. Where rocky reef systems are home to sufficient flora they can act as blue carbon sinks, providing essential regulation of both the local and global environment [34]. Rocky reef habitats encourage tourism to rural areas, greatly influence the local economy, and provide a strong tradition (often through fisheries) that fuels a sense of community [29]. Rocky reefs support sandy beaches and therefore also benefit the activities that are linked to them: sports, recreational fishing, and even casual time outdoors [28].

Rocky reef systems composed of chalk substrates are globally rare. 57% of European coastal chalk is found in Britain, and it is still scarce there, composing only 0.6% of coastlines predominately in Kent and Sussex [39]. Chalk is a relatively soft rock, though there are varying levels of hardness depending on its composition [40]. Associated fauna and flora utilise and exploit this feature to their benefit: boring invertebrates, as an example, can penetrate the chalk more easily than other substrate materials [41]. Chalk habitats can be flat planes of smooth chalk or contain boulders, cobbles, and other substrate types, such as rock, mud, or sand. Often a combination of these structures and materials compose the entire substratum and they can occasionally form distinct reef areas wherein the chalk substrate is “topographically distinct from the seabed” [42].

While coral reefs are highly valued and widely publicised to be in decline, other marine reef systems are also vulnerable to the combination of human impacts and climate-exacerbated events [34], but these impacts are less well understood. The lack of focus on them means that they are far less monitored and assessed. Because of limited surveying, dedicated and relevant methods and metrics are not commonplace. The differences in type of organisms present on these reefs and in substrate composition, when compared to coral reefs, would suggest that the assumptions made when examining coral reefs should not be assumed true for other systems, and that the same pressures and responses cannot be applied by default.

The loss of reefs would be catastrophic to the marine environment and those that rely upon it, directly or indirectly. Monitoring and, where possible, counteracting decline in structure, diversity, and all associated features is essential for the future of these systems and the prosperity of oceans and people alike.

### 1.3 Environmental monitoring of marine reef ecosystems

The ability of coral reefs to provide vital ecosystem services is declining worldwide as they are continually degraded [43]. Management and monitoring of these systems is vital to maintain their health and function, but must be done with a focus on reef structure to increase the resilience of reefs [10]. The monitoring of reef systems is a complex and challenging task with many techniques used globally. Quadrat and/or transect surveys can be used to assess species richness, species abundance, percentage cover, and other metrics [44, 45, 46]. These assessments are repeatable to a certain extent, but rely heavily upon *in-situ* SCUBA work and so are limited by time, conditions, cost, diver skill (in both diving itself and in the tasks required by the survey), and the subjective view of the diver.

As technology has progressed, the use of 3D modelling to extract coral reef data has become more common, often by image or video collection through SCUBA diving and sometimes followed by Structure-from-Motion (SfM) 3D modelling or digital elevation models (DEMs) [3, 17, 47]. These methods benefit from greatly reduced time constraints as once data/images are collected they can be reused in any number of ways (e.g. for continuous/repeated assessment in the future). As such, the methods for this data capture are varied, but all follow along the same vein.

Most prevalent are single camera data capture methods, with a single action camera or DSLR used to capture images at a set interval (i.e. 1 frame every 1, 3, or more seconds) or to take video footage with stills to be extracted post-survey. These methods are often restricted to a top-down view of the reef that limits the model accuracy to a birds-eye view of the substrate, poorly rendering or excluding the overhangs and crevices that are commonly found in reef systems [17, 47, 48, 49]. Analysis of data from remote sensing surveys can be more intensive, particularly with video and photo data. They are also often restricted to a top-down view of the reef that limits the model accuracy to a birds-eye view of the substrate, poorly rendering or excluding the overhangs and crevices that are commonly found in reef systems [17, 47, 48, 49].

The choice of camera in underwater modelling is a balance of price, image/video quality, and the number of cameras needed. While there are many types of camera available, generally those used underwater are limited to mirrorless, DSLR, “rugged” cameras (those that are waterproof, drop resistant, etc.) and action cameras. Popular choices include

GoPro™ and other similarly styled action cameras [48, 50, 51, 52] and DSLRs with a wide-angle lens or standard lens set to a wide angle ( $\leq 35$  mm) [47, 53, 49, 54, 55, 56, 57]. Action cameras are widely available, cost-effective, and waterproof to a certain depth, with inexpensive casings available to extend their maximum operating depth. They are also exceedingly user friendly with very few buttons and simplified settings. These cost benefits are balanced by more restrictive customisation, a single lens with 1-3 preset focal lengths, and lower image and video quality than DSLRs at the more affordable side of the scale. Current, more modern or higher-cost action cameras have much improved image quality compared to their predecessors. Although DSLR and other fully customisable cameras do provide a quality and adaptability advantage, the increased cost of the camera and of a separate waterproof housing puts them out of reach of most monitoring programs. Cost plays an even larger role when considering multiple camera set-ups [17, 58].

With further advances in computational power, automated annotation in marine monitoring is becoming a more prevalent and powerful tool [59, 60, 61, 62, and others]. It allows for images to be captured *en masse* and labelled by a trained computational network, speeding up data analysis for researchers. When considering coral reef systems, generally an image is cropped to only show 1 class per frame [63] or, where a wider-scale image is used, a selection of pixels are annotated rather than an entire image [64]. Gómez-Ríos et al. [63] used publicly available data to compare the use of different convolutional neural networks (CNNs) and related techniques. Of the two datasets used, one used eight semantic labels (all but two of which were scleractinian coral) another used 14 (most of which were species specific), while the last used nine (delineated only as five coral and four non-coral). Data augmentation techniques of random image rotations, flips, shifts, and zooms were not found to improve the accuracy of their best performing models significantly, with a shift augmentation improving the accuracy in one data set by 0.18% and zoom improving another by 0.68%. Misclassifications highlighted the challenges of using a *dead coral* class, most probably because it incorporated all coral types when dead so morphology and texture would more closely match an image with other classes than this class in many cases. They also had issues with morphologically similar species distinctions, which would require many more images with expert annotation to train upon and, as noted in their findings, may be helped by the use of full coral colony images aside from exclusively close up frames. Mahmood et al. [64] utilised an Australian data set to

train a deep CNN to annotate coral reef images. Their training image annotation labelling covered the most common benthos within one region (Western Australia) and applied to 50 pixels within each image. The algorithm best performed when trained and tested on images from one year (97.00 % accuracy) and worst performed when trained on one year and tested on others (92.45 % accuracy). This is likely a reflection on the highly fluctuating structure of reef systems. Reef-wide events such as storms and bleaching can change the appearance of many substrate types rapidly, while the form of faster growing species can also be more fluid and change on a smaller scale year on year. Some attempts have been made to use CNNs to capture the health of corals: in the Persian Gulf, coral disease has been detected to 95 % accuracy [60].

ImageCLEF<sup>1</sup> is a global effort aiming to advance the field of automatic image annotation and eliminate language as a barrier to semantics. Research groups can propose tasks that they think are valuable and interesting, and which individuals and teams can sign up to develop a methodology and compare it to others in the same task, with the overarching outcome of furthering the tasks results rather than “winning” a competition. The first marine themed ImageCLEF task was LifeCLEF, a fish species identification task (2014-15) that developed into SeaCLEF from 2016-17, identifying both fish and whales. Both tasks utilised the abundance of image and video data from ecological surveys that would otherwise require a large amount of time and effort to annotate. When considering the increases in marine image data each year, automatic annotation is likely to become an essential tool for ecosystem monitoring.

---

<sup>1</sup><https://www.imageclef.org>



## 1.4 Research objectives

The overarching aim of this research was to develop a feasible method for monitoring marine reefs through 3D modelling. This should be simple to perform and relatively quick to execute and analyse on both large and small scales. After a review of associated literature, a series of tools and metrics were investigated and developed to achieve this aim through the thesis research questions.

### **RQ1 - Can multiple cameras be used to the same accuracy of single cameras in Structure from Motion photogrammetry in less time?**

Single camera methods of capturing coral reef data are common and there are instances of stereo image/video capture, but both require several, if not many, passes to capture reef areas in their entirety [48, 49]. The time required for this is extensive, with few areas of relatively small scales, often 2 m by 2 m areas, captured per dive [48]. Multi-camera methods are essential for more rapid surveying, particularly with the scale of changes occurring on reef systems during this time of global change. With multiple cameras comes the question of number of cameras, placement, and angles. The number of cameras impacts the total field of view of the device, and therefore the effectiveness and speed of surveying. Modelling software best performs with 60-70% overlap in adjacent images, so position on a frame and angle need to account for the necessary overlap while also capturing the widest area of reef possible. Collected data needs to build models to the same or better quality as single camera methods and allow for data extraction to be just as accurate and reliable, if not more so, to be a viable replacement methodology - inaccurate results would negate the benefits of faster surveying. As such, they need to both provide accurate reconstruction and look realistic enough to be used as visual aids when communicating research. The survey method and software pipeline for building the 3D models must therefore provide a precise model quickly enough to be viable for practical use in reef monitoring.

This research objective is explored in chapter 3, where the proposed approach is developed and tested in a coral reef environment, and in chapter 4, where it is used in a temperate chalk reef survey.

**RO2 - Are coral reef complexity metrics developed for tropical systems of use to temperate habitats?**

The structural complexity metrics used in coral reef surveys and assessments often look at the diversity of benthic organisms or at small scale topographic changes provided by the varied substratum [65, 66, 48]. Though there are some general metrics [65, 66], most have either been developed specifically for coral reef systems or adjusted to suit them prior to use [66, 65, 48]. Their suitability for other reef types is unknown and links to local biodiversity, structure, and other site characteristics may not be legitimate if the metric does not represent the substrate accurately. Comparing the relationships of commonly used metrics on different reef types would demonstrate each measures' appropriateness. Novel measurements of complexity may be required that are tailored to individual ecosystem types and can represent topographical changes that complexity metrics do not adequately measure in rocky reef systems. These metrics can then be explored with other ecosystem variables, such as species abundance, diversity indices, and damage assessments.

This research objective is explored in chapter 4, where unchanged metrics for coral reefs are applied to a temperate chalk reef, and chapter 5, where adapted metrics are tailored to the chalk reef habitat.

**RO3 - Can coral reef substrates be automatically annotated from 2D images accurately?**

The most time consuming element of marine surveying, both *in-* and *ex-situ*, is species diversity and the subsequent indices associated with diversity and abundance. Automating the process would not only reduce the time needed for species counts and identification, but could also eliminate the need for human interaction with the dataset outside of uploading images. Neural networks are often used in image detection and recognition, but the varied morphology within coral reef species', and even genera, mean that developing an accurate and reliable network is extremely challenging. Some morphological groups may be easier to identify, but even they may still be too narrow for an algorithm in its early stages. A convolutional neural network (CNN) trained on coral reefs will inevitably be skewed in favour of the particular reefs it is trained on, but making one generic enough to be applied globally

is an essential element of a useful annotation network. Similar networks could also benefit the monitoring of other reef types as they are less biodiverse than coral reefs and may be both easier to detect and easier to recognise to genus or species level.

This research objective is explored in chapter 6, where a new task is developed for ImageCLEF to annotate coral reef images, and chapter 7, where an attempt at developing a network to annotate the ImageCLEF data set with additional images from other sources is described.

## 1.5 Research contributions

Research contributions made throughout this thesis are listed per research objective below.

For research objective 1:

1. Collection of coral reef images and reconstruction of 3D models, and subsequent extraction and analysis of model and substratum data in chapter 3. Substratum complexity data was used to form part of an *in-prep* paper on multi-camera arrays for 3D modelling.
2. A comparative assessment on the accuracy of a custom 5-camera data capture method versus standard single camera data capture in chapter 3. This provided the groundwork for integrating further cameras in image data capture approaches.

For research objective 2:

1. Extraction and analysis of substratum data from 3D models of the Cromer Shoal Chalk Bed MCZ and analysis of related species abundance data in chapter 4. This provided the data for a formal advisory report sent to the Eastern Inshore Fisheries Agency (EIFCA) to highlight current and potential substrate damage, and to inform management and further research at the site.
2. Development of a complexity assessment method in chapter 5 to better relate the Cromer Shoal Chalk Bed substrate structure to organism abundance on the chalk reef. This was independently developed as a novel method for extracting this complexity type in a chalk reef environment and a novel python script (Appendix IV).

For research objective 3:

1. Annotation of image data in chapters 6 and 7 as well as administration of images annotated by others. This data-set was used and expanded upon in each year of ImageCLEFcoral.
2. Participation in the 2020 NOAA GPU Hackathon as preparation for an ImageCLEFcoral 2021 submission in chapter 7. This included working within a team to replicate and troubleshoot a previous ImageCLEF submission as a first exposure to neural networks.
3. Further testing of a neural network to automatically annotate coral reef images with the addition of non-standardised publicly available data and colour enhancements in chapter 7, and coordination of the task participation group. This submission to ImageCLEFcoral 2021 was the first edition of the task to use alternative data sources and demonstrated potential issues that can arise from this.

## 1.6 Research publications and presentations

Publications and presentations are listed per research objective below, with the specific contribution stated.

For research objective 1:

1. An in-prep article demonstrating the theory and application of a novel camera layout in 3D photogrammetric data capture. Contributions include *in-situ* testing; model building and analysis; and drafting and editing the paper.

[J. Chamberlain, L. Clift, [J. Wright](#), and A. Clark, “Multi-camera photogrammetry using dodecahedron-based structures for terrestrial and underwater surveying,” *in-prep*, 2023]

2. A public talk on 3D modelling in marine environments and post-modelling complexity extraction for Pint of Science. Contributions include creating the slides for complexity analysis and giving the presentation.

For research objective 2:

1. A research report to provide a preliminary assessment of potential damage at the Cromer Shoal Chalk Bed MCZ. Contributions include project planning, *ex-situ* data extraction, statistical analysis, figure creation, and drafting and editing the report.

[F. Tibbit, J. Love, J. Wright, J. Chamberlain, “Human impacts on Cromer Shoal Chalk Beds MCZ: Chalk complexity and population dynamics of commercial crustaceans,” Natural England, Tech. Rep., 2020.]

2. An in-prep article demonstrating the use of a novel relief assessment on the Cromer Shoal Chalk Bed MCZ and comparing relief to other common structural metrics, as well as contrasting these results with those of a coral reef system. Contributions include the capture and building of coral reef models, conceptualising the method, developing the code required, analysis of 3D models, and writing the paper.

[J. Wright and J. Chamberlain, “Investigating Human Impacts on Rocky Reefs Using Measures of Complexity and Relief from 3D Photogrammetry,” in press, 2024]

3. An oral presentation to the Natural England Norfolk project team covering the basics of 3D reconstruction with SfM and common complexity metrics that could be applicable to the chalk reef. This presentation was given at the start of the project before specific plans were set to demonstrate the capabilities of computation analysis. A similar presentation was given over zoom two years later to a new group of staff on the project. Contributions include creating the slides for complexity analysis and giving the presentation.

For research objective 3:

1. A conference paper detailing the motivation, planning and results of the first ImageCLEFcoral task. Contributions include determining substrate annotation labels; training of image annotators; image annotation and administration; and reviewing the paper draft.

[J. Chamberlain, A. Campello, J. Wright, L. Clift, A. Clark, and A. García Seco de Herrera, “Overview of ImageCLEFcoral 2019 task,” in *CLEF2019 Working Notes*, ser. CEUR Workshop Proceedings, vol. 2380. CEUR-WS.org, 2019]

2. A conference paper detailing the motivation, planning, and results of the 2020 ImageCLEFcoral task. Contributions include determining substrate annotation labels; training of image annotators; image annotation and administration; and reviewing the paper draft, as per the previous year.

[J. Chamberlain, A. Campello, J. Wright, L. Clift, A. Clark, and A. García Seco de Herrera, “Overview of ImageCLEFcoral 2020 task: Automated coral reef image annotation,” in *CLEF2020 Working Notes*, ser. CEUR Workshop Proceedings, vol. 2696. CEUR-WS.org, 2020]

3. A conference paper outlining the submission of a run to the ImageCLEFcoral 2021 task. Contributions include project planning, image colour enhancements, submission run troubleshooting, creating figures, and writing the paper.

[J. Wright, I-L. Palosanu, L. Clift, A. García Seco de Herrera, and J. Chamberlain, “Pixelwise annotation of coral reef substrates”, in *CLEF2021 Working Notes*, ser. CEUR Workshop Proceedings. CEUR-WS.org, 2021]

4. An oral presentation outlining coral reef substrate identification for each ImageCLEF semantic label and the use of custom software to annotate images. Contributions include creating and giving the presentation.
5. An oral presentation outlining the motivation and outcome of the ImageCLEFcoral 2019 task. This talk was designed to provide others in the Natural Language and Information Processing research group with context on the research. Contributions include creating and giving the presentation.
6. An oral presentation outlining the ImageCLEFcoral 2021 paper submission for other ImageCLEF participants. Contributions included creating the presentation and presenting the motivation and theory behind the project as well as the results.
7. A poster outlining the context and design of the ImageCLEFcoral 2019 task. This poster was targeted to Biological Science research students to demonstrate the use of image annotation in conservation research. Contributions include creating the poster and discussing it at a general poster session.

## 2 | Literature review

### 2.1 The importance of structural complexity in reef systems

Structural complexity is a vital component of a healthy and biodiverse reef habitat [67, 68, 69, 70] - it provides the architecture for organisms to become established and is also sustained by those same organisms. It is a measure of the physical diversity of a system and its 3D characteristics, often also looking at the quality of structures to determine the state of the habitat. A wide range of terms have been used to describe the concept. Risk [46] defined *spatial heterogeneity* as the “actual surface area of a substrate as compared to its horizontal projection area,” and was referred to by Luckhurst and Luckhurst [71] who used the term interchangeably with *habitat complexity* and *substrate complexity*. McCormick [66] described habitat complexity as the spatial arrangement and diversity of surface types. Pittman et al. [45] took *topographic complexity* to be a measurable form of surface heterogeneity, but offered no further definition. Di Franco et al. [38] further characterised habitat complexity as the “tri-dimensionality of the habitat ... determined by abiotic (e.g. the physical rugosity) and biotic (e.g. the architecture of the benthic cover) elements.” These terms all encompass the same idea - that structural complexity is a mathematical description of the fundamental morphology of a system that, in ecology, has long been used as a measure of ecosystem health and resilience.

#### 2.1.1 Coral reef structure, health, and biodiversity

The most commonly thought of reef type is coral, wherein scleractinian corals make up the dominant organism in a biogenic marine habitat. A coral reef is one part of a connected biological system, linking with other reefs, terrestrial environments, seagrass meadows, and mangrove forests and augmenting reef resilience [1, 72]. This connectivity allows for ontogenetic species dispersal, providing nursery grounds and refuge for a variety of reef-associated organisms [72], and for carbon sequestration (though individually coral

reefs act as a carbon source [73] their interaction with other ecosystems allows for greater carbon uptake and increases coral calcification [74]).

Structural complexity is widely studied on coral reefs and is a key to maintaining a biodiverse system [67]. Many biological functions are enabled or supported by this complexity [53] so it is often used as a proxy for reef health and resilience; greater structural complexity is connected to increased food sources, breeding areas, refuge and settlement for the organisms living in these environments [3, 4, 65]. Complex structures support diversity, which brings organisms that provide more complex structures (Fig. 2.1). The different morphologies of substrate-bound benthic organisms provide an intricate framework of crevices, overhangs, and refugia that not only support other reef-associated organisms but also provide settlement and expansion grounds for new or expanding substrates. With increasingly strong environmental stressors, complexity is being lost as corals bleach and die out [23] or are damaged by extreme weather and inattentive human actions (from divers, snorkellers, and swimmers, boat anchors, etc.) [9].

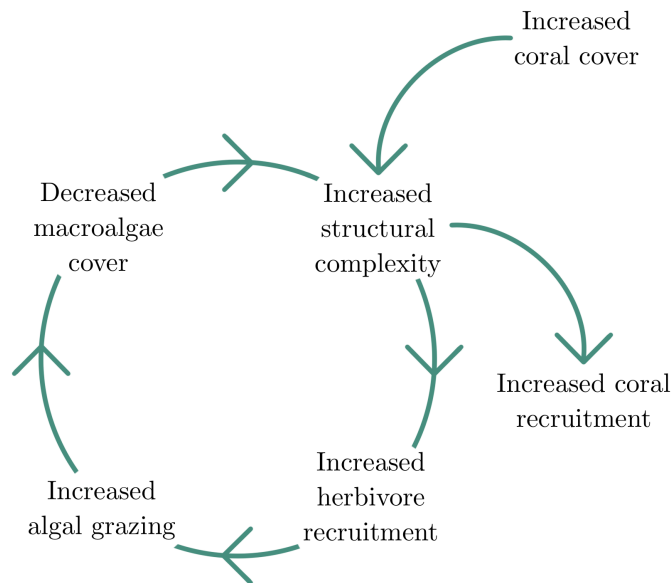


Figure 2.1: Positive reef interactions creating a feedback loop that maintains coral dominance on a reef system and promotes structural complexity and recruitment of reef fauna.

General consensus across studies is that structural complexity in a reef system is a vital driver of biodiversity and therefore ecosystem health [67, 65, 75, 76]. Greater complexity is reflected in greater coral cover [77], greater abundance of fish (as biomass and density) [65, 78] and invertebrates [79], and reduced algae cover which could be reflective of intensified herbivorous activity [65].



Structural complexity also has positive implications for coastal protection in reef areas. While reefs are thought of as a form of protection outright, qualitative evidence has been found showing that structurally complex reef systems offer greater protection than their less complex counterparts. An analysis of research on the impact of structural complexity on reef systems by Graham and Nash [65] showed that the effect was consistent despite geographic distance from the shore, although the scale of the effect may vary. Some studies within their review were inconclusive when assessing coral cover, algal cover, and sea urchin density in the Caribbean region but when compared with other studies in the review, trends held with other regions.

### **2.1.2 Coral reef complexity decline in the Anthropocene**

Although slowly changing climates are a natural process, the increased rate of change due to anthropogenic pressures is well recorded [80, 81]. The compounding pressures of stress events, both long and short term, cause damage to reef systems across the globe [24, 82]. The outcomes of this can in turn create a cycle of damage that acts as a feedback loop, continuing and compounding reef degradation to an irrecoverable state [83]. With every harmful impact on coral reefs, structure can be lost.

Increasingly warming sea surface temperature (SST) has a multitude of direct and indirect effects that can diminish structural complexity. Increased temperatures are well-recognised to cause coral bleaching in many regions of the world [82, 84, 85], an effect compounded by higher levels of ocean acidification [86]. Increasing atmospheric CO<sub>2</sub> causes greater uptake of CO<sub>2</sub> into the ocean, leading to a greater volume of H<sup>+</sup> thus reducing pH. Lower oceanic pH can reduce the density of coral skeletons, weakening their structure, and reduce calcification rates [87].

Rising sea levels can increase local sedimentation through land run-off, which can smother coral polyps and prevent feeding, stressing, and starving corals to the point of bleaching and death [9, 19, 88]. Pollutants can not only poison reef systems and encourage disease [19, 89], but also reduce light penetration and encourage algal blooming [90]. Algal blooms compound the reduced light effect, or create it, by blocking the sunlight (specifically photosynthetically active radiation) from coral reefs, preventing photosynthesis in the coral holobiont which stresses and starves the coral [91]. Algal mats can increase sediment accumulation which leads to increase nutrient loads, smothering, and coral disease,

and excessive algal presence could lead to an extreme spectrum of dissolved oceanic  $O_2$  causing shifts in community composition and lowered local pH [92], which itself can result in reduced accretion rates, stunted growth, and dissolved coral skeletons [83]. These effects cause brittle coral skeletons that are easily fragmented in storms or by human impact, leading to rubblisation of the coral and reduced structural complexity [83].

A more immediate example of reef structural loss from the effects of climate change is the increased frequency of destructive storms. Cyclones, tornados, tsunamis, and other natural disasters can be catastrophic for reef systems. Harmful effects, both direct and indirect, can devastate a reef's structure and its ability to recover. The strength and force behind water movement can fragment and uproot coral colonies, with those colonies then fracturing further colonies still attached to the substratum [93]. More complex corals are more susceptible to this type of damage - branching corals are most often broken up by storms [67, 93]. Fragmented and broken coral can take decades to recover, and storms can occur multiple times a year on some reefs, which compounds the effect of these weather events and damages the reefs' capability to maintain a diverse and robust ecosystem [9].

Anthropogenic activities can also directly harm system complexity through removal of, or damage to, marine substrates. Exploitation of reef resources is common in several industries, including the food, aquarium, and jewellery trades [1, 94, 95]. Harmful fishing practices are prevalent in poorer regions where coral reefs are vital for individuals as a resource of income and food. Blast fishing, mostly with dynamite or fertiliser, kills many fish with minimal effort - maximising profit - but can decimate the area where the bomb was thrown. Coral, sponges, other animals, and even the rock below the benthos can be destroyed, removing structure and species abundance in an instant. Cyanide fishing is a more opportunistic method that supplies the food and aquarium trades with fish, invertebrates, and coral [9]. Cyanide fishing is particularly harmful to corals when repeatedly done, stressing the colony to the point of death [19], and because fishers will break corals open to extract hiding fish [94], immediately removing their microhabitat and structure from the reef.

Terrestrial development can cause considerable degradation to reef systems [19, 96, 97, 98]. Development often leads to pollutants in coastal waters, particularly sewage water with high nutrient levels. The increase in nutrients can lead to phytoplankton blooms that increase light attenuation thereby reducing coral health and resilience and propa-

gating algal growth in areas previously dominated by corals [90]. Building on shorelines, particularly on intertidal zones, often leads to increased sedimentation in the water column that increases light attenuation and can block coral polyps, reducing the corals' ability to feed [9, 19, 88].

### **Phase shifts**

Coral reefs are so called because scleractinian corals are the dominant organisms. Changes to community structure can alter this dominance and push the reef into a phase shift: an ecosystem-wide shift in community structure that leads to a change in the dominant organism(s) (Fig. 2.2). These phase shifts, exacerbated by climate and anthropogenic stressors, can be detrimental to reef complexity and health. Competition for dominance on coral reefs is a constant shifting pressure between slow and persistent organisms, such as corals, and faster growing organisms, such as algae or Crown of Thorns starfish. Sponge reefs are also now considered a possible phase shift outcome for hard coral dominant systems in some regions [99, 100], as are corallimorpharians, soft corals, and some other benthic groups [100].

The balance of species abundance within a reef system is delicate. Hard corals often can't outpace the growth of other species and instead rely upon herbivores, spongivores, and even tidal action to remove or maintain the level of competing benthic organisms [101]. The removal of these animals can upset reef dynamics and, when buoyed by other disturbances, a phase shift can be unavoidable. Many reefs in the Caribbean have moved to algal dominance through extensive herbivore loss, storm impacts, and disease [102], as well as sedimentation and eutrophication [103]. Overgrowth of coral can cause their smothering, suffocation, and eventual death. Dead corals easily fragment to form rubble, eradicating structure and further alienating a range of species' that would otherwise aid in maintaining relative species abundances [88]. This creates a feedback loop that perpetuates the new reef phase (Fig. 2.2).

Coral reefs have been able to recover from phase shifts in some instances. Though a spatially restricted study, the Dairy Bull reef on the north coast of Jamaica, which was an algae dominated system before 1998 in part due to a loss of herbivorous activity, showed a dramatic decline in algae (~90% loss) and increase in scleractinian corals (~132% gain) between 1995-2004 that resituated hard corals as the dominant group. This change

was potentially due to a high abundance of *Montastraea annularis* coral colonies, which provide a significant contribution to reef structural complexity and are resilient to extreme weather events [104], and reflected by increased black sea urchin, *Diadema antillarum*, density which may have in turn been influenced by the grazing of other urchin species [105]. In the Florida Keys, the herbivorous crab species *Maguimithrax spinosissimus* was able to remove 50-80% on algae cover which subsequently led to great increases in coral recruitment and fish abundance [106]. Cases of recovery are uncommon, but do provide some hope for amelioration with and without human intervention.

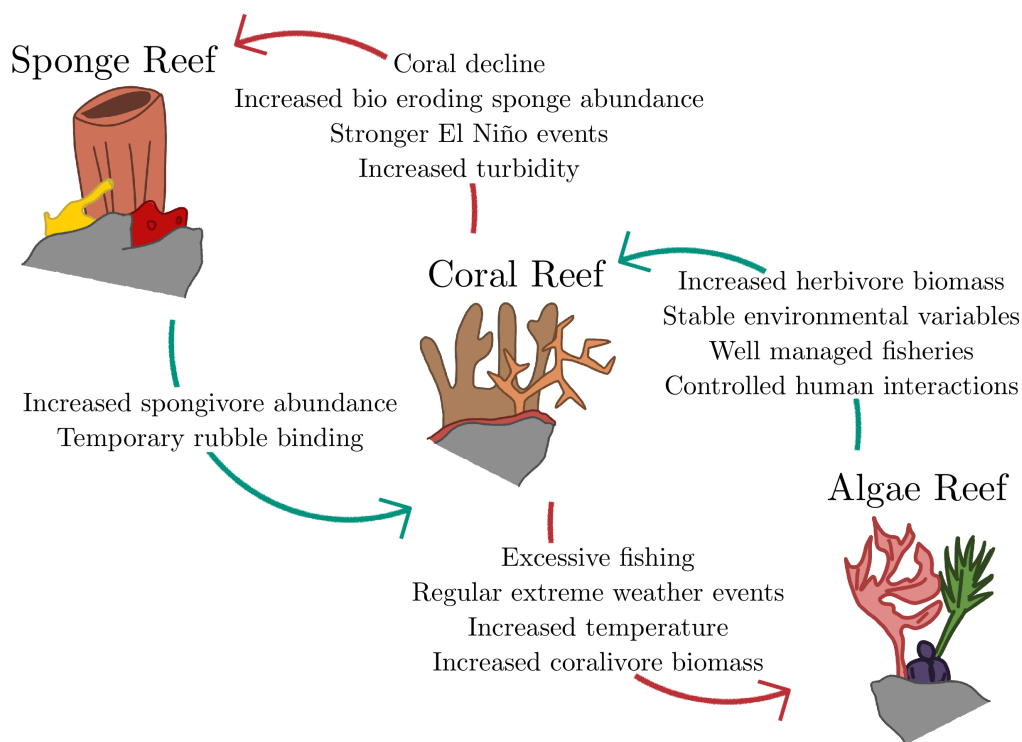


Figure 2.2: An example of the causes of phase shifts between a coral reef, an algal reef, and a sponge reef.

### 2.1.3 The structure of non-coral reefs

Coral reefs are not the only type of reef. Natural reefs are geological bars formed from any number of organisms or materials. Oyster reefs, for example, are formed from living and dead oysters and provide structure and habitat for nekton species (those that are able to move freely in the water column) in normally muddy-bottomed ecosystems, allowing more diverse substrate to be exploited through “physical ecosystem engineering” [107].

Sponge reefs are also becoming more common and, for bioeroding sponges, could increase the complexity of reefs even after out-competing corals [108]. Alternatively, abiogenic reefs are commonplace in marine and freshwater environments and can be formed of sand, rock, chalk, and other similar materials. Each of these form in different ways, creating unique and varied structures that can greatly differ from each other in their complexity.

There has been comparatively little research into non-coral reef systems. Where it occurs, it generally focuses on organisms living on/around the substrate rather than on the substrate itself. Where structural complexity has been assessed a range of relationships have been found, dependant on the reef type. Temperate rocky reefs, for example, show a positive association with rugosity and small fish biomass but a negative one with larger fish in some instances, potentially through a flora-associated enhancement of resource availability and refuge provisioning [35]. An experiment with oyster reefs of varying complexity showed that higher rugosity systems showed higher densities of many, though not all crab species, with the larger crabs showing the greatest preference for more complex areas [109]. Contrasting these findings, habitat complexity is not always found to have an impact on fish assemblages in temperate rocky reef environments, showing that not all ecosystems follow expected patterns [110]. In some cases, the type of benthos impacted a rocky reef's biodiversity more than structure and no-take fishing zones did [38].

There is a clear need to continue to monitor the physical structure of coral reefs to track and predict topographical shifts, and an even more prevalent need for investigation into other reef types to assess if they are following the same trend and, if so, whether they are losing complexity for the same reasons. Large scale, cost-effective, and time-efficient methods are required for future efforts to keep up with the scale of marine systems and the potential changes to their substrate.

## **2.2 Reconstructing marine environments**

Mapping and reconstruction of underwater structures is an intensive task with a range of methods and applications. Measuring the changing depths of the ocean is known as bathymetry, and is the foundation of early mapping. The first bathymetric map was created in 1853 and is extremely coarse in detail compared to those in later centuries (Fig. 2.3). Weighted lines were originally used in these surveys, also known as “plumb lines”

[111], before sound waves became a common method to gather underwater depth data. Single beam echo-sounders were developed to emit a beam of sound and record the speed at which this beam returned. The resulting data allowed for large areas of ocean depth to be measured, but had no way to determine if the depth measurement was coming from directly below the device or anywhere within its 30-60° focus beam [112]. Following this, multibeam echo-sounders greatly improved the resolution of resulting data by using cross-beam like soundwaves and noting the intersections of said beams. This advancement in technology allowed the entire seafloor to be mapped in much greater detail than before [112]. With both single and multibeam echo-sounders, the shallower the water the more accurate the data - the less distance a sonic wave has to travel, the less of a spread area the angle of the beam can reach, meaning a smaller region is surveyed in greater detail.

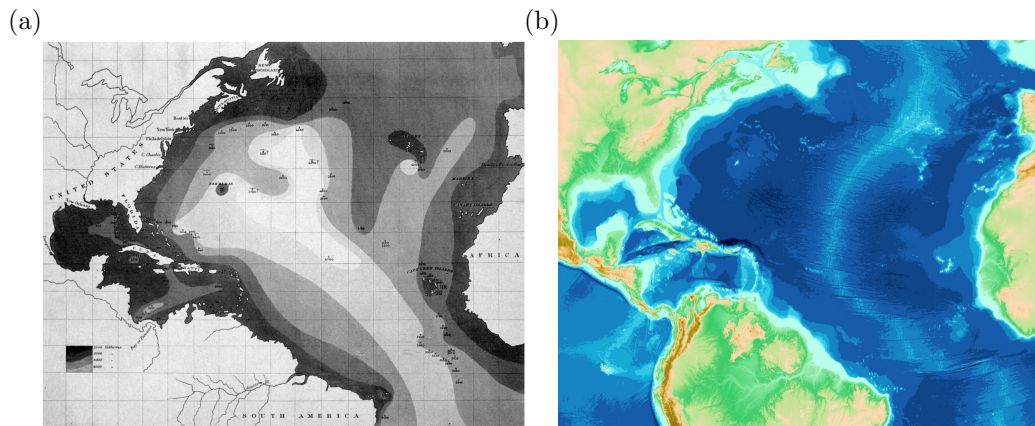


Figure 2.3: Bathymetric maps of the North Atlantic ocean, from (a) 1853 by Matthew Fontaine Maury<sup>1</sup> and (b) 2021 generated through the GEBCO Grid<sup>2</sup>.

### 2.2.1 The history of photogrammetry

Photogrammetry allows for the extraction of measurements from objects within an image or set of images. It was developed - using a foundation of Leonardo da Vinci's principles of object perspectivity - relatively soon after the invention of photography (1839) and the development of the first camera (1851), with measurements from camera images used in documenting public buildings from 1858 [113]. Photogrammetry was initially carried out by hand before becoming automated from the 1950s, allowing for "basic to photogrammetric restitution" to project 2D image coordinates into associated object coordinates in

3D [113].

Photogrammetry may have been imagined before the photograph was even invented. Notebooks from da Vinci depict “points, lines angles, surfaces and volumes on the picture plane” [114], beginning his work into optical projection. Mathematicians used da Vinci’s work to develop the field of projective geometry - looking at central projection, or how geometric objects and their projections onto other surfaces relate to each other.

Konecny [113] divided photogrammetry’s advancement into 4 stages, defined by the rapid development early on in each. Plane table photogrammetry (1850-1900) used, and was named for, plane table surveying principles to map topography [115]. The start of this stage is attributed to the French engineer, Colonel Laussedat, who lead experiments into topographical surveying is the first instance of extracting measurements from images for mapping [116]. Analogue photogrammetry arose from 1900 to 1960 with the invention of the aeroplane and development of better equipment allowing for aerial mapping [117]. The improvements in technology lead to new instruments; 1908 saw the invention of the stereoautograph from Eduard von Orel - a plotter utilisable in mountain surveys [117]. The use of aerial surveys was revolutionary, particularly as a resource in both World Wars. A short period between 1960-1985 was known for analytical photogrammetry with improved outputs from both computing developments and a new mathematical process [115]. These improvements overcame most previous constraints in photogrammetry and allowed for further uses, including in extraterrestrial missions [118]. Despite the advancements made in such a short time, the expense required for photogrammetry kept it out of reach for most.

From 1985 to the present day, computational photogrammetry has risen as a simple, relatively inexpensive tool. The rapid increase in computing power and the normalisation of technology in schools and homes lent itself to great steps forward. The development of imaging capture and processing tools led to vastly improved accuracy in photogrammetry; digital cameras, with charged couple devices instead of film, are both more accurate and much easier to interface with computers [119]. Digital computers replaced photogrammetric plotters and enabled large datasets to be utilised with better hardware (i.e. larger HDDs, then SSDs, and more powerful RAM) and software that allowed for user-friendly

---

<sup>1</sup><https://photolib.noaa.gov/Collections/Voyage/History-of-Oceanography-Collection/Bathymetric-Maps-Collection/emodule/1287/item/72846>

<sup>2</sup><https://download.gebco.net>

data processing with fully automated algorithms. The ease of access into digital technology and related software has led to a boom in 3D modelling and subsequent photogrammetric data extraction in marine monitoring and surveys [3, 56, 17, 120]. Low-cost approaches have been developed using more affordable equipment and software [48, 121, 122], allowing more research to access these methods and move towards computational approaches.

### 2.2.2 3D modelling of underwater systems

3D reconstruction can occur through several methods. The most common by far in marine applications is Structure-from-Motion (SfM) photogrammetry, which determines the environment and camera positions to project a 3D reconstruction accurately through recovering the position of shared points in images. This can be done with one moving camera or with multiple cameras capturing different angles simultaneously [48, 123]. Other methods include photometric stereo and shape-from-shading, both of which utilise a single camera in a static position while a light source moves in each still, and reflection on the camera lens is used to determine object position in 3D space. The practicality of these in real-life marine survey situations is limited, considering the time constraints of SCUBA and light refraction in water.

3D reconstruction of reef systems is becoming a prevalent and promising method for quantifying substrate variables and visualising reef changes [3, 56, 17, 120]. The use of modelled systems has allowed for easier and more advanced metrics to be taken, improving the accuracy and speed of data collection. Currently many 3D modelling techniques only cover a small area of the reef at a time, with 2x2m areas generally used per model. This limited scale reduces the efficiency of data collection as, though more metrics can be used, the number of dives required is still high. Image collection of large scale areas in single dives is an essential next step in 3D reconstruction of coral reefs to optimise data collection and increase the efficacy of monitored reefs.

Generating a 3D model using SfM requires images of an environment wherein the modelled objects do not move. These images can come directly from photographs (images) or taken as video frames (stills). The use of stills and images is not consistent between data collectors, though the effect this has on the validity of data extracted from a model is unknown. The convenience and insurance of a video still extraction can be highly beneficial to combat image blurring and a need for more images than anticipated, but



there is a trade-off with the data embedded into stills being considerably less than that in images. Some papers [3, 124, 49] suggest that calibration of cameras is preferable during data collection, but others suggest that this is unnecessary [125, 48], likely due to the processing involved during SfM incorporating processes that account for unknown calibrations.

Most papers working in SfM of coral reef systems utilise one camera [47, 49, 48, 54, 55], though some use two [58], and predominantly use Metashape<sup>3</sup> (previously named Photoscan) for processing and generating 3D models. The workflow used is consistent across papers, with many following the procedure set out in Burns et al. [49]. As a relatively low cost, commercial program, Metashape is well suited to model development while remaining accessible and there are many informed papers and guides to allow for a wide range of people to use it. This is beneficial for pushing 3D modelling to widespread use in short- and long-term research and monitoring. Some papers rely on other algorithms and mapping software in model creation, i.e. VisualSfM to MeshLab [124], or on in-depth user interaction throughout processing [58], which may produce accurate results but is inaccessible, particularly to monitoring projects, and is unlikely to be replicated by others unless it becomes more comprehensible, despite being open source.

Any camera used in image/still collection needs to be of good enough quality so that common points across images can be found. This is particularly true of underwater data collection, as light refraction, light attenuation and turbidity can all contribute to inadequate image collection. To combat this, the distance of the camera from the modelled object/area is often closer than it would be on land. Camera type may also come into effect with clarity, as higher resolution cameras will be able to generate clearer images. The use of digital SLR cameras in underwater housing is common when images are used instead of video stills [3, 47, 53, 54, 120] and generally capture images from 2m [47, 120] to 3m [3, 53, 54] above the substrate, though up to 5m distances have been used [120]. Closer capture is used when video footage is captured, from 1m-2m [126, 122] with high-definition video cameras to as close as 0.5m-1m using GoPro<sup>TM</sup> action cameras. Stereo camera set-ups, while not common in modelled reef capture, have been used from 1.5m above the substrate [127]. DSLR cameras provide the widest photographic footprint across literature, but their cost and the price of housings required have lead to lower cost meth-

---

<sup>3</sup><https://www.agisoft.com>

ods using action cameras to be identified and used [48] to make modelling systems more accessible to monitoring and other research groups, and these camera types have been found suitable for both trained researchers and “citizen scientists” for 3D modelling [50].

A major practical component to 3D modelling habitats is the scale that can be covered. Smaller areas offer a much quicker processing time and may be well suited for some projects. To truly proliferate through research and monitoring, the ability to model large areas is vital and, to an extent, have been modelled by some groups [47, 54, 58]. As with any program, increasing the images used in model generation also increases processing time. Larger areas need more images by default, but ensuring that generation is optimised requires only enough for accurate modelling. To ensure this, adequate image overlap is required. While there have been suggestions of up to 90 % overlap being necessary [120, 128], many have found that less, between 70-80 %, is sufficient [53, 49, 125, 54, 127, 51]. There are of course some exceptions, with overlaps as low as 60 % [48] and as high as 95 % [47].

### **2.2.3 Processing 3D models in Agisoft Metashape**

Imaging a reef is only the first step in creating a 3D reconstruction. The building of a model can utilise many varied techniques, but SfM is both common across marine monitoring and assessment [3, 17, 48, 122], and is relatively inexpensive and simple to carry out compared to many other reconstruction methods. It relies on the extrapolation of camera position in 3D space through common points between adjacent images to build an accurately scaled and positioned model of the environment. Metashape is one of several software options available in generating SfM 3D models and is commonly used, potentially because it has automated these steps into user-friendly software with customisable settings and interactive models [3, 49, and others].

#### **Selecting workflow settings for SfM reef modelling**

A common theme in adjusted settings is the aim of minimising processing time as much as possible while maximising the model quality. Some studies adjust a few settings in one or more steps, while others fully customise model creation in each stage of the process. A subset of studies using Metashape (or Photoscan prior to the renaming) with adjusted settings are compared below. Where a setting is not mentioned or is called standard/generic, it is presumed to have been left to the default.

When aligning photos, accuracy was generally set to high [47, 54, 51, 129], though it has been set to medium [48] and low [124] with success, though the low quality did show increasing error with models that contained structurally complex features when combined with the other adjusted settings (see [124] for details). This study was also the only one to turn off pair preselection. Key point limit was only changed once, increasing to 50,000 initially and further to 70,000 if any images were not aligned [54]. Tie point limit was also increased in some cases, to either 5,000 (or 8,000 if images were not aligned) [54] or 10,000 [17, 47] and was once decreased to 1,000 [124]. Dense cloud quality was lowered to “medium” in some cases [124, 48, 54, 51] but no other settings appear different to the standard. Mesh face count was set to high in some cases [54, 51], but a custom value of 3,000,000 was used once to increase the resolution of a relatively small scale model [48]. Only two studies altered the texture settings. One increased texture size to 30,000 [51] while the other increased size to 16,384 while also using the adaptive orthophoto mapping mode [54]. Little clarity was provided in the above studies as to why settings were specifically selected and what impact they had on model quality or processing speed.

Photogrammetry has become increasingly common in marine monitoring, particularly in the reconstruction of coral reef systems [3, 56, 17, 120, 48, 122]. Its use shows a clear benefit over exclusively *in-situ* assessments by providing reusable data that can be utilised in a range of studies with limited SCUBA diving requirements. This data could even enable future research to be carried out on soon-to-be “historical” datasets with assessments that may not yet exist, effectively future-proofing substrate data. Linking 3D reconstruction with previously collected “analogue” structural complexity metrics is key to driving research towards computational analysis and providing a stepping stone between exclusively *in-situ* versus *ex-situ* research.

### **2.3 Measuring structural complexity in marine habitats**

Measuring complexity *in-situ* is complex and often inaccurate but is accepted as a relatively easy-to-replicate and cheaply performed assessment. Many *in-situ* methods of reef surveying rely on the use of transects, quadrats, or both. These provide areas for study that can be chosen at random or be selected for repeated measures over a period of days, months, or years. The two can be combined to survey habitat complexity and

species interactions as part of coral reef monitoring [130].

The classification of reef substrate can give an insight to the composition, complexity and functions of a reef system. There are many ways to approach this classification and choice is dependent on the question being answered by surveying. Species abundance and distribution measures can be used as they provide an in-depth view into substrate composition, although when only looking at complexity it can be more appropriate to measure at a higher taxonomic level or via growth forms.

### **2.3.1 Reef complexity with analogue metrics**

While many habitat surveys include a complexity assessment of some sort, the range of metrics available have led to a large amount of research that is relatively incomparable. The act of measuring complexity *in-situ* can be a challenge in and of itself. Rugosity is the most common metric in reef ecology for determining the complexity of a system. It has been used consistently for decades [4, 71, 65, 131]. Rugosity of a reef system is often determined from a spatial index assessed using the common chain-and-tape measure. This is limited by chain link length, the presence of organisms such as soft corals that can bend and twist under the chain weight, crevices and overhangs that cannot easily be navigated around, and the difficulty of repeating measurements in the same place that they have been done previously. Subjectivity in chain placement can limit the replication of the method, as can chain link length, which can cause misleading distance errors at larger scales [132].

Having this metric allows for comparisons to be drawn from different reef sites, but chain-link length is an important factor to consider when undertaking cross-study analysis [133]. Visual assessments of complexity are also relatively common, especially in research where only a descriptive appraisal of *in-situ* complexity is needed [4]. These are more subjective than rugosity due to the influence of observer skill and experience, however they do allow for large areas of reef to be assessed rather than isolating one specific complexity component as a representation of the whole system.

### **2.3.2 Computational methods to extract complexity**

With the current shift in monitoring techniques to digital methods, more sophisticated analyses of structural complexity are possible. Metrics that are difficult or impossible to

carry out *in-situ* are now available to research teams, allowing those that are more accurate or suitable to be utilised [48]. There are, of course, those that are both common *in-situ* and feasible in 3D model data extraction. Linear rugosity is an example of this and has been consistently used throughout the rise of reef mapping in modern monitoring either linearly as done *in-situ* [48] or across an entire substrate area [47]. Other metrics include the rare use of vector dispersion in 3D modelled complexity [48, 134] many years after it was adapted for use on coral reefs *in-situ* [135], as well as fractal dimension [56] and slope [56]. These metrics, and others, are explored in Section 2.3.3.

3D modelling is becoming more commonplace in marine ecology as a way of mapping reef systems and extracting complexity measures [47, 48, 122]. The use of 3D maps is thought to provide more precise measures for complexity and be more replicable in repeated studies and monitoring programs [48]. Newly proposed methods of collecting structural data from models are often compared to *in-situ* data gathered from the same site. This ground-truthing is a vital part of developing a new method, but can be challenging in the context of metrics and environments that have complex or time-consuming *in-situ* data collection methods, but *ex-situ* testing can show the strength of a test that is then assumed to be reflective of *in-situ* measurements [48]. Generally, the extraction of complexity variables is done with different software than that used to build the 3D model. The most common of these are Rhinoceros 3D from Robert McNeel and Associates<sup>4</sup> and ArcGIS from the Environmental Systems Research Institute<sup>5</sup>. Each offers a different toolset for analysis. Rhino provides the ability to run python scripts that allow for completely customised assessments, though this requires at least some knowledge of writing script and in depth knowledge of the metric in question. ArcGIS provides many built-in assessments with far less user input required, which is more user-friendly and more restrictive to available metrics. Open-use software is available, such as Gwyddion<sup>6</sup> and R<sup>7</sup>, which enable anyone to analyse models to some extent, though as they are not designed for use with 3D models. Analysis can also be performed within Metashape, allowing the entire methodology to be performed with a single piece of software, though there are far more restricted capabilities compared to other software options [17].

When standard top-down imagery is used, models can struggle to capture for crevices

---

<sup>4</sup><https://www.rhino3d.com>

<sup>5</sup><https://www.arcgis.com>

<sup>6</sup><http://gwyddion.net>

<sup>7</sup><https://www.r-project.org>

and caves in reef systems [56], but time is often a prohibitive factor in marine surveying. When collecting data, efficiency is key to keep constraints caused by access to sites, budget and any seasonality from affecting the ecosystem. To increase the accuracy of many *in-situ* methods would require greatly increasing the time taken to carry out data collection and this is often not feasible. The use of computers to aid data collection can reduce the amount of time currently spent in water collecting data [48], which also provides a safety benefit to research by minimising the risks associated with SCUBA as much as possible.

### 2.3.3 Complexity metrics in marine monitoring

With the importance of structural complexity in marine research comes an influx of metrics, some with their own variations. Complexity measurements can become incomparable with those from other studies, even when the research is done in the same area. Below, some of the more common metrics are described. A summary table follows to provide a quick overview of key features (Table 2.1).

#### Rugosity

Rugosity is a common complexity metric in ecology and measures the ratio of two distances - the linear distance of a substrate as a contour and as a straight line. There are various manners to measure the rugosity of a substrate, with the customary method utilising a chain-and-tape. The first instance of chain-and-tape complexity had a chain draped to follow contours in a 1m<sup>2</sup> quadrat (Eq. 2.1) [46].

$$T = \sum_{i=1}^n (t_1 + \dots + t_n)^2 \quad (2.1)$$

Where  $T$  is total substrate topographic complexity,  $n$  is the number of chains laid and  $t$  is the length of chain required to follow the contour over a set area, first demonstrated by Risk [46]. Although this is not a ratio, it is the earliest instance of rugosity in marine ecology. The surface area of the substrate was assumed to be a function of the linear contours found using the chain, as per “point-counting,” and to be a representation of heterogeneity.

Having rugosity as a ratio allows for greater comparisons to be drawn between surveyed points, though often important features for replication such as chain-link length are

excluded from publications [4, 71, 65, 131]. Depending on the requirements/parameters of the survey being carried out, the chain-and-tape method (Fig. 2.4) can be applied in one of two ways, with the key difference being one uses a set chain length and only traverses the relative contoured distance of that chain (Eq. 2.2) and one stretches across a preset distance of substratum, often used with a quadrat of set size (Eq. 2.3). The first instance of this ratio used Equation 2.2 [71]. There are notable issues with using a chain on coral reefs. Where the benthos has tightly grouped complex regions, a chain may not be able to follow the contour as it is and instead have to drape over top, missing much of the viable area. Holes and crevices that are deep or difficult to get into may also be omitted from measurement due to the inability to accurately map the chain to them. In both instances, the resulting measurements can be highly variable [132]. The use of a chain itself can also be troublesome, particularly if it gets caught on substrate and causes damage.

$$R = \frac{\text{length of undraped chain}}{\text{length of draped chain}} \quad (2.2)$$

$$R = \frac{\text{contoured distance}}{\text{linear distance}} \quad (2.3)$$

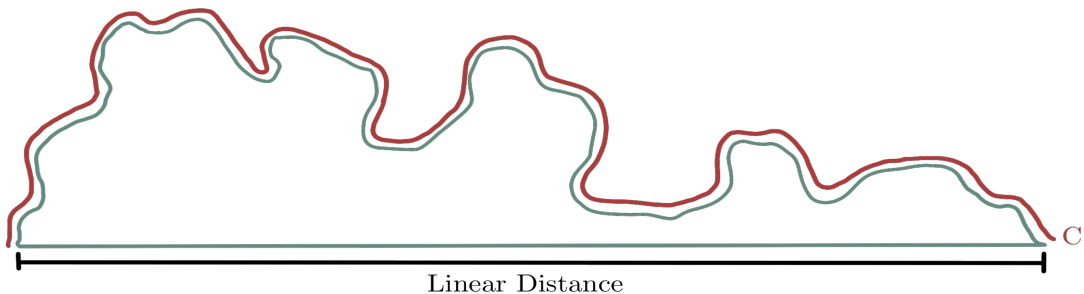


Figure 2.4: Rugosity calculated using linear distance and contoured chain distance,  $C$ .

Rugosity has also been applied non-linearly to cover the surface of an area [58, 136, 137], sometimes called a Relief Index [138], though this is far less common than the linear projection of complexity. It is similarly calculated to linear rugosity (Eq. 2.4).

$$R = \frac{\text{surface area of contoured terrain}}{\text{projected surface area of uncountoured terrain}} \quad (2.4)$$

The introduction of computational complexity assessment has not steered studies away from the use of rugosity, so it is often used for comparison when testing new methods of data collection. In a study testing the power of digital metrics, Young et al. [48] found that

*in-situ* rugosity strongly correlated with virtual chain rugosity extracted from Structure-from-Motion (SfM) models. Friedman et al. [137] used Triangular Irregular Network (TIN) based reconstruction to compare *in-situ* chain and tape rugosity measurements to both virtual chains and virtual area rugosity measures. A strong correlation between *in-situ* and virtual chains showed that the two were similar when compared, though *in-situ* measurements were found to be higher in virtual ones. The variation found in virtual chain measurements lead to testing with surface area rugosity, which showed similarly strong correlations with *in-situ* chains with less variability than that found with virtual chains. Similarly focused on surface rugosity over chain rugosity, Bryson et al. [58] used SfM models to determine the accuracy of the measure and found that variance occurs with changing environmental conditions. This is an important consideration when collecting data, particularly in regions with variable weather and/or where surveying requires multiple days.

### Vector dispersion

Carleton and Sammarco [135] described vector dispersion as a mathematical “estimate of vector variance for all vectors normal to the individual planar surfaces considered;” a normal vector is one that is perpendicular to the surface (which in this instance is a reef substrate). It was measured using a 3D profile gauge and calculated *ex-situ* (Eq. 2.5) wherein  $\frac{1}{k}$  is vector dispersion and  $R_1$  is found through Eq. 2.6.

$$\frac{1}{k} = \frac{i - R_1}{i - 1} \quad (2.5)$$

$$R_1 = \sqrt{\left(\sum \cos_{x_i}\right)^2 + \left(\sum \cos_{y_i}\right)^2 + \left(\sum \cos_{z_i}\right)^2} \quad (2.6)$$

Wherein  $\cos_{x_i}$  = directional cosine of vector normal to the surface of the individual triangle,  $i$ , with respect to the X-axis, and equivalent for  $\cos_{y_i}$  and  $\cos_{z_i}$  in their respective axes, where (0, 0, 0) is the midpoint of the triangle.

Though vector dispersion has been long established as a complexity assessment [139] and metric [135], it has not often been compared between *in-situ* values and digital values. Carleton and Sammarco [135] determined vector dispersion to be highly suited to measuring surface irregularity compared to other metrics assessed in the same study using a 3D



profile gauge *in-situ*. This approach poses similar data collection issues as the rugosity chain: difference in step between points on the gauge would provide highly variable results. The only test of vector dispersion accuracy on coral reef systems digitally was carried out by Young et al. [48] using 3D printed structures and submerged concrete structures of the same shape. They found SfM modelled vector dispersion to be highly accurate and repeatable.

### Vector ruggedness

Vector ruggedness is conceptually similar to vector dispersion [48] but uses square planes to generate vectors instead of triangular planes [53, 54]. First developed by Sappington, Longshore and Thompson [140] and calculated by Eq. 2.7, it looks at the variation of slope and aspect to provide an alternate view of the environment to a single metric.

$$R = 1 - \frac{|r|}{n} \text{ where;} \quad (2.7)$$

$$|r| = \sqrt{\left(\sum x\right)^2 + \left(\sum y\right)^2 + \left(\sum z\right)^2} \quad (2.8)$$

where  $|r|$  is the magnitude of the resultant vector of  $x$ ,  $y$ , and  $z$ , and  $R$  is a dimensionless value between 0 (flat), and 1 (complex).

Vector ruggedness has not been used *in-situ* for complexity assessment: Sappington et al. [140] used ArcView to calculate the metric. Fukunaga et al. [57] found that vector ruggedness strongly correlated to both surface area rugosity (called surface complexity) and slope using digital elevation models (DEMs).

### Angular standard deviations

A 2D representation of vector dispersion, called vector standard deviation, was described in McCormick [66]. The equation for this is:

$$R_1 = \frac{\sqrt{\sum (X_i - \bar{X})^2}}{n - 1} \quad (2.9)$$

Where  $X$  is the angle of a vector,  $i$ . A similar metric was also proposed as substratum angle standard deviation and calculated as above with  $Y$  in place of  $X$  (Fig. 2.5).

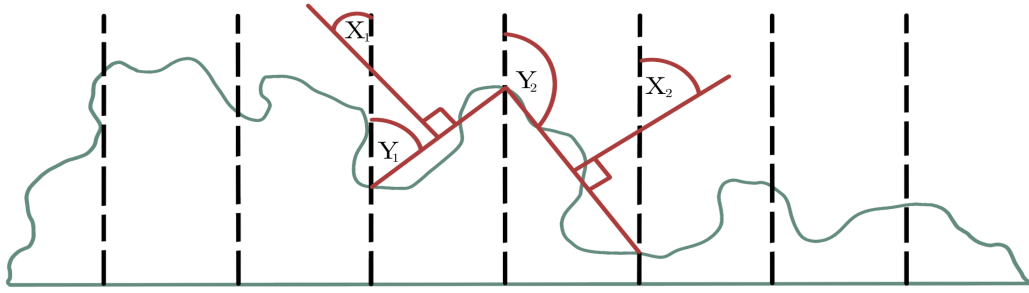


Figure 2.5: Measurement of angular standard deviations of vectors  $X$  and angles  $Y$ .

Both of these metrics were carried out *in-situ* by McCormick [66] using a 2D profile gauge. Vector standard deviation was noted as a 2D equivalent to vector dispersion. Neither has since been used in standard *in-situ* or 3D modelled assessments, though vector standard deviation was successfully used with laser lines to detect differences between substrate types [141].

### Verticality

Verticality is a measure of the changing height of the substratum [17] along a transect (Fig. 2.6):

$$A(x) = \left| \frac{f(b) - f(a)}{i} \right| \quad (2.10)$$

Where  $A(x)$  is the average rate of change in bathymetric height,  $f(a)$  and  $f(b)$  are positions on the substrate relative to intervals along the substrate of length  $i$  (chosen based upon other relevant information such as mean body size of organisms of interest).

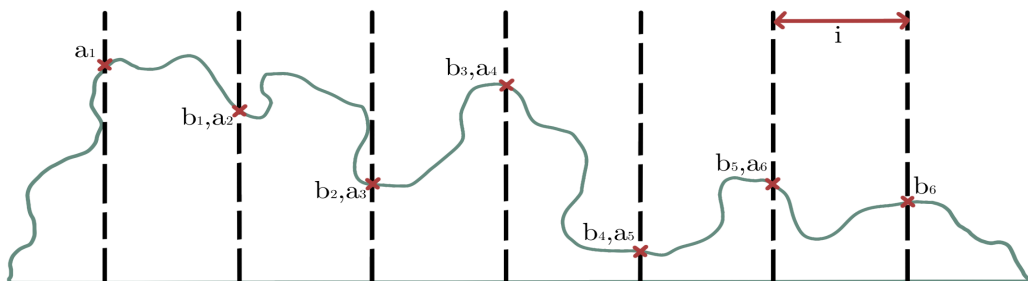


Figure 2.6: Measurement of verticality of a linear section of substrate.

Verticality may be a better assessment of linear complexity in environments that are not formed with small scale complexity changes but are instead notable for their larger

shifts in topography. Adapting  $i$  to suit the environment is a far simpler change than increasing the size of rugosity chain links (either *in-situ* or computationally). This has also been called slope in some instances, where slope is not in reference to the rate of change of variables in a figure [57].

### Curvature

Originally described as the rate of change of slope [142], curvature is becoming a more common metric in complexity assessment [3, 54, 134, 57].

$$Z = Ax^2y^2 + Bx^2y + Cxy^2 + Dx^2 + Ey^2 + Fxy + Gx + Hy + I \quad (2.11)$$

Where  $A$  through  $I$  are calculated by Lagrange polynomials of a 9x9 matrix of elevations  $Z_1$  through  $Z_9$ , per Zevenbergen et al. [142].

Where  $Z = 0$  the surface is flat, while positive and negative values show convex and concave substrates. It has been suggested having a range of values for an area is more suited to describing complexity than a mean value, and that it may be more reflective of complexity than vector ruggedness [134], though pairing the two could be beneficial for capturing the structural variation across the morphologically varied coral growth forms and of overall reef structure [57].

### Consecutive substratum height difference

First described in a method comparison paper [66], consecutive substratum height difference is a simple linear measure looking at changing substratum height, much like verticality (Fig. 2.6). The equation was not printed but in-text explanations indicate:

$$\Delta h = \sum (a_1 - b_1)^2 + (a_2 - b_2)^2 + \dots + (a_n - b_n)^2 \quad (2.12)$$

It has been referred to as  $\sum dh^2$  as it is “the sum of squared differences in height from one point to the next” [143].

McCormick [66] originally described the metric and found it to be a slight improvement on other metrics tested.

## Fractal dimension

Fractal dimension ( $D$ ) is a metric that links complexity to size categories by demonstrating changes in 3D structure across given spatial scales. Though first described for linear dimensions [144], the equation for fractal dimension can be used in 3D as well:

$$D_{x_1-x_2} = \frac{\log\left(\frac{N(x_1)}{N(x_2)}\right)}{\log\left(\frac{x_2}{x_1}\right)} \quad (2.13)$$

Where  $x_1 = \text{size 1}$ ,  $x_2 = \text{size 2}$ , and  $N = \text{number of times } x \text{ is required to cover the substrate surface}$  (Fig. 2.7). As with most metrics, the higher a value, the greater the complexity.

Fractal dimension is a metric first applied to the study of coral reefs in 1983 [145]. The scale of study reported fractal dimensions between 1.9-2.0, later refuted and shown as between 1.13-1.16 [146], which contrasts with more recent equations that calculate this metric between 2.0-3.0 [48, 54, 134, 138]. Several other uses of fractal dimension show different ranges of values, making it hard to cohesively compare fractal dimensions across studies [56, 143, 144, 147].

A study [148] utilising rugosity chains of differing link sizes calculated fractal dimensions of a reef system as:

$$D = 1 - \frac{\log(R_2) - \log(R_1)}{\log(C_2) - \log(C_1)} \quad (2.14)$$

Where  $R$  is rugosity and  $C$  is chain link length for link sizes 1 and 2.

More recently [48, 54, 57], fractal dimension has been calculated as:

$$D = 2 - \text{slope of } \left[ \frac{\log S(\sigma)}{\log(\sigma)} \right] \quad (2.15)$$

Where  $\sigma$  and  $S(\sigma)$  represent the resolution of a DEM or 3D model and the 3D surface area at that resolution. This allows for the  $D$  to fall between 0-1, which is much simpler when comparing fractal dimensions with other metrics, particularly graphically.

The limits of  $D$  are set by the topological dimension of the substrate in question. As a fractal,  $D$  must be greater than the topological dimension of the surface: planes have topological dimension 2 and so, in theory,  $D$  should always be greater than 2. As evidenced above, this is not always true, potentially due to substrates not necessarily being

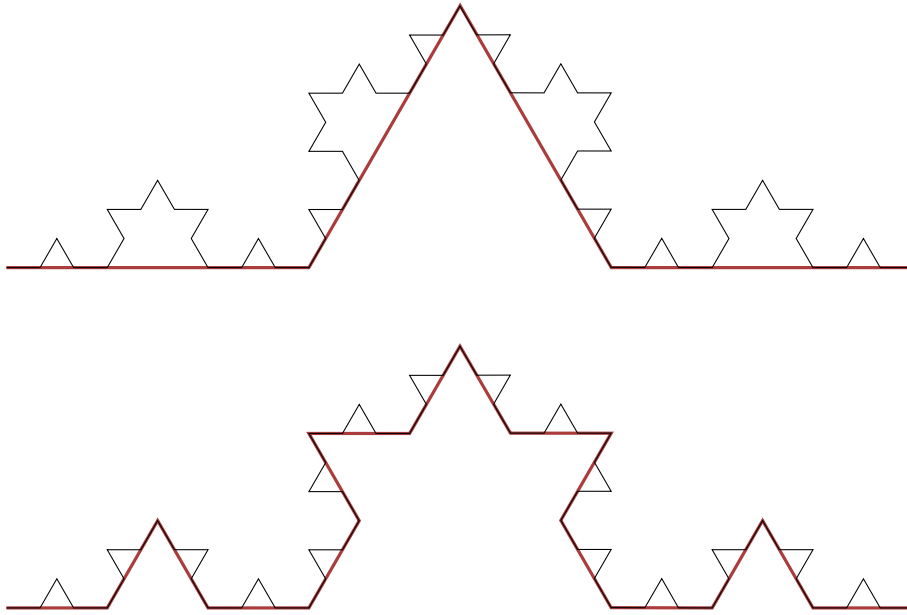


Figure 2.7: A Koch snowflake (black) example of fractal dimension (Eq. 2.13), where dimension,  $x$ , is shown in red. The top snowflake demonstrates  $x_1 = 3$  and  $N(x_1) = 4$ , and the bottom shows  $x_2 = 1$  and  $N(x_2) = 16$ . In this instance,  $D_{1-3} = 1.26$ .

self-similar [138]. Likely the most applicable of the methods used to calculate  $D$  are those using varied resolutions, as they create self-similar planar areas of squares.

## Viewshed

Viewshed is a proportion of an area that is visible from a set point. While commonly used in terrestrial terrain planning, it has been adapted for marine substrate complexity assessments in recent years [136] and used to determine how “open” an area of reef is from the view of an imagined observer [54].

$$V = \sum A(v_{(p)}) \text{ where;} \quad (2.16)$$

$$v_{(p)} = \{q \in \tau \mid d_{(p,r,\theta,\sigma)} \leq r \text{ and } q \text{ is visible to } p\} \quad (2.17)$$

Where  $V$  = total viewshed,  $v$  = viewshed of a point,  $q$  on terrain,  $\tau$ ,  $A$  = area of  $v$ ,  $p$  = observer,  $r$  = detection range,  $\theta$  = horizontal field of view,  $\sigma$  = vertical field of view,  $d$  = distance of maximum visible range.

A similar but alternative method has been used to assess the potential for a fish to detect predators whilst feeding [17].

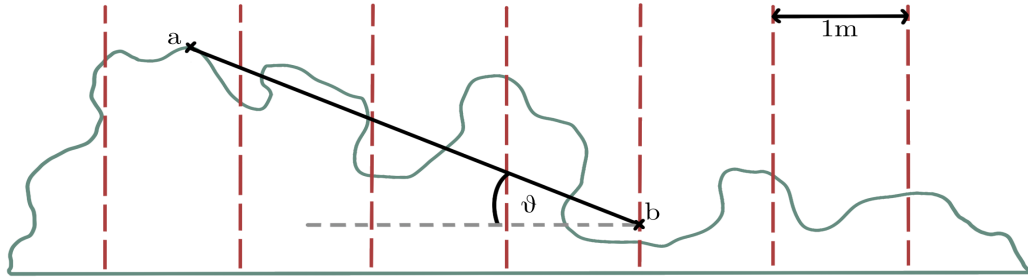


Figure 2.8: Field of view of a fish when grazing where  $a$  is the highest point of the substrate,  $b$  is the eye a fish grazing 2.5cm off the substrate and  $\theta$  is the angle between the eyeline and a secant to point  $a$ .

### Complexity metric summary

A summary of the above metrics is provided in Table 2.1 below.

Structural complexity is a key component of coral reef health with a myriad of metrics to accompany its many facets, but the organisms that provide this structure are equally important [101]. Different organisms provide different types of structure and therefore different ecosystem functions and services. Current assessments are heavily skewed to *in-situ* quadrat and transect surveys with manual identification and counts [11, 65, 149]. With the push towards computational assessments of structural complexity, similarly computational methods by which coral reef substrate organisms are identified and counted would also be of great benefit to reef monitoring. Increasing the speed and automation of these surveys would both free up researcher time and allow for much larger data sets to be used.

## 2.4 Automatic image annotation

Annotation of features has been essential in the development of image retrieval. This was first carried out manually and was then driven towards content based image retrieval (an automatic method that relies upon simple image features) to negate human subjectivity in annotations. The disparity in results showed the difference between human semantics in labelling and computational assessments of image colour, texture and other features. Automatic image annotation (AIA) then developed to connect images to semantic labelling which allows for searching images with keywords [150].

Automatic image annotation is an invaluable tool in a world with an ever increasing amount of photographs and pictures. When processing an image, the aim is to detect

Table 2.1: A brief summary of habitat complexity metrics.

Metric	Key notes
Linear Rugosity	Widely used and easily performed. Restricted linear view.
Relief Index	Encompasses entire substrate area. Not commonly used.
Vector dispersion	Accurate view of surface irregularity. Only one computational use.
Vector ruggedness	Correlates well to other metrics. Only possible computationally.
Angular standard deviations	Linear form of vector dispersion. Restricted linear view.
Verticality	Suited to environments with larger topographical change. Restricted linear view.
Curvature	Range of values for broader view. Not yet widely used.
Consecutive substratum height difference	Compasses larger height changes.  Restricted linear view.
Fractal dimension	Links complexity to target species. Size scales could be restrictive.
Viewshed	Highly distinct metric of complexity. Assessed for specific points on terrain.

objects (i.e. a car, a person, a building) by relating the pixel information within the image to the context of it. Labels of the image and/or the objects within it are then produced based on an analysis of pixels and predictions derived from them. Manually annotating images, aside from the time required, is cumbersome in data analysis due to the training required and sheer volume of images needed to produce a viable dataset. The more specific the image content, the more training required and the more time each image could take to annotate. This then leads to the overarching goal of AIA - to label unseen images appropriately with reliable accuracy, without the need for human intervention.

#### 2.4.1 Methods for automatic image annotation

There are numerous approaches to automatic image annotation, many of which have slightly different aims and assumptions that provide their distinctions. Some models base

their algorithms on the premise that visually similar images contain the same labels to some degree, and therefore search for already labelled images when presented with a new query, such as with nearest neighbour models. Others, such as conditional models, focus on labels themselves and the boundary between them to determine the probability of a class' presence in a new image.

Before deep learning became wide-spread, image segmentation occurred with relatively simple algorithms compared to those used today. Deep learning techniques have improved the accuracy of image segmentation efforts [151]. Initial processing requires a convolutional neural network (CNN) to determine the features within an image, then a separate technique is applied to assign semantic labelling to each feature [151]. This is commonly based on either pixel level relationships with labels (semantic) or distinction of specific objects (instance). Semantic segmentation utilises predefined categorical labels to classify an image on a pixel-by-pixel basis whereas instance segmentation further characterises an image by defining adjacent objects of the same type distinctly, rather than as one segment (Fig. 2.9).

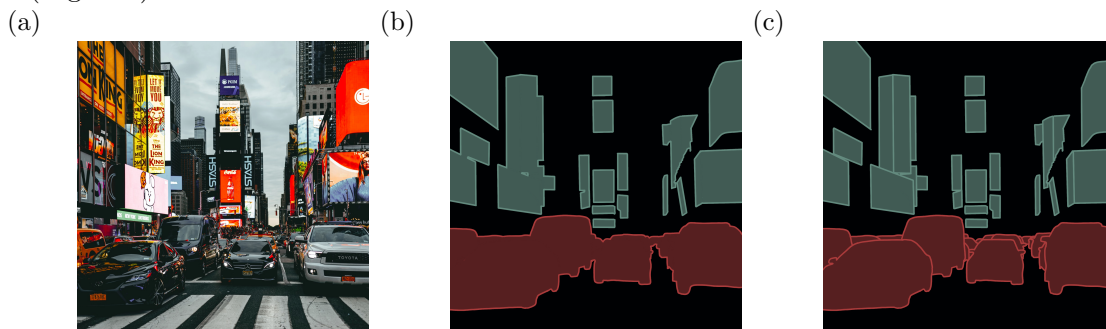


Figure 2.9: (a) An image with cars and billboards sectioned as in (b) semantic segmentation, where any adjacent pixels with the same semantic label are joined as one object, and (c) instance segmentation, where every instance of a semantic label is grouped individually whether it is adjacent to other objects or not.

## Convolutional neural networks

CNNs are a type of artificial neural network that take an input image array (consisting of the number of images, each images width and height, and the number of image channels) and run it through a series of “layers,” or processing steps, to provide a subsequent output array (Fig. 2.10). The input moves sequentially through the layers producing an output for each layer that acts as an input for the next. Pre-annotated images are used to train the CNN, wherein the processing parameters are learnt. A training image is passed



through the model to a “loss layer,” which assesses the difference between the training images ground-truth and its predicted output and signals the CNN to adjust the model parameters and continue training. Parameter adjustment is done in epochs, where 1 epoch is one run of all training images followed by appropriate parameter changes, as these changes must consider all training images to ensure that reducing the ground-truth to prediction discrepancy in one does not increase it in others.

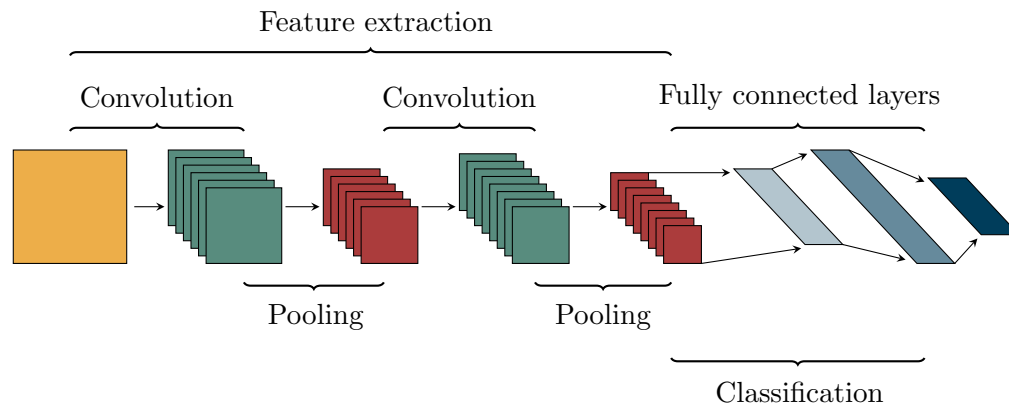


Figure 2.10: The classification of an image through a simplified convolutional neural network model, beginning with an input image (yellow), through to convolutional (green) and pooling (red) layer outputs, to the fully-connected layer outputs from flattening (light blue) and assigning a semantic label to features (mid blue) to a final result with associated semantic labels and their probabilities (dark blue).

Determining the appropriate number of epochs for model training is a balance of increasing accuracy/reducing loss while avoiding overfitting. Early stopping is a common technique to prevent overfitting as much as possible, wherein a subset of training images are used to monitor the error rate with every epoch and act as the “canary in a coalmine” to stop model training. However, increasing error rate can be a false flag as models can have a decrease-increase-decrease pattern to error per epoch, known as double descent [152]. Too many epochs in training overexposes the model to specific data, causing it to learn the specifics of the training data set rather than gaining a generalised view of features and labels.

Once training is complete, the model can be used on previously unseen and unlabelled data. Once imported, images are run through a series of layers (Fig. 2.10). The first layer of a CNN is a convolution layer, which passes a kernel (filter) over each image to create a feature map with predicted classes. This layer takes each image and determines the scalar product of a portion of the image and one or more smaller kernel matrices (composed

of learnable parameters), reducing the image to a 2 dimensional map per kernel stride (to cover all image pixels, stride = 1). Following this, pooling layers reduce the scale of each image further by calculating either the maximum or average of a portion of the image, moving similarly to a kernel to cover the entire image. This minimises the volume of detail to be passed on through the model while ensuring the essential details pass through. The convolution and pooling layers can be repeated as many times as desired, with several convolutions occurring before any pooling in some models. The fully connected layers lead to the output, and begin by flattening the previous outputs before giving each feature a label by applying weights. Each label is then given a probability when the output is produced showing the likelihood that the associated label is correct.

#### **2.4.2 Coral reef image annotation**

There have been a variety of attempts to utilise the power of automatic image annotation to aid in coral reef research and monitoring. The first, by Marcos et al. in 2005 [153], looked at simple delineation of living coral, dead coral, and sand or rubble from video footage using colour and texture features only. The premise for these features was the distinct colours and regular texture of live coral, the monochromatic whiteness of dead coral, and the monochromatic and varied texture of sand and rubble. They compared results of their video stills using a neural network and a two-step classifier, both of which showed considerably good outcomes considering both the novelty and difficulty of the task set. Though the network provided a higher recognition rate with a lower error, they noted that the classifier benefits from a simpler approach with the capability to add new features if needed. This work shows the capabilities of automatic annotation to be useful in coral reef imagery, but is severely limited by its broad categories. Despite this limitation, as the first method to develop an algorithm for reef benthos annotation, it signified the possibility of an innovative step forward in coral reef research.

In 2012, Beijbom et al. also utilised the varying colour and texture combinations of reef benthic substrates in their annotation model [154]. They built on a previous method by allowing for multiple patch sizes (to account for the different scales within their coral reef data set) and adding colour as a variable. They highlighted the difficulties a changing reef-scape poses to annotation, as their results worsened when testing across different yearly images, with the exception of identifying coral versus not coral objects. Results

were improved in their third iteration, training on 2 years of data and testing on a third, which they attribute to an adjusted random classification baseline level. A follow-up paper from Beijbom et al. [155] altered their algorithm with the aim of increasing accuracy while decreasing the model's runtime. They tested a semi- and fully automatic system, with the former allowing the algorithm to “flag” images that it finds too challenging to a human annotator and the latter running without human interaction. While promising, the need for human interaction to such a degree is impractical for the large scale datasets produced in coral reef monitoring. Their use of a semi-automatic model showed predictions were similar to those done entirely by a human annotator when 50% of annotations were done each by the system and a human annotator. Their fully automated system results highlighted the need for a greater input of training images.

A more recent use-case of automatic image annotation of coral reef imagery by Hopkinson et al. [156] attempted to map semantic labels to a 3D reconstruction of a coral reef. They began by building the 3D model, then determined the images associated with a particular triangle within the models mesh layer. For a subset of the mesh triangles, these images were presented to a human annotator to label with one of ten classes covering 10 benthic substrate groups, some at functional group level (i.e. algae) and others at genus/species level, to produce network training data. Their algorithm was then trained and used to predict the labels of all other images. They then applied three distinct classification methods to associate a label with each mesh triangle; (1) the class with the most predictions across all associated images was chosen, (2) the class with the greatest averaged probability was chosen, or (3) using a neural network designed to merge multiple views into one label. Their technique applied to 3D reconstructions well, but notably was unable to annotate vertical or overhanging reef areas due to their imaging technique. They did find that increasing the number of different viewpoints of the mesh triangles subsequently increased class prediction accuracy in most cases. However, the method is highly restricted, focusing on semantic labels for substrates associated to reefs within the study area only, and is not generically applicable to other reef systems.

## 2.5 Summary

While many coral reef habitat surveys include a complexity assessment of some sort [65, 66, 11], the range of metrics available have led to a large amount of research that is relatively incomparable. *In-situ* surveying is rarely repeatable as assessing the exact points of a specific location accurately underwater, even when removing the challenges of SCUBA-based research, is functionally impossible. The push to computational reconstruction and assessments is therefore key for accurate, reliable, and future-proof data sources [48, 47, 49]. The limitation of this assessment type is often in its execution, with the most common approach providing top-down views from a solitary camera that insufficiently captures the complex and shifting topography of marine reef substrates [50], and time requirements, where a single camera has to cover one portion of reef multiple times to capture it well enough for 3D reconstruction [48]. Increasing the number of cameras used and varying their viewpoints could provide a faster image capture technique, and is the focus of research question 1.

Throughout this section, the prevalence of coral reef research over that of other reef types is clear. This demonstrates a clear gap in knowledge of both the current state of structural complexity in other reef systems, as well as the appropriate assessment of it and potential factors affecting it. Research question 2 therefore focuses on assessing a non-coral reef environment and comparing its apparent structural complexity using a range of metrics.

The 3rd research question of this thesis focuses on automatically annotating coral reef benthos and was motivated by the need to link structural complexity to coral reef composition. The lack of research in this area is likely a reflection of the difficulty of annotating highly complex images such as those of coral substratum, but a push into this field is needed to further enhance coral reef research with computational analysis and allow for vast data sets to be utilised to their fullest potential.

# 3 | 3D models in coral reef monitoring

## 3.1 Introduction

The intricate morphology of scleractinian corals supports a wide range of ecological niches, creating a diverse and robust system [65]. As such, reefs dominated by complex coral types support a greater number of niches than their less complex counterparts [67]. Substrate complexity has a well-established relationship with ecosystem health and biodiversity. It is often monitored as a reflection of this [65, 67, 129]. The methods for these assessments, however, are often time consuming and limited in scale. Even with the advancement of 3D technologies and remote sensing, there are limits to the size of areas that can be assessed within pragmatic time scales (such as the duration of a SCUBA dive). The efficiency of surveying methods for projects with a limited budget that monitor marine systems repetitively should be a priority to support marine conservation.

The complexity of marine reefs is in decline [157]. Monitoring these systems can track this change, but often cannot trace the cause, so assessments should additionally measure defined substrate damage, tailored to either the ecosystem type (e.g., coral reefs, rocky reefs, sand banks, etc), the specific region of interest, or both. Any newly proposed method for substrate monitoring needs to not only be rapid and robust, but also as cost-effective as possible [48]. It also needs to include metrics that can relate to past data, or the monitoring risks becoming obsolete and may suffer from shifting baselines.

Though there are many computational processes available to monitor ecosystems, Structure-from-Motion (SfM) 3D modelling is become a popular approach [48, 56, 3, 17, 47, and others]. Building a 3D model from a set of images requires specialist software. There are many commercial and open-source tools for SfM models, all with varying user control

and settings. Agisoft Metashape (previously Agisoft Photoscan) is a popular choice in marine surveying for its relatively affordable pricing and simple interface [3, 17, 48, 120].

This chapter compared the use of single camera data capture to that of a custom multi-camera array when 3D modelling coral reef environments. A comparative assessment of build quality settings was performed on single-camera image data to clarify the use of specific settings when creating models, as often these are not explained or justified (see Section 2.2.3). The construction of a multi-camera array was then described. As this array relied upon overlapping camera views, the field of view of commonly used action cameras was tested *ex-situ* against the settings claimed by manufacturers. Finally, models generated of a coral reef by single and multi-camera approaches were used to find reef complexity, which was then compared to assess the accuracy of the multi-camera array.

## 3.2 Methodology

### 3.2.1 Reef model sites

The Wakatobi Marine National Park of Indonesia (WMNP) is located in South East Sulawesi, encompassing 4 main islands (Wangi, Kaledupa, Tomia, and Binongko) and several smaller ones within 1.4 million ha of sea. It is in the centre of the Coral Triangle, an area known to be a hotspot of marine biodiversity that is home to 627 species of hard coral (74% of all species) [158]. The area hosts several mangrove forests and seagrass beds - both essential habitats connecting to coral reef systems [1]. Its status as a national park and a hub of diversity has pushed the WMNP to a priority area for marine conservation.

Communities within the WMNP rely on reefs for food and income but, when combined with regional and global stress events and historically poor management practices, degradation has occurred throughout the park [159]. Blast fishing with dynamite is commonplace and can decimate the structure of the reef, negatively impacting reef complexity and biodiversity [9, 159]. Dive tourism is common and has potentially harmful impacts on coral reefs as divers can knock into the reef and may remove things from it [160].

Pulau Hoga, an small island north east of Kaledupa, is home to several reef sites on the island's fringing reef and is close to several others, including a highly degraded site (adjacent to the Sampela Bajo village) and a mangrove site (on Kaledupa island). Hoga reef encompasses a range of microhabitats with few direct stressors, although localised blast

fishing may have led to increased rubble load on the reef [161] and decreasing complexity.

A Pulau Hoga home reef site, Pak Kasims, is part of the island’s fringing reef. It begins 350 m off shore, with a shallow crest and flat (5 m) moving to a 40-70° slope, which descends to sand flats at 50 m (05°27.569S, 123°45.179E). It is considered a more pristine area than many others surrounding Pulau Hoga. Though in better condition, it has still been affected by fishing activities leading to an increased rubble load [161].

The Sampela reef site, a lagoon reef subject to overfishing, crests at 1-5 m and slopes to sand flats at 10-15 m interspersed with coral bommies along one side and sparse reef on the other (05°29.300S, 123°45.100E). It has shown such a loss in coral that it only had 10 % cover from 2014-2016 [162, 163]; this is likely higher than current coral cover if decline has followed its recent trends. The reef has been heavily impacted by fishing and high sedimentation. The decrease in herbivorous fish has lead to increased algae and sponge cover, with subsequent coral loss reflected in a low complexity region [164].

As the Sampela reef has more challenging environmental conditions that can impede data collection (i.e. increased sedimentation and benthos that moves in currents), there may be a site impact on model creation to be considered through the processing pipeline.

### 3.2.2 Single camera data capture

Four sites of six 4 m<sup>2</sup> quadrats, forming a 4 m by 6 m rectangle, were randomly placed along each reef’s slope for survey between depths of 5-16 m (Fig. 3.1). Metal pins were inserted into non-living substrate to semi-permanently mark areas for re-imaging as needed.

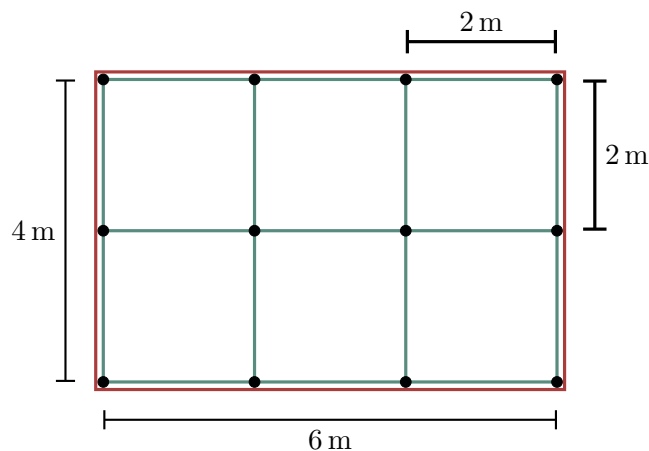


Figure 3.1: Positioning of quadrats at each reef site showing the placement of semi-permanent metal pins (black) that were used to mark quadrats. Six 2×2m quadrats (green) were placed within one 6×4m quadrat (red) per site. The 6×4m quadrat is offset for visualisation but shared the outer border of the 2×2m quadrats *in-situ*.

When collecting data, images can be taken directly or an area can be recorded with stills extracted at a later time. Both approaches have advantages to be considered. Photographs taken directly are generally of higher quality than extracted stills and contain useful metadata (e.g. focal length) [3]. Stills extracted from video, while of lesser quality and without some metadata, can avoid blurred or otherwise unusable images by extracting another frame to maximise the usable data for model generation [48]. Depending on the environment and equipment used, both have their place. Land-based surveys, those in clear water, or those that utilise high quality camera equipment are more able to capture images reliably enough for use, while lower quality equipment or less favourable conditions (e.g. turbid environments) are more likely to produce lower-quality images with blur, obscured areas, or backscatter that impedes model creation and benefit from the flexibility that video provides [59].

The images or stills all have an ideal overlap, where they feature the same section of reef over a portion of the image (most commonly 70-80% [53, 49, 125, 54, 127, 51]), to create an accurate reconstruction. To obtain this overlap, a swimming pattern is repeated - a straight line for transect lines or the “lawnmower” or “expanding circle” (Fig. 3.2) for quadrats [17, 48]. These methods require the camera to be consistently facing directly downward. The patterns are used to cover the entire quadrat with the optimal overlap between every adjacent image even, in the case of the lawnmower pattern, when the same area is imaged non-sequentially. Here, the lawnmower method was performed.

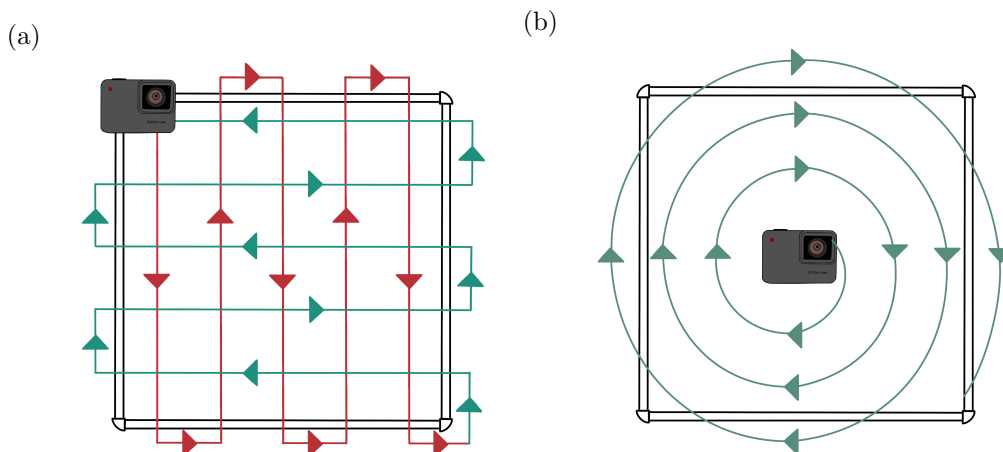


Figure 3.2: Substrate image capture using a single camera method with (a) the lawnmower pattern and (b) the expanding circle pattern.

Field of view (FoV) is often provided in a camera or lens’ instructions, and can be calculated with the distance above seabed to determine substrate area captured in each



image (Eq. 3.1). This can then be used to calculate image overlap - a camera with  $100^\circ$  horizontal and vertical FoV held 1.5 m above the seabed would capture a  $2.38 \times 2.38$  m area of substrate and would therefore need a 1.43-1.67 m overlap between adjacent images.

$$E = 2 \cdot \frac{D}{\tan(a)} \quad (3.1)$$

Where  $E$  is the captured distance of the substrate,  $D$  is the distance between the camera and substrate, and  $a$  is found through  $90 - \frac{FoV}{2}$  (Fig. 3.3).

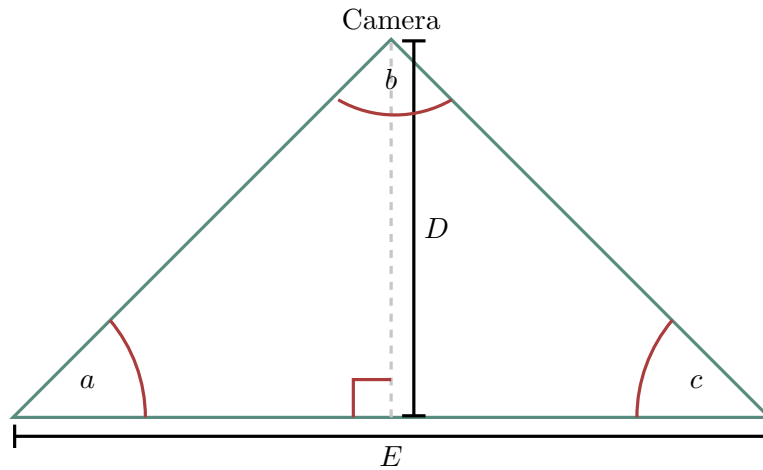


Figure 3.3: 2D representation of the captured area of a camera held a set distance above the seabed. Angle  $a = c$ , angle  $b$  represents the cameras field of view, length  $D$  is the distance between the camera and substrate, and length  $E$  is the captured distance of the substrate.

### 3.2.3 Single-camera 3D model build quality

Quadrats stills were extracted at 1-3 frames per second depending on the swimming speed during filming to provide an approximately even number of stills per model with a  $\sim 70\%$  overlap using a free video to image converter<sup>1</sup>.

A four-stage process is used to generate models. First images are aligned to determine the cameras' position and orientation and the moment of capture. This generates a sparse point cloud of the area using common points within adjacent images. Step 2 involves building a dense point cloud, where camera depth is taken into account for positioning, then step 3 builds a mesh from these points. The mesh is a connected polygon combining all points with those adjacent to them. Texture is added to the polygon mesh in step 4, which uses the polygon mesh and original images to project appropriate colouring

---

<sup>1</sup><https://www.dvdvideosoft.com/products/dvd/Free-Video-to-JPG-Converter.htm>

onto the model. Within this, a variety of settings are customisable to suit the model requirements and computing capabilities (Appendix I). Photo resolution scaling is the most easily adjustable setting, where faster processing speed is balanced with lower processing quality.

A combination of settings were tested across eight coral reef quadrats ( $2 \times 2$  m) in Agisoft Metashape to determine the impact of lower quality processing on model rendering and associated data to assess build quality. The top-left quadrat from each site at Pak Kasims and Sampela reef were used to cover a range of substrate compositions.

Each *align images* quality setting (“Lowest,” “Low,” “Medium,” “High,” and “Highest”) was tested to determine the most optimal choice for model rendering. The setting with best image alignment was taken forward to the *build dense cloud* testing.

Dense clouds were built at each quality setting (“Lowest,” “Low,” “Medium,” “High,” and “Ultra high”). The clouds were imported to CloudCompare<sup>2</sup> for a cloud-to-cloud distance comparison between adjacent settings per quadrat (i.e. “Lowest” compared to “Low,” then “Low” to “Medium”). The setting used was selected by comparing the mean dense cloud points and cloud-to-cloud distances with processing time for each setting.

At the *build mesh* stage, custom maximum face count values were used. The default “High,” “Medium,” and “Low” settings were calculated by Metashape based on each model’s dense cloud. A custom face count allowed specification of the number of polygons in the generated mesh, providing standardisation. Starting values were set at 3 million and 10 million, from Young et al. [48] and the Agisoft Metashape user manual (which states that any value above 10,000,000 “is likely to cause model visualisation problems in external software”) [165], respectively. A further face count was set at 6.5 million to provide a middle ground between these two settings, and the default medium value was also used to test its capabilities against custom numbers. Cloud-to-mesh distances were calculated in CloudCompare for each face count level against the models associated dense cloud.

### 3.2.4 Multi-camera arrays

A multi-camera method of data capture that uses 5, 10, or 20 cameras across a whole or half dodecahedron frame was then compared to the single-camera approach. The cameras

---

<sup>2</sup>CloudCompare version 2.12 for MacOS: <https://www.cloudcompare.org/>

were spaced evenly and positioned to face outward from the frame, not downward, to provide overlap and greater accuracy in construction of all angles of benthos, including those protruding sideways or overhanging.

To obtain the minimum overlap desired consistently, the cameras used must be set and positioned appropriately according to its FoV. For a 20 camera array, a  $360^\circ$  total FoV should be provided, with other setups covering the FoV required to capture the entire substrate of a system. The angle of overlap can be calculated by considering any 2 adjacent cameras on the array (Fig. 3.4). For the standard array, SJCam action cameras are used, set to  $170^\circ$  FoV, length  $F = 1$  m and  $G = 20$  cm. Using this and the equation for captured substrate area (Eq. 3.1), the angle for a 70% overlap,  $d$ , can be found.

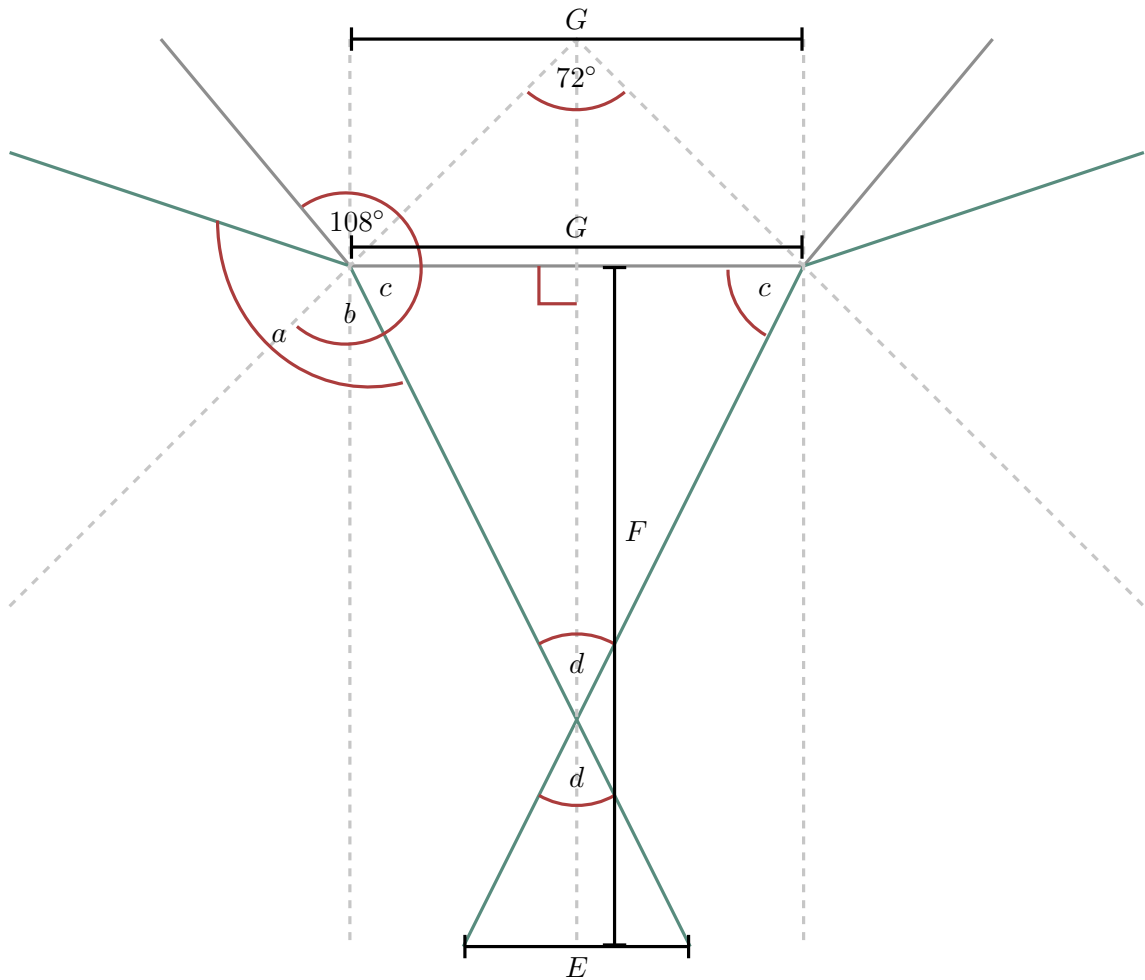


Figure 3.4: Angles associated with 2 cameras of a multi-camera array based on a regular dodecahedron frame with pentagonal faces (not to scale).

Assuming the  $170^\circ$  FoV (i.e.  $a = 170$ ):

$$c = \frac{360 - 108 - 170}{2} \quad (3.2)$$

Therefore  $c = 41$ , so:

$$d = 180 - 2(41) \quad (3.3)$$

The angle of overlap in this instance is  $98^\circ$ . From this, to calculate the captured seabed from these two cameras, the distance from the camera array frame can be calculated (Equation 3.4, assuming that  $G = 20$  as with the standard array, then the captured sea floor can be calculated with Equation 3.5, in this case assuming that  $F = 100$  i.e the array is held 1 m above the substrate).

$$\text{Distance to overlap} = \frac{10}{\tan(41)} \quad (3.4)$$

By splitting the area between the array and initial overlap into two right-angle triangles to find that Distance to overlap = 11.5 (to 1 d.p.), the distance from the initial point of overlap to the sea floor is  $100 - 11.5 = 88.5$  m. Therefore from Equation 3.1:

$$E = 2 \cdot \frac{88.5}{\tan(41)} = 203.6 \text{ cm, or } \sim 2 \text{ m} \quad (3.5)$$

The expanded FoV of the array therefore allows a simpler camera path. When compared to a lawnmower method, the array could cover a  $4 \times 6$  m area in two quick passes, whereas the single camera lawnmower method required six separate quadrats, each taking 6-8 passes and 3-5 minutes each.

### 3.2.5 Action camera field of view

The custom array used SJCam action cameras, but can use GoPros or a combination of both, so the field of view (FoV) of these cameras was tested at a range of distances from an imagined substrate. FoV on the SJCam can be set to  $70^\circ$  or  $170^\circ$  FoV, while the GoPro provides “medium” or “wide” without stating the angle.

Each camera was held 1, 2, 3, 4, 5, 7, and 10 metres from an imagined substrate (a wall) in portrait and landscape. A tape measure was moved until it could just be seen at the edges of the captured area from top to bottom, then left to right, to show distance captured and FoV was calculated for the 1 m and 2 m distances, as this is a common height at which to swim above substrate in surveying.

### 3.2.6 Single versus multi-camera complexity

To test the array’s capabilities, a comparison of extracted complexity took place with a single-camera technique [48]. First, the multi-camera array was used to model the Pak Kasims reef sites previously captured with the single-camera method. The array was swum over each 6×4 m quadrat (Fig. 3.1) in 2 passes as opposed to the lawnmower pattern (Fig. 3.2a) used in the single-camera imaging. Models were built to the same processing level, per Young et al. [48] (all settings default, medium quality, 3 million face count).

### 3.2.7 Data analysis

To assess the impact, if any, of quality setting and site (degraded or pristine) on each 3D model generation stage, Kruskal Wallis testing was performed due to the non-parametric nature of the data sets. Cloud-to-mesh data was normalised and a two-way ANOVA was used to assess any effect face count or site had on the measured distance. No testing was carried out for texture generation, and standard settings were used, as it is used for visual purposes only and does not alter the structure of the model.

Differences in complexity (rugosity, vector dispersion, and fractal dimension) between 3D models generated with a multi-camera array compared to a single camera approach were assessed by pair-wise t-tests.

## 3.3 Results

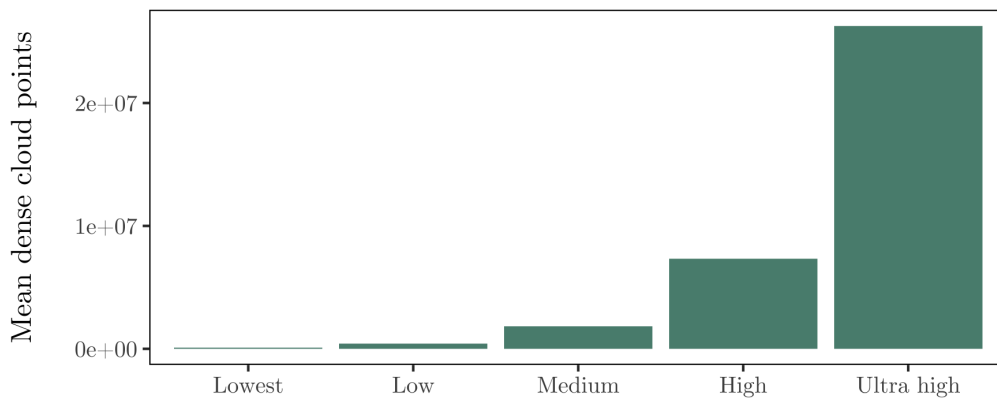
### 3.3.1 Build quality testing

When aligning images of coral reef quadrats (4 m<sup>2</sup>,  $n = 48$ ) in Metashape, reef site had no impact on the percentage alignment ( $p > 0.05$ ), but quality of alignment did ( $H_6 = 31.934$ ,  $p < 0.001$ ). Post-hoc testing showed that the “Lowest” quality setting significantly differed from all other settings ( $p < 0.005$ ), while no other settings differed. Despite this, the “Medium” setting was taken forward to the *Build dense cloud* testing as it showed 100% alignment in all quadrats, whereas “Low” quality alignment had some unaligned images in two cases, and the processing time difference between the two was negligible (within 5% for all models).

The total number of points created in the dense cloud did not vary by site ( $p > 0.05$ )

but did vary by quality setting ( $H_4 = 37.463$ ,  $p < 0.001$ ), with each setting increase showing a significantly greater number of points within the dense cloud (Fig. 3.5a). The cloud-to-cloud distance between adjacent qualities also did not vary by site, but did per quality comparison ( $H_3 = 16.401$ ,  $p < 0.001$ ). The smallest range was seen when comparing “High” and “Ultra high” quality dense clouds (range = 0.04), showing the smaller variance in dense cloud output between these quality levels (Fig. 3.5b). When considering the mean dense cloud points and cloud-to-cloud distance comparison with processing time, high quality dense clouds were used for the *Build mesh* stage.

(a)



(b)

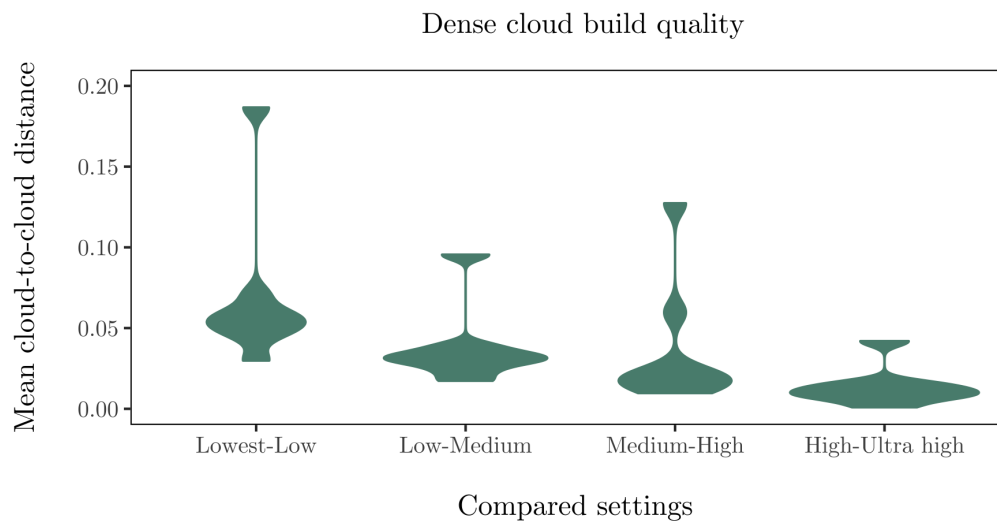


Figure 3.5: (a) Mean points generated and (b) mean cloud-to-cloud distance per dense cloud build quality across models rendered with medium image alignment quality.

When building model meshes, face count had no significant effect ( $p > 0.05$ ) on cloud-to-mesh distance, whereas the site did impact the distance between the mesh and dense cloud points ( $F_1 = 9.298$ ,  $p < 0.01$ , Fig. 3.6). Site and face count did not have any interaction effect on the cloud-to-mesh distance ( $p > 0.05$ ). Increasing the face count did not appear to change the processing time in any noticeable way. Considering only the

models tested here, the pre-set medium face count setting was used to generate the model texture.

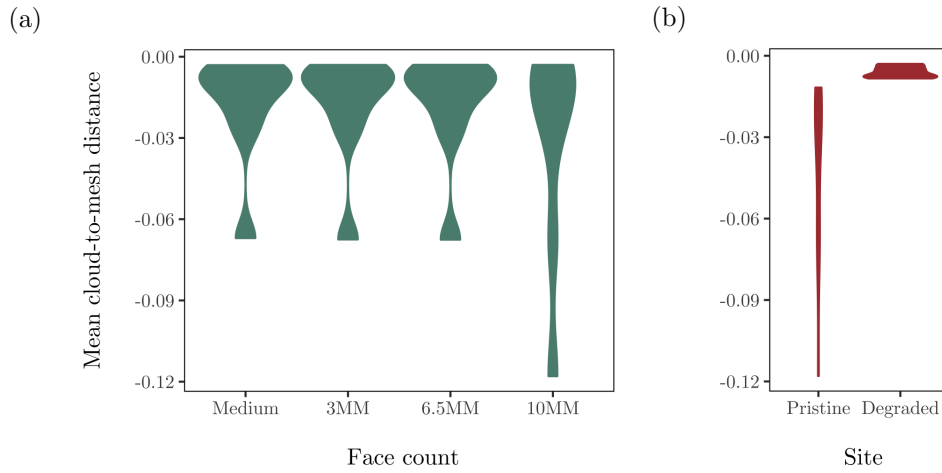


Figure 3.6: The mean cloud-to-mesh distance across a range of models rendered with medium image alignment quality and high dense cloud quality per (a) face count setting and (b) site.

Each stage of the model building process can be seen in Fig. 3.7.

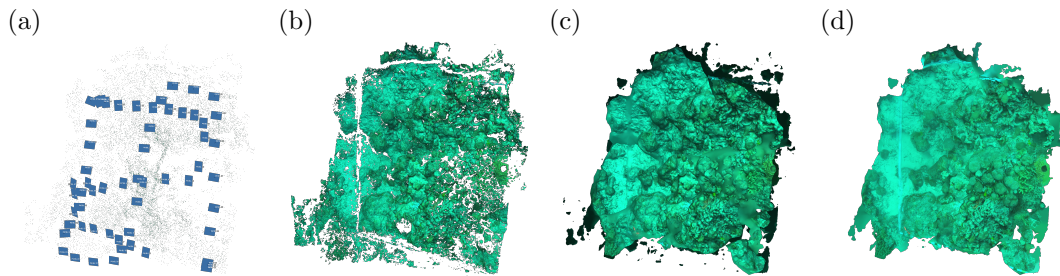


Figure 3.7: A section of coral reef modelled in Agisoft Metashape at different stages of processing showing (a) aligned photos (at medium quality), (b) the dense cloud (at high quality), (c) the mesh (at medium face count), and (d) the final model with texture.

### 3.3.2 Action camera field of view

Measured captured distance increased in a linear pattern when action cameras were held in portrait and landscape mode (Tables II.1 and II.2). For both camera brand at all FoVs, landscape orientations appeared to capture a wider area than portrait orientations, showing a data error. Using Equation 3.1 and Fig 3.3, FoV was found at 1 m and 2 m (Table 3.1). None of the FoV's found matched with those reported.

Table 3.1: Field of view (FOV) calculated per action camera at all FoV settings, at 1 m and 2 m, where the camera is positioned to capture landscape and portrait images.

Camera & FOV setting	FOV at 1 m (°)		FOV at 2 m (°)	
	Portrait	Landscape	Portrait	Landscape
SJCam - 70°	21.5	33.5	22.0	31.2
SJCam - 170°	41.7	58.9	39.6	51.7
GoPro - Medium	33.4	47.8	35.3	52.0
GoPro - Wide	48.6	60.7	47.8	61.6

### 3.3.3 Single versus multi-camera complexity

There was a significant difference between the complexity extracted from 3D models created from single-camera and multi-camera approaches in terms of rugosity ( $t_{143} = -2.6628$ ,  $p < 0.01$ ) and vector dispersion ( $t_{1535} = 13.935$ ,  $p < 0.001$ ), but no difference when considering fractal dimension at any scale ( $p > 0.05$ ) (Fig. 3.8). Several attempts were made to extract rugosity and vector dispersion values from models with adjusted positioning of the associated helper files for each metric, but placement was never at the exact same point due to the differences between models in scale.

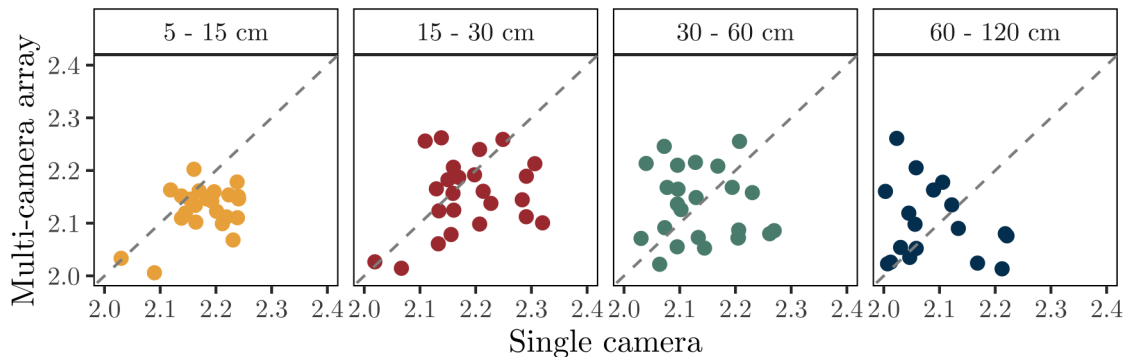


Figure 3.8: Fractal dimension at 4 size scales of coral reef models generated by a single or multi-camera method.

## 3.4 Discussion

### 3.4.1 3D model build quality

The varied and highly detailed composition of coral reefs provides a challenging task for 3D modelling software. The number of images provided for model creation was varied due to the nature of still extraction. Differences in video length can occur due to changes



in swimming speed, current, or conditions (e.g. increased sedimentation, changing substratum height, etc.). This could have been countered and precise frame extraction could provide the same number of images per quadrat, but this would not reflect the “real-world” use of the data capture technique [48]. As there was no impact of site on image alignment when creating models, it is unlikely that there was an impact from the number of stills provided.

When aligning photos in Metashape, only the “Lowest” quality setting showed a difference in overall alignment. This may show the power of the software when performing this process, or the increasing quality of modern camera equipment, but could change on larger modelled areas with many more images and more varied substrate. Further testing would be needed on large scale areas to assess this further.

As with aligning photos, when building the dense clouds no setting was impacted by site but quality provided an increasing number of points per cloud, as could be expected. With each improved quality setting, a non-linear increase in dense cloud points was found. This was reflected by a greater concentration of points in the higher quality clouds (shown by shorter cloud-to-cloud distances as quality increased). Selection of dense cloud is likely a balance between the desired use of the model output, processing power, and available time. Where a model is required very quickly, many must be created, or where they are only used for visual demonstration and not measurement, would be well-suited to lower quality dense clouds. Where data is to be extracted, higher quality settings may be required.

Site-related effects were seen when building meshes, with the Sampela quadrats showing far smaller cloud-to-mesh distances than the Pak Kasims quadrats. Further tests could be performed to further define the cause of this difference, generating models of the same sites using a range of cameras, image counts, image overlaps, and prior build quality settings. This would demonstrate whether the cloud-to-mesh distance was truly impacted by the site itself, or if image and model quality were more important than currently seen. Contrastingly, changing the face count when building meshes did not impact cloud-to-mesh distance significantly. This may be due to the relatively small scale models rather than a lack of required processing power, though more testing with image sets or varying scales would be required to determine any size-related effect.

### 3.4.2 Action camera field of view

Field of view testing showed a variation in angles at different distances, likely highlighting a flaw in data collection rather than a changing FOV within the cameras. Averages could be taken, but the variation in some measurements suggests that these may not represent the FOV accurately (a  $30.4^\circ$  discrepancy is seen with the wide angle GoPro in the landscape orientation). Nevertheless, the smallest angle between the 1-2 m range would provide the minimum overlap position needed for each camera when held at the standard distance for this type of substrate survey.

*In-situ* testing of FoV would be beneficial when testing image collection methods and related equipment. The water-related distortion of images may reduce the captured substrate area. Wide-angle views may be more susceptible to this type of distortion, particularly as they already tend to feature a “fish-eye” effect that may impact the edge of images [48]. Any array built should either be tailored to the specific camera used to ensure adequate image overlap, or be based on the minimum likely field of view to ensure that all images are identical to at least 60% of their adjacent images.

### 3.4.3 Single versus multi-camera complexity

When comparing the substrate complexity of models created by single and multi-camera methods, both rugosity and vector dispersion differed. The helper files used to extract these metrics [48] intersect with the model mesh at a specific point and replication on the same model would require the precise location to be found again, or would produce a different result. Extracting complexity from a different model, though the model was of the same site, is therefore extremely challenging and finding the same point is unlikely.

Fractal dimension did not face the same issue, likely as it used the whole quadrat to create a single value, instead of averaging values from individual regions of the quadrat. This removes the need for such precision and benefits replication, as demonstrated by the lack of difference found in fractal dimension at any scale.

## 3.5 Summary

Using multiple cameras to capture an area of substrate requires more preparation and equipment than a single camera approach, but saves on time and increases the area imaged

per dive/survey [122, 123]. Monitoring of larger areas of reef would likely benefit from a method using 5 or more cameras (with the number determined by the sites topographical characteristics) to increase the efficiency and scope of data collection.

Comparing *in-situ* models' extracted complexity from single versus multi-camera capture methods showed a difference in values of rugosity and vector dispersion, which is unsurprising when considering the placement of associated helper files is nearly impossible to match perfectly and subsequent data would reflect different portions of the model due to the nature of the metric calculations [48]. The similarity in fractal dimension, which relies upon the entire area rather than set points, is expected when models are reflective of the environment captured and show the power of the multi-camera array in accurately capturing and reconstructing marine substrates.

The shortened imaging path, faster surveying time, and replicated fractal dimension values demonstrated proof-of-concept for the multi-camera array. Following this, the subsequent chapter details the testing of this array in distinct rocky reef environment with different structures to those of a coral reef.

# 4 | Assessing structural damage on a chalk reef system

## 4.1 Introduction

Chalk benthic habitats form rocky reefs in temperate waters and are relatively rare. They are formed through deposition from calcareous ooze and calcite shells that build up into stretches of chalk reef with different characteristics [166]. The complex structures formed by the erosion of chalk result in varied habitats that allow a wide range of organisms to thrive. They provide spawning, grazing, and hunting grounds, refuge from predation, and a range of environmental conditions that suit species' occupying different ecological niches. The complexity of chalk is created by the layering of deposits over millennia [167] and so any damage done, either naturally or anthropologically, is permanent and prolonged destruction of the system could lead to a dramatic ecological change [168].

Shellfish fisheries are the second largest in the UK and traditional potting is a common approach. Potting most often involves shanks, consisting of pots (or creels, or traps), rope, and anchors (Fig. 4.1) deployed in lines. Pots are known to cause damage from their contact with the seabed, through abrasions caused by water movement, and when they are set and removed [169]. The use of single pots as opposed to a shank has been tested experimentally; single pots' heavier weight had a more damaging impact when being deployed and in water, but a lesser impact when being hauled in as pots were not dragged along the seabed [170]. Pots are known to cause damage from their contact with the seabed, through abrasions caused by water movement, and when they are set and removed [169].

Though potting is a long-used fishing technique, there is little-to-no research into the structural damage caused by it. Research into potting damage often finds no evidence of

significant harm caused directly. Often, however, these studies are limited in scope either due to their lack of temporal or spatial comparisons, or a lack of ecologically contextualising data.

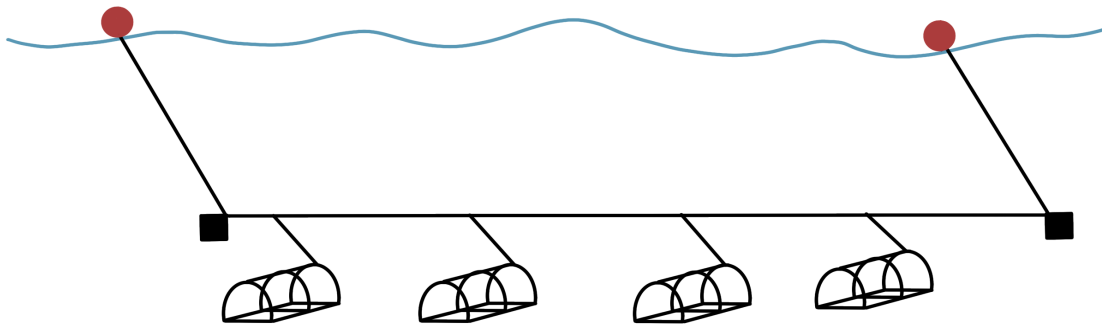


Figure 4.1: A typical potting shank used in crustacean fisheries, with anchors and surface marker buoys at each end and rope tethers attaching each pot to the main shank line. A typical shank used in the Cromer fishery is  $\sim 200$  m in length with 10 pots attached.

This chapter details a preliminary survey into the impacts of crustacean potting undertaken in collaboration with Natural England (NE; an advisory body to the government aiming to protect and manage the environment) to provide statutory advice to the Eastern Inshore Fisheries and Conservation Agency (EIFCA; a government agency aiming to manage inshore fisheries and their associated environments) on their management of the Cromer Shoal Chalk Bed MCZ. The assessment aimed to provide this advice by determining whether adult and juvenile crustaceans are more prevalent in more structurally complex chalk reef areas and if more complex chalk features show a greater incidence or severity of human impact. Surveying also provided the opportunity to test the capabilities of the multi-camera array described in Chapter 3 in a challenging non-coral environment to assess the connection between structural complexity and species' abundance.

## 4.2 Methodology

### 4.2.1 Study sites

The Cromer Shoal Chalk Bed was designated as an MCZ in January 2016 (Fig. 4.2). This classifies it as a site of “nationally important, rare or threatened habitat,” with the objective of maintaining the system of specified features [171]. The MCZ stretches from Weybourne south-eastward to Happisburgh in Norfolk, UK. It begins 200m offshore (of Mean Low Water) and extends for 5-10 km seaward, to a total of  $320.5 \text{ km}^2$  [172].

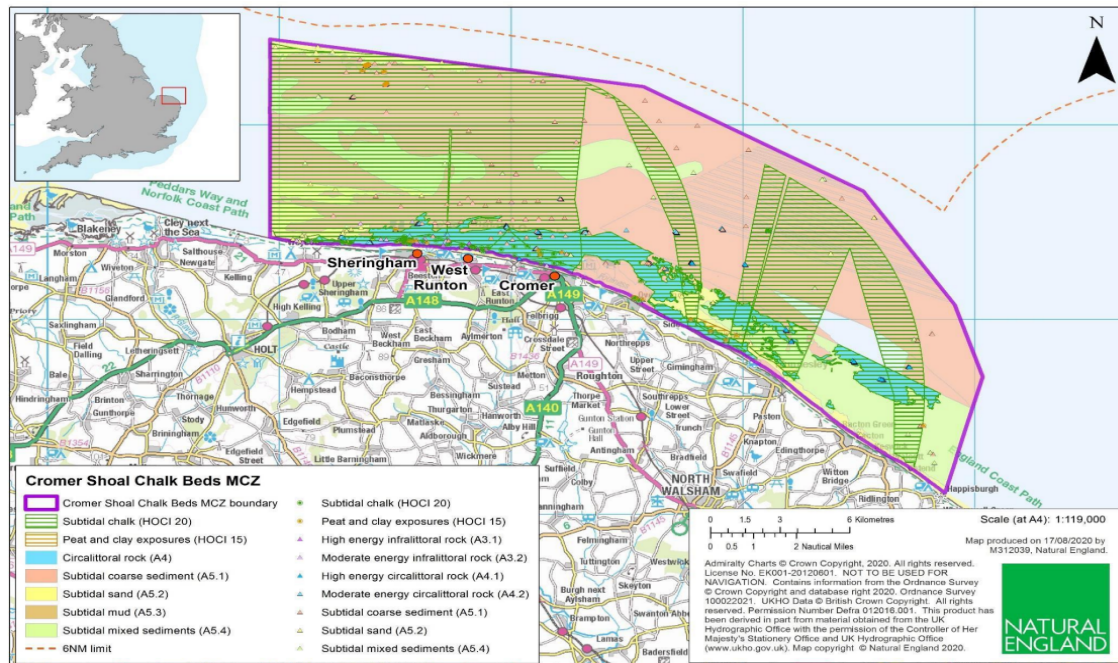


Figure 4.2: Cromer Shoal Chalk Bed Marine Conservation Zone (MCZ) map with annotated designated features [172].

The EIFCA are responsible for the fisheries management of the Cromer Shoal Chalk Bed MCZ. They are required to assess it and, where possible, support the conservation of the area. The crustacean fishery on the chalk reef follows the minimum landing sizes of the EIFCA region: 115 mm carapace width for *Cancer pagurus* and 87 mm carapace length for *Hommarus gammarus* [173]. This is smaller than other UK regions [172].

Despite being fished with fewer boats, advancements in fishing gear have allowed each boat to have a larger region of operation, and landings from crab and lobster from this region provide over £1.75 million to local business and fishers [29]. The smaller boats of local fishers, generally  $\leq 10$  m in length, stay closer inshore (within 2 nautical miles) over the larger areas of chalk reef. This, particularly as a potting fishery, puts the fishing gear over a delicate system that is particularly susceptible to damage [174]. The shanks used by North Norfolk fishers are known to be stored at sea when not in use. These pots are thought to be stored on flatter ground past the reef itself (EIFCA, personal communication, 2019), but stored and lost post have been seen damaging areas of complex chalk on the reef [175].

Four actively set shanks were used as transect lines to survey across the accessible regions of the The Cromer Shoal Chalk Bed MCZ chalk reef; two at West Sheringham

(WS1 and WS2), one at West Runton (WR), and one at East Runton (ER)<sup>1</sup>. Each transect was approximately 200 m and had 10 pots each (up to five of which were used as surveying sites (4 m<sup>2</sup> quadrats) per dive). The sites had unique features that presented different areas of interest:

- WS1    A flat area of flint, sand, gravel and chalk cobbles with no areas of exposed chalk bed.
- WS2    A region of reef predominantly covered in a thin algae layer with 2 m high ridges and gullies between 5 - 10 m wide composed of flat chalk and sand. There were minimal regions of cobbles.
- WR    A similar area to WS2 with smaller ridges of approx. 1 m high and less well defined gullies of sand, chalk, and cobbles.
- ER    An area of small ridges approx. 0.5 m high with ill-defined chalk, rubble, cobble, and sand regions.

No control site existed as no area of the chalk reef is free from pot fishing.

#### 4.2.2 Chalk reef imaging

The *in-situ* data collection was carried out by a team of six divers - four in water and two standby divers on the surface. The in water divers were then split into two teams; the imaging team gathered topographical and damage data, and the biological team collected abundance and habitat assessment data.

Each imaging team diver used a five-camera array to gather modelling data with an additional camera recording perpendicular to the seabed for damage analysis. Five SJCAM action cameras were attached to a plastic frame facing outwards at an oblique angle and an additional GoPro camera was set facing directly down (Fig. 4.3). All were set to video mode and still frames were extracted in post-processing. Although image capture provides higher quality data for 3D reconstruction, the extraction of lower quality stills from video footage was more beneficial due to the logistical difficulty of surveying the reef.

Recording began at the start of a transect. Each diver held a multi-camera array and swam along one side of the transect (~2 m apart with the shank between them) at ~1 m above the substrate. Each array was held in the same position and direction throughout the survey and divers swam at a consistent pace when moving. After each pot was encountered, one of the team swam ahead (a random number of fin kicks approximately 5-10 m from

---

<sup>1</sup>GPS locations of the study sites have not been released as per agreement with the fishing industry.

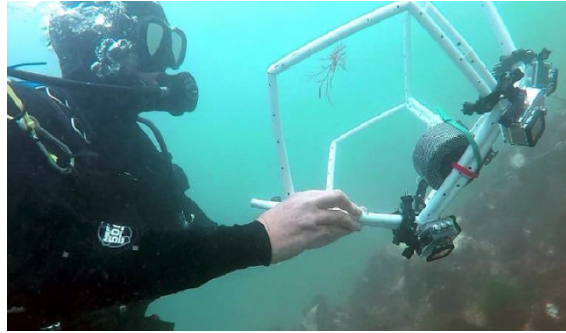


Figure 4.3: The camera array used for surveying the Cromer Shoal Chalk Bed MCZ.

the pot) to place an A4 control marker under the shank before returning and continuing with the video survey (Fig. 4.4). The team continued to the end of the transect or until the maximum dive time was reached.

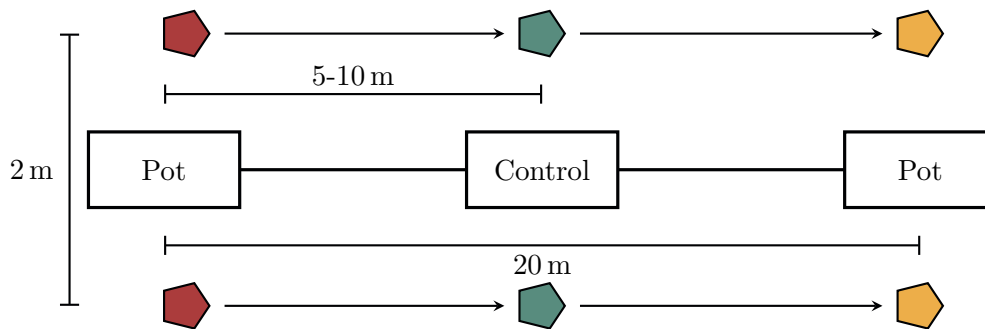


Figure 4.4: Transect surveying layout between 2 pots on a shank line with a control marker between them, showing the camera array (pentagon) and the location of the first (red), second (green), and third (yellow) point of image collection for 3D model generation.

### 4.2.3 Substrate damage assessment

The video footage from the sixth camera added to each array was reviewed by three annotators, each working independently to identify and categorise damaged chalk across each transect area as well as the timecode of each incidence. The start and end of each transect were also noted, as well as any pot or control markers in the footage. The data was then consolidated first by timecodes (recordings within 4 seconds of each other were considered the same instance), then by category (where 2+ annotators agreed on damage type the instance was automatically included, where damage was not agreed it was reviewed before determining to include or discard). Annotator 1 had experience at the sites and developed the assessment, annotator 2 had experience in annotation of video footage of marine environments and annotator 3 was an intern with Natural England with no prior experience at the time of the surveys.



To carry out a damage survey on the site a categorisation system was developed using evidence collected from the biological team action camera footage, anecdotal evidence from both dive teams, and evidence from consultants. 11 distinct damage categories were identified, described in appearance and severity, and probable causes were determined (Table 4.1). Damage type was assessed visually and severity was classed by the degree of disturbance to the chalk. Epiflora was removed in all cases.

Low	Only surface chalk was removed.
Medium	Chalk structure was broken but not removed.
High	Chalk structure was broken and removed/detached.

#### 4.2.4 Crustacean assessment












The biological assessment began with a visual habitat characterisation survey as standard for Natural England surveys. This included a site description and noted physical characteristics of the reef and the community upon it. The team then followed the transect after the imaging divers, with one diver on each side of the rope. When they encountered a pot or control marker, they recorded a count of all commercial crustaceans (*C. pagurus* and *H. gammarus*) as well as their age (juvenile or adult, determined by catch limit sizes) within a 4 m<sup>2</sup> quadrat directly ahead of the pot/marker. Control markers were removed as they were passed. Information on each pot encountered was noted, including size.

#### 4.2.5 Data analysis

3D models were built for pots and control markers along the first 100 m of each transect (WS1  $n = 6$ ; WS2, WR, and ER  $n = 10$ ). Stills were extracted from videos at 1 frame per second and were colour corrected. Models were built in Agisoft Metashape using medium settings for image alignment and dense cloud construction. They were then imported into Rhinoceros (version 7) to extract complexity metrics per Young et al. [48], using either the pot length (90 cm) or control marker (A4) for scale (Tables III.2, III.3).

Comparisons of complexity at the four sites aimed to identify high level characteristics of the sites before investigating species abundance and human damage. Each models' ( $n = 34$ ) rugosity ( $R$ ) and vector dispersion ( $\frac{1}{k}$ ) was considered as a mean value ( $n_R = 6$ ,  $n_{\frac{1}{k}} = 64$ ), while fractal dimension produced one value per size scale.

Table 4.1: Damage categories observed on the chalk bed, with most likely causes and severity indicated. Low severity was classed as damage that only removed the surface chalk layer, medium severity caused broken chalk structure without removal of chalk, and high severity caused broken and removed chalk. Natural causes are shown in italics.

Damage	Description	Diagram	Likely causes	Severity
Lift (LIF)	Shattered chalk at edges with one edge lifted out.		Pot, Anchor	High
Grating (GRA)	Rubbed epifauna and chalk of non-horizontal areas creating uneven grooves and chalk debris below the site.		Pot, Anchor, <i>Scour</i>	High
Angular Rubble (RUB)	Angular chalk cobbles that indicate disturbance but with no clear cause.		Pot, Anchor, <i>Water movement</i>	High
Saw (SAW)	Broken angular rubble in a line as a result of continued vertical burns.		Rope	High
Cut (CUT)	Single line of horizontal indentation of approximate equal width.		Rope	High
Level Shear (LSH)	Horizontal and flat area of exposed chalk as a result of a complete cut.		Rope	High
Unlevel Shear (USH)	Flat (but not horizontal or level) area of exposed chalk from an incomplete cut or a large amount of chalk disturbance in one impact.		Pot, Anchor, Rope, <i>Water movement</i>	High
Strike (STR)	A vertical strike with a visible impact site and shattered chalk in edged pieces.		Pot, Anchor	Medium
Drag (DRA)	Single lines of chalk indentations of unequal width.		Pot, Anchor	Low
Abrasion (ABR)	Rubbed epifauna and chalk forming a flattened horizontal plane.		Pot, Anchor, Rope, <i>Scour</i>	Low
Burn (BUR)	Single line of vertical indentation of approximate equal width.		Rope	Low

Damage annotation agreement was initially assessed using Fleiss' kappa,  $\kappa_f$ , followed by the removal of annotator 3 and the use of Cohen's kappa,  $\kappa_c$ . Annotator 3's responses were removed to highlight the value of experience in video annotation in marine environments when performing this type of surveying method. Agreement to disagreement moves linearly from +1 to -1.  $\kappa < \pm 0.4$  is considered poor,  $\pm 0.7 < \kappa \leq \pm 0.4$  is considered fair to good, and  $\pm 0.7 \leq \kappa$  is considered strong.

Sliding windows of damage were used to investigate any association between chalk reef damage and complexity (Fig. 4.5). A pot or control marker's damage window began and ended at the pot or marker either side of it, i.e. pot 3's window was from control 2 to control 3, to form an approximately 20 m by 2 m quadrat. WS1 was removed from damage analysis as there were no incidences observed and it was not on the chalk reef. Low incidence of damage in several categories limits statistical analysis of this variable.

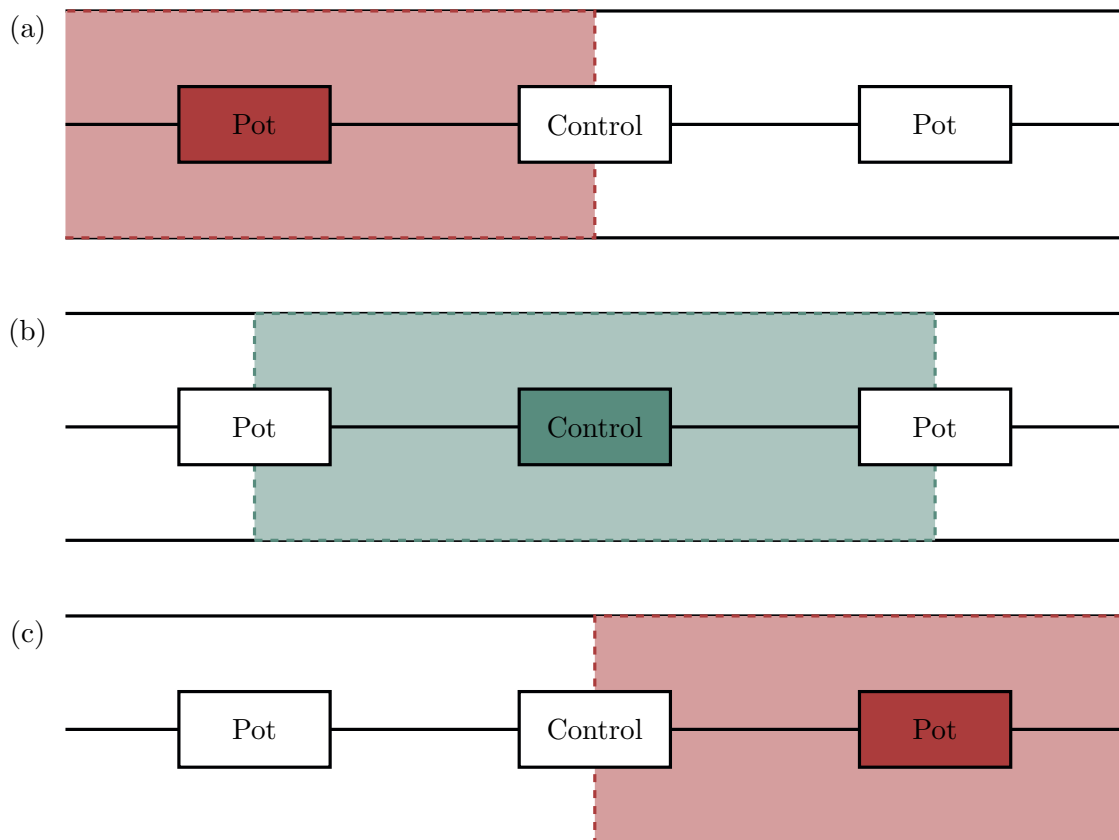


Figure 4.5: Sliding windows of damage showing the transect region where (a) damage annotations would be associated with a pot, (b) the following damage window associated with a control marker, and (c) a third damage window associated with another pot.

Abundance data were combined into catch and non-catch crabs, determined by local minimum catch size, and lobster counts were excluded due to their low occurrence (Table

III.1). All ER quadrats and two WS1 quadrats were excluded from analysis as no counts were carried out due to diving restrictions.

Statistical analyses of the variations between sites, abundances and complexity were performed using t-tests (paired and unpaired) and one-way ANOVAs. Pearson correlation coefficients were used to test correlations between variables.

## 4.3 Results

### 4.3.1 Complexity metric variation between chalk reef sites

There was a significant difference in rugosity ( $n = 216$ ) between the sites ( $F_{3,212} = 6.425$ ,  $p < 0.0005$ ), with WS1 being less rugose than all other sites ( $p < 0.0001$ ). WS2, WR and ER showed no difference in rugosity ( $p > 0.05$ ).

Vector dispersion ( $n = 2304$ ) also differed between sites ( $F_{3,2300} = 12$ ,  $p < 0.0001$ ). There was no difference between WS1 and WS2 ( $p > 0.05$ ), nor between WR and ER ( $p > 0.05$ ). There was, however, a difference when considering WS1 and both Runton sites (WR and ER) ( $p < 0.0005$ ,  $p < 0.0001$ ), and WS2 and both Runton sites ( $p < 0.001$ ,  $p < 0.0005$ ). In both cases the Runton sites showed higher vector dispersion than the Sheringham sites.

Fractal dimension ( $n = 36$ ) showed differences across the sites at the scales  $D_{60-30}$  ( $F_{3,32} = 2.944$ ,  $p < 0.05$ ),  $D_{30-15}$  ( $F_{3,32} = 4.775$ ,  $p < 0.01$ ), and  $D_{15-5}$  ( $F_{3,32} = 12$ ,  $p < 0.05$ ), but not at  $D_{5-1}$  ( $p > 0.05$ ). A post-hoc Tukey test showed no significant differences between sites at  $D_{60-30}$ , however.  $D_{30-15}$  differed between WS1 and WR ( $p < 0.01$ ), as did  $D_{15-5}$  ( $p < 0.05$ ).

Complexity at pot and control sites ( $n = 36$ ) differed in terms of rugosity ( $t = 2.2458$ ,  $p < 0.05$ ) and vector dispersion ( $t = 4.7274$ ,  $p < 0.0001$ ), with pot complexity being higher in both cases. There was no difference in complexity between the two in fractal dimension of any scale.

### 4.3.2 Damage annotator agreement

Analysis of annotator decisions using Fleiss' kappa,  $\kappa_f$ , showed significant but poor agreement between all three annotators for when damage occurred ( $\kappa_f = -0.226$ ,  $p < 0.001$ ) and the category of damage ( $\kappa_f = 0.203$ ,  $p < 0.001$ ). Weak disagreement was

found when detecting incidence of damage in all cases. For all other agreement where  $\kappa_f$  was significant, the strength of agreement was increased with two annotators instead of three. Categories with fewer instances of damage generally had lower agreement or non-significant agreement, whereas abrasion damage, that which had the cumulatively greatest incidence, had significantly strong agreement in all cases with two annotators, approaching  $\kappa_f = 1$  at WR and ER.

Removing annotator three (who had no experience in marine annotation) then found 47.76% initial agreement of damage incidence across all sites, with 65.13% agreement at WS2, 46.88% agreement at WR and 28.24% agreement at ER. Using Cohen's kappa,  $\kappa_c$ , could then be used to reassess agreement with only 2 experienced annotators (Fig. 4.6).

$\kappa_c$  no significant agreement was seen with regards to damage incidence when considering all sites and when looking at WR ( $p > 0.05$ ). At WS2, a significant, though poor, agreement was seen ( $\kappa_c = 0.229$ ,  $p < 0.001$ ) and there was fair disagreement when looking at ER ( $\kappa_c = 0.473$ ,  $p < 0.001$ ). Where an incident of damage was agreed upon,  $\kappa_c$  was used assess agreement of damage category. When considering all damage types collectively, there was fair to good agreement at all sites ( $\kappa_c = 0.481$ ,  $p < 0.001$ ) combined and individually (WS2  $\kappa_c = 0.426$ ,  $p < 0.001$ ; WR  $\kappa_c = 0.549$ ,  $p < 0.05$ ; ER  $\kappa_c = 0.505$ ,  $p < 0.01$ ).

Drag damage showed strong agreement at all site combined and at WS2 ( $\kappa_c = 0.658$ ,  $p < 0.001$  and  $\kappa_c = 0.655$ ,  $p < 0.001$  respectively). Abrasions were strongly agreed upon at WR and ER ( $\kappa_c = 1.000$ ,  $p < 0.01$  in both instances) and fairly agreed upon at WS2 and when considering all sites ( $\kappa_c = 0.426$ ,  $p < 0.001$  and  $\kappa_c = 0.481$ ,  $p < 0.001$  respectively). Grating showed fair agreement at WS2 ( $\kappa_c = 0.481$ ,  $p < 0.005$ ) and significant but poor agreement at all sites combined ( $\kappa_c = 0.353$ ,  $p < 0.01$ ), and showed no significant agreement at WR and ER ( $p > 0.05$ ). Angular rubble was recorded with very strong agreement across all sites combined ( $\kappa_c = 0.815$ ,  $p < 0.001$ ) and at ER ( $\kappa_c = 1.000$ ,  $p < 0.01$ ), with good agreement at WS2 ( $\kappa_c = 0.642$ ,  $p < 0.001$ ). Level shears were significantly but poorly agreed upon at all sites ( $\kappa_c = 0.299$ ,  $p < 0.05$ ) and at WS2 ( $\kappa_c = 0.323$ ,  $p < 0.05$ ), but showed no significant agreement at WR ( $p > 0.05$ ). Unlevel shears were agreed upon fairly well at all sites ( $\kappa_c = 0.467$ ,  $p < 0.001$ ) and at WS2 ( $\kappa_c = 0.549$ ,  $p < 0.001$ ) but were not significantly agreed upon at WR or ER ( $p > 0.05$ ).

Other damage could not be tested using  $\kappa_c$  as only independently noted instances were

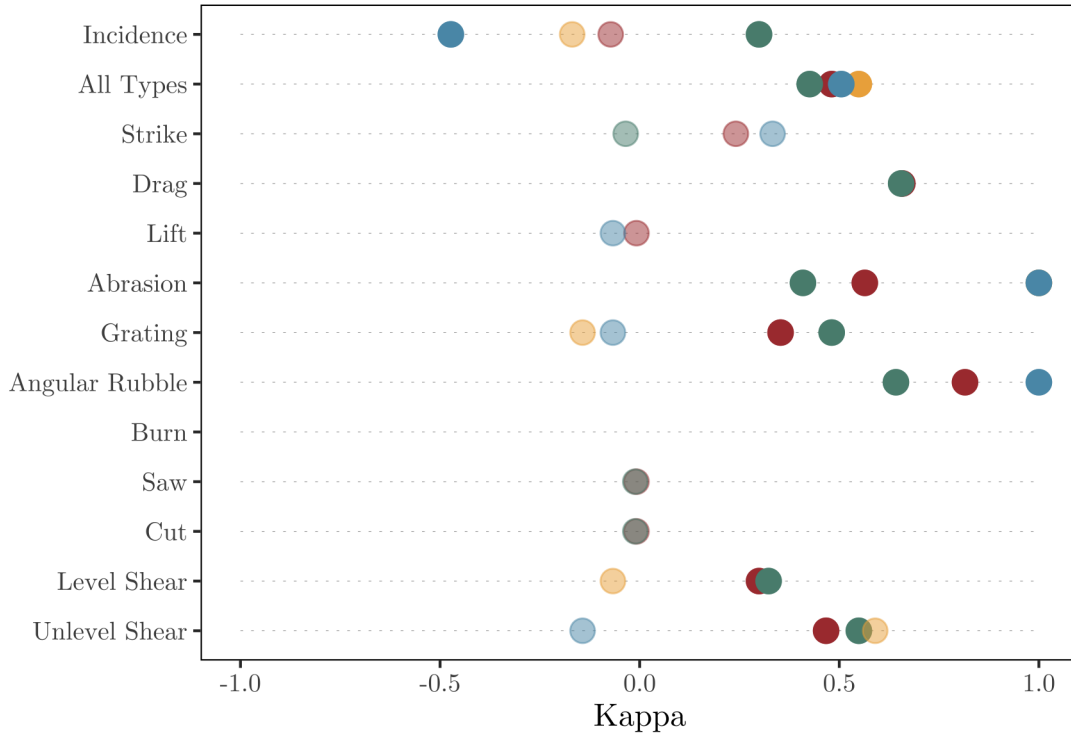


Figure 4.6: Cohens' Kappa ( $\kappa$ ) between two experienced annotators in damage annotation at all sites (red), WS2 (green), WR (yellow), and ER (blue). Significant agreement ( $p < 0.05$ ) is shown as solid colour with non-significant agreement as transparent. Agreement to disagreement moves linearly from +1 to -1.  $\kappa < \pm 0.4$  is considered poor,  $\pm 0.7 < \kappa \leq \pm 0.4$  is considered fair to good, and  $\pm 0.7 \leq \kappa$  is considered strong.

included. Any recording of these categories occurred after consolidating annotations.

### 4.3.3 Complexity and observed human impacts

WS1 was excluded from damage analysis as it was not a chalk reef site. WS2 had 83 instances of damage, WR had 37 and ER had 72 across each category (Table 4.2).

Of this damage, 65 incidents across all sites could be directly attributed to human impacts, either because the damage only had human causes or the damage cause itself was present at the time of the survey (i.e. a pot was observed to be causing an impact).

Grouping damage by severity ( $n = 65$ ) showed variation in damage per site ( $\chi^2_4 = 16.2131$ ,  $p < 0.05$ ), with more instances of high and low severity damage seen at WS2, and more medium severity damage seen at ER (Fig. 4.7). When focusing on potting impacts specifically ( $n = 65$ ), pots and anchors caused more low and medium severity damage and ropes cause the most high severity damage ( $\chi^2_2 = 13.9719$ ,  $p < 0.05$ ) (Fig. 4.7).

No correlations were found between damage observed in sliding damage windows (Fig. 4.5) and the complexity metrics from the associated pot or control quadrat ( $p > 0.05$ ).

Table 4.2: Damage to the Cromer Shoal Chalk Bed per type at the sampled sites.

Damage type	WS2	WR	ER
All	83	37	72
Lift	0	0	2
Grating	3	3	4
Angular Rubble	5	3	26
Saw	1	0	1
Cut	1	0	1
Level Shear	7	1	1
Unlevel Shear	11	6	13
Strike	2	3	12
Drag	1	0	0
Abrasion	49	20	12
Burn	2	1	0

#### 4.3.4 Complexity and species abundance

No difference was found in any complexity metric and species abundance overall ( $n = 28$ ), as adults, or as juveniles at pot or control sites ( $p > 0.05$ ). Species abundance did not correlate with complexity in most cases, except for with adult crabs in terms of rugosity,  $D_{60-30}$ , and  $D_{30-15}$  (Table 4.3).

All biological data is archived in Appendix V of the report published with Natural England from this survey [172]. *C. pagurus* and *H. gammarus* abundance is additionally detailed in Appendix III.

## 4.4 Discussion

### 4.4.1 Human-attributed impact to the chalk bed

The damage assessment here shows that permanent damage is occurring to the chalk bed as a result of human activity and crab and lobster potting. The ecological significance of this damage is as yet unknown and should be the focus of further studies in the MCZ. Previous reports have highlighted that the soft nature of chalk leaves it vulnerable to abrasion pressures generated by static fishing techniques [176, 177]. Hartnoll [176] acknowledged the potential for repeated incidents of damage from the same rope, pot, or anchor.

The visually raised features of the West Sheringham site seemed to attract the most

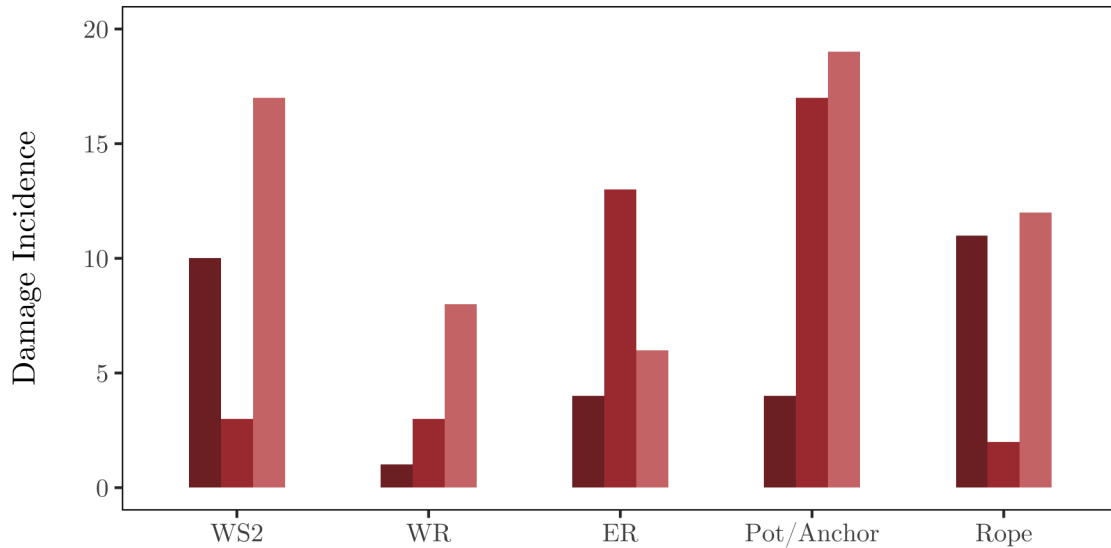


Figure 4.7: Incidence of high severity (dark red), medium severity (red), and low severity (pink) damage at Cromer Shoal Chalk Bed sites and caused by pots and anchors or ropes.

level shears, suggesting that the ropes of a shank were pulled taught across raised chalk when pots settled, shearing off these features. At WS2, divers noted that pot tethers ( $\sim 2$  m) were not of adequate length to allow the pot to rest on the chalk bed, and instead pots were left hanging over the chalk (Fig. 4.8). Subsequent severe chalk damage (from grating, shears, and other damage types) was observed across the top of the chalk features. The swinging and movement of the pot is also a culprit of damage, more so than if the pot was settled securely on the chalk bed. Extending rope tethers between pots and shank lines could minimise chalk damage by both taut rope and hanging pots, though too much loose rope can also be a risk, particularly to boats moving across the reef. Ropeless pots, as trialled in Scotland and the United States (US) [178, 179], could be a solution to both not enough and too much rope causing chalk damage. All of these observations were anecdotal and not shown by correlations in the data. A more extensive approach covering more transects is required, but was out of the scope of this preliminary survey.

Human-attributed damage is not isolated in itself but combines with natural damage and erosion to weaken the structure and resilience of the reef [180]. Natural degradation of chalk could be sped-up by the smallest instances of damage from pots, ropes, anchors, or other man-made objects. Chalk covered in epifauna is likely to weather at a slower rate than exposed chalk, and therefore small-scale impacts from potting may be speeding up the natural process of erosion, which will eventually impact the structure of the chalk.



Table 4.3: Pearson correlation coefficients between median rugosity and crab abundance across the Cromer Shoal Chalk Bed.

Metric	Abundance	r	$r^2$	$p$
Rugosity	Total crab	-0.0214	0.0005	0.0024
	Adult crab	0.6717	0.4512	<b>0.0003</b>
	Juvenile crab	-0.1440	0.0207	0.5020
Vector Dispersion	Total crab	-0.1591	0.0255	0.4580
	Adult crab	0.3113	0.0969	0.1387
	Juvenile crab	-0.2142	0.0459	0.3153
$D_{60-30}$	Total crab	-0.1061	0.0113	0.6220
	Adult crab	0.5361	0.2874	<b>0.0069</b>
	Juvenile crab	0.0063	0.0000	0.9767
$D_{30-15}$	Total crab	0.0555	0.0031	0.7967
	Adult crab	0.5627	0.3166	<b>0.0042</b>
	Juvenile crab	-0.0483	0.0023	0.8237
$D_{15-5}$	Total crab	0.0457	0.0021	0.8321
	Adult crab	0.1593	0.0253	0.4576
	Juvenile crab	0.0158	0.0002	0.9416
$D_{5-1}$	Total crab	-0.0880	0.0077	0.6826
	Adult crab	0.1372	0.0188	0.5226
	Juvenile crab	-0.1117	0.0125	0.6056

The lack of association between damage and complexity has several implications. The least likely is that damage is simply not more commonly seen in areas with large, complex chalk features. A review of video footage showed that more damage was seen on larger outcropping chalk (WS2 footage) and that flatter chalk areas showed only abrasion type damage. Kaiser et al. [181] have shown the detrimental affect of bottom-towed fishing gear is exacerbated with increased structural complexity so a logical assumption would be for the relationship to apply to static fishing gear as well, though perhaps less severely. A more comprehensive study would provide more conclusive answers.

#### 4.4.2 Annotation of damage

Damage analysis showed varying agreement between annotators of damage incidence across all sites. The variation could be for any number of reasons, including video quality, turbidity, experience of the site conditions, experience of video annotation, etc. The good-to-strong agreement found for damage categories overall, at WS2, and at WR shows the capability of similar assessments in producing robust data but there is always a need for

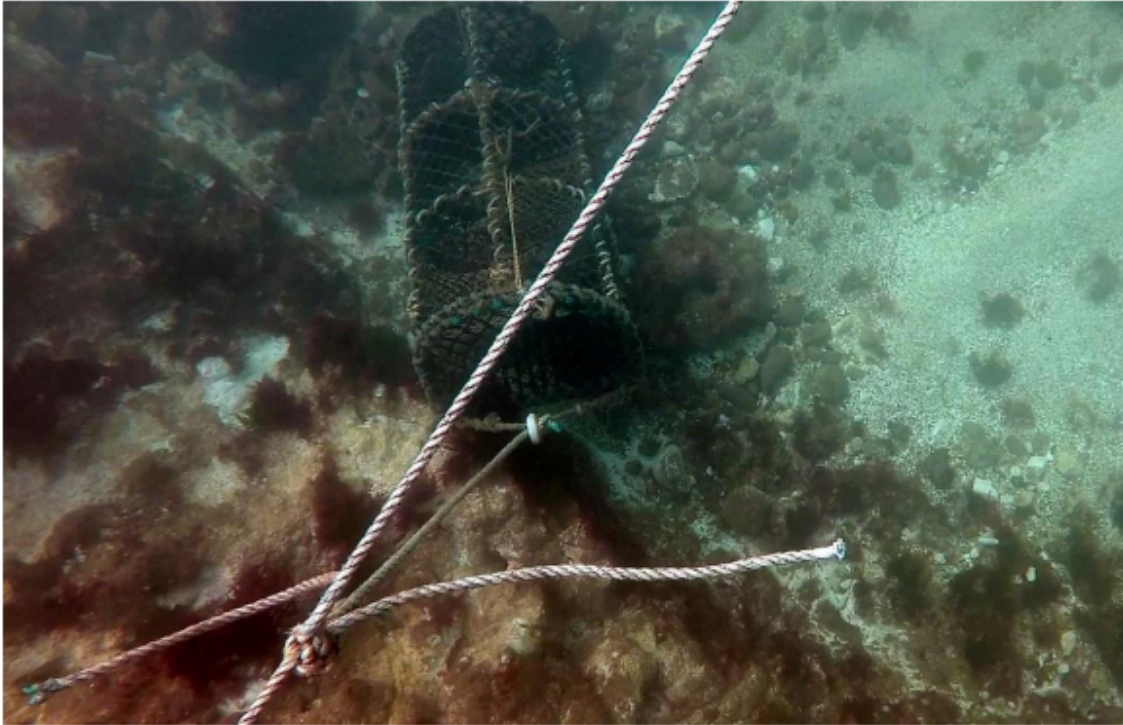


Figure 4.8: A pot attached to a shank by a rope tether  $\sim 2$  m long. The tether is too short to allow the pot to sit on the chalk bed substratum so it is left hanging with the ropes pulled taut on the chalk reef.

annotator training and a consolidation stage to resolve disagreement. In this project, data were consolidated and agreed upon by the annotators after independent assessment.

The lack of strong agreement between annotators highlights issues with the damage categorisation, annotator training, the video quality, or all three. Categories may have been too similar; lifts, grating, angular rubble, sawing, and strikes may all show rubble-like debris that could have made them difficult to distinguish from one another, particularly when combined with the relatively poor video quality. Consolidating categories with similar appearance or impact may enable better agreement between annotators, and possibly easier and quicker analysis. This would, however, remove the fine detail analysis enabled by the more distinct categories. With more surveys, the benefits of more extensive training and/or fewer categories may be seen.

Greater agreement was seen for damage categories that were more prevalent across the sites, such as for abrasions and angular rubble, indicating that greater exposure to damage categories increases familiarity and recognition. This also appeared to be the case for drag damage and unlevel shears to some extent, perhaps due to the distinctness of these damage types in the chalk. Categories that look similar, like strikes and level shears,

may be harder to ascertain with both limited instances and lower quality video footage.

Increasing the number of annotators should not be considered a solution unless video quality is so poor that greater corroboration and consolidation are needed. Better training and understanding of damage is a more desirable outcome so that videos can be annotated and verified/consolidated between 2 annotators to minimise the time spent collecting data.

The disparity in annotator agreement highlighted the difficulty in annotating footage that is of poor quality, as here through sedimentation and poor light. Scaling up surveying is essential for continued monitoring, but impractical with the current annotator burden. To reduce the required effort and scale up monitoring, an automatic benthic annotation method could be developed for use, though this would be an intensive imaging and development task.

#### 4.4.3 Commercial crustacean preferences in habitat complexity

The significant positive correlation between adult *Cancer pagurus* abundance and rugosity, fractal dimension at 30-15 cm, and fractal dimension at 60-30 cm demonstrated that adult commercial crab are more often seen in areas containing large, complex chalk features. The lack of correlation between juvenile *C. pagurus* abundance and any complexity metric conversely suggests that juveniles show no preference for either flat or structurally complex regions. A possible cause of this variation in crab density is the crevice and refuge size in areas with lower complexity (particularly fractal dimension) cannot support the larger crab and as such they will move to more complex areas, whereas smaller crab do not face the same size issue. The territorial and cannibalistic nature of adult crabs could also be a factor, leading to the exclusion of juveniles from the preferred, more rugged areas of chalk [182]. Consequently, juvenile crustaceans can find suitable refuge in both highly and lesser complex areas of chalk, unlike the larger adults, potentially because their size may enable them to fit into the smaller cracks and fissures.

Hunter and Sayer [183] have previously noted a preference for complex habitats in *C. pagurus* on temperate rocky and artificial reefs. This relationship between commercial crustaceans and habitat complexity suggests that a reduction in the complexity of the chalk would also lead to a reduction in abundance of crab and lobsters. This would have knock-on effects both on local marine biodiversity and the North Norfolk fishery.

#### 4.4.4 Survey limitations

The survey faced constant and numerous complications. The logistics of collecting field data were more complex and more expensive than anticipated. The field techniques required training that could only occur during the excursions and ate into the surveying time. The 5 day assessment was also subject to bad weather, boat failures, and inconvenient launching facilities. The most unfortunate ramification of this was a limited amount of data collected.

*In-situ* limitations included a limited amount of commercial crustacean data, particularly with *H. gammurus* being so rare that analysis of them could not occur. Adult *C. pagurus* were also rare but could still be analysed, although the low abundance did provide less robust conclusions. The complexity assessment was undertaken using metrics tailored and scaled to coral reef studies. The different compositions and structural styles of chalk and coral reefs likely mean that the metrics used were not able to fully encompass the sweeping shifts of chalk reef topography. Even fractal dimension scales used here were tailored to those of coral reef fish abundance [48]. Rugged chalk was a focus of this study by default (the assumption being that more complex topography would be most sensitive to impact based on photographic evidence), so the flatter plain of chalk reef was ignored particularly with the time constrictions faced.

The damage assessment, mostly due to its novelty, was a source of potentially subjective data. Though the assessment and severity categories were determined by experts and experienced divers, the variation in reef damage could easily lead to discrepancies between individual assessors. Some categories are similar in appearance and some areas may have experienced two impact types, which could change the damaged chalk's appearance and therefore categorisation. The nature of severity is also inherently subjective. Minor amounts of a high severity damage, such as a shear, may be less destructive than masses of abrasion damage, which was designated as low severity.

Some of these limitations are unavoidable without more resources and funding for regular and repeated surveying at a greater scale and/or further study into damage extent on chalk. The use of potentially improper complexity metrics is however simpler to test as an *ex-situ* comparison of already generated models.

## 4.5 Summary

The preliminary survey carried out in this chapter acted as both proof-of-concept for assessing the Cromer Shoal Chalk Bed MCZ and to provide an indication of the current state of the chalk reef. Surveying marine environments with multi-camera arrays and 3D photogrammetry can drastically reduce fieldwork surveying time and cost, and provide accurate measures of complexity across survey sites. However, these complexity measures may not be relevant to the environment surveyed if as the topography is vastly different to that of coral reefs, which the metrics were tailored to. Developing one or more complexity metrics specifically suited to chalk reefs, or to any protected marine environment, is essential when monitoring substrate to generate ecologically meaningful results.

The following chapter takes the survey data and applies tailored complexity metrics in an attempt to clarify any relationships present between chalk reef complexity, *C. pagurus* abundance, and chalk damage.

# 5 | Adapting complexity to a rocky chalk reef

## 5.1 Introduction

The layered deposition of chalk and continuous water movement creates a gradually changing structure with transitions between high and low areas characterised by the presence of gullies, arches, stacks, and ledges [42]. This may limit the appropriateness of many established marine complexity assessment metrics as they are often tailored for small changes to a system, such as branching corals on tropical reefs, rather than shifts in the topography of a rocky seabed [66, 48]. This was evident when comparing site descriptions and physical characteristics of each transect to the apparent complexity produced from measurements of rugosity and vector dispersion in chapter 4.

In marine monitoring, substrate height can be described by a wide range of reef metrics. Several height measurements were developed by McCormick [66] relating to height that showed varying success in plotting height changes, separating substrate types, and correlating to fish abundances. Elevation is usually used to describe the height of something above sea level or a given point. Slope and gradient are also common measures used in ecology that may refer to the same value in some cases. Gradient is measured as the ratio of vertical to horizontal distance between two points. Slope refers to either this measurement or the angle of the horizontal to vertical points, with the horizontal being  $0^\circ$ . Reef gradient is also used in coral reef ecology to refer to the different areas of a coral reef (i.e. crest, slope) without using any quantitative measurement.

Relief measures the height difference between 2 points that may not necessarily be directly vertical (as with height) nor do they need to be set (as in elevation). Relief has been found to correlate with an abundance of reef-associated fish on a rocky reef area

in Sweden [184], experimentally tested through constructed, high-profile structures. This relationship, and visual assessments of the type of structures on the Cromer Shoal Chalk Bed MCZ, determined that relief would be tested as a metric on the chalk reef.

The chapter presents an alternate assessment of the Cromer chalk reef survey data (Chapter 4) to propose a novel measurement of relief through 3D reconstructions of marine environments. First, the relief metric must provide a distinct view of complexity when compared to other metrics in rocky reef environments. To benefit the Cromer MCZ survey, relief must also be assessed for any link to commercial species or to human impacts on the chalk reef. Here, relief is taken as the absolute vertical increase of a substrate within a given area. This took the linear assessment of verticality/slope [17] and applied it to a surface area for a targeted view of the complex substratum.

## 5.2 Methodology

### 5.2.1 Model analysis

The chalk reef models analysed here were created in Chapter 4 from West Sheringham (WS1 and WS2), West Runton (WR), and East Runton (ER). Coral reef models were also analysed from Pak Kasims and Sampela reef (Chapter 3). The Cromer chalk reef site (see Section 4.2.1) was compared to the two coral reef regions (see Section 3.2.1), exploring the suitability of the relief metric for these less complex reef types.

A computational approach to assessing relief was performed on all models, where the total height difference across an area was calculated (Fig. 5.1). All models were assessed to determine the largest scale area that could be consistently used, then a closed object was created - in this case a 64 m<sup>3</sup> cube. The object was placed to intersect with the model mesh and encompass the area, then was split across the intersection to provide halves ending in the contour or inverse contour of the reef surface.

$$Relief = |a - b| \tag{5.1}$$

Where  $a$  = height of split object with surface contour, and  $b$  = height of split object with inverse surface contour. A novel script for relief was developed (Appendix IV).

A key feature of fractal dimension ( $D$ ) is the connection between an organism and its

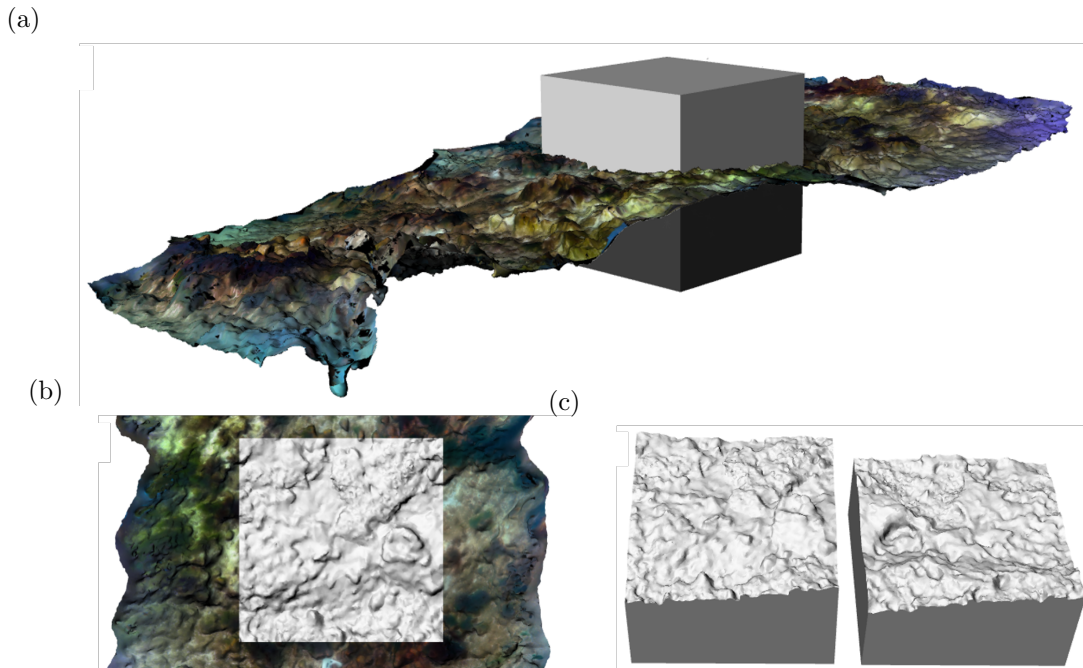


Figure 5.1: Relief assessment of an area of reef. (a) A solid box scaled to be greater than the largest relief across all models was intersected with the model mesh. (b) The box was split across the intersection, matching the contour of the mesh. (c) The box was separated to show the contour of the substrate and the inverse. The height of one split was then subtracted from the height of the other and the absolute value was the relief of the area.

habitat when considering spatial scale (Section 2.3.3). In Chapter 4,  $D$  was carried out to size scales appropriate for coral reef fish [48], likely limiting the usefulness of the results. To rectify this, a tailored approach was taken and size categories were adjusted to suit the carapace width of *Cancer pagurus* catch size:  $D_{\text{catch}}$  for  $D$  between 345 mm and 115 mm, and  $D_{\text{non-catch}}$  for  $D$  between 115 mm and 28.75 mm. Coral reef models were not evaluated for fractal dimension here as the size scales used are irrelevant to that ecosystem.

### 5.2.2 Ecosystem data

*C. pagurus* classification as adult or juvenile was determined by catch size limits so counts remained, per Chapter 4 (Table III.1). *Hommarus gammarus* were not incorporated as there were so few seen and they were excluded from analysis. Damage categories, severity (Table 4.1) and counts (Table 4.2) remained as originally determined. Surveying time restrictions limited the number of pots and control markers that could be imaged on each transect. To account for this, only the first 100 m of each transect was used for further analysis as all pot and control quadrats were within this area.



### 5.2.3 Statistical analysis

A replication of previous tests was performed (Section 4.2.5). Pearson correlation coefficients were used to test correlations between complexity metrics. Analyses of the variations between sites, abundances and complexity were performed using t-tests (paired and unpaired) and one-way ANOVAs. Low replication and incidence of some damage types limited analysis. Damage was then grouped by severity and tested.

## 5.3 Results

### 5.3.1 Relief and metrics of complexity in coral and chalk reefs

Relief had a weak-moderate positive correlation with rugosity ( $r = 0.3781, t_{34} = 2.3817, p < 0.05$ ), but not with vector dispersion,  $D_{\text{catch}}$  or  $D_{\text{non-catch}}$  ( $p > 0.05$ ) on the chalk reef (Fig. 5.2c). Pak Kasims coral reef site showed a moderate correlation between vector dispersion and relief ( $r = 0.4657, t_{22} = 2.4685, p < 0.05$ ), and a potential moderate correlation between rugosity and relief ( $r = 0.4023, t_{22} = 2.0608, p = 0.051$ ) (Fig. 5.2a). The Sampela coral reef also showed a moderate correlation between vector dispersion and relief ( $r = 0.4934, t_{22} = 2.6609, p < 0.05$ ) and a moderate-strong correlation between relief and rugosity ( $r = 0.6703, t_{22} = 4.2361, p < 0.0005$ ) (Fig. 5.2b).

### 5.3.2 Relief and species abundance on chalk reefs

No difference was found in  $D_{\text{catch}}$ ,  $D_{\text{non-catch}}$ , or relief between pot and control sites ( $p < 0.05$ ).  $D_{\text{catch}}$  showed variation ( $F_{3-32} = 4.461, p < 0.01$ ) across the sites; WS1, the non-chalk site, was less complex than WS2 ( $p < 0.05$ ) and WR ( $p < 0.01$ ).  $D_{\text{non-catch}}$  did not differ ( $p > 0.05$ ). Relief followed the same trend as  $D_{\text{catch}}$  between sites ( $F_{3-32} = 4.606, p < 0.01$ ); WS1 and WS2 ( $p < 0.01$ ), and WS1 and WR ( $p < 0.05$ ).

When considering tailored fractal dimension, adult crab ( $\geq 115$  mm) abundance correlated with  $D_{\text{catch}}$  but not  $D_{\text{non-catch}}$ . Juvenile crabs ( $\leq 115$  mm) did not correlate with either  $D$  at either size scale, supporting the original findings that juveniles do not rely upon complexity in their distribution, but adult crabs prefer more complex areas (Table 5.1). Relief did not correlate with crab abundance overall or by age group.

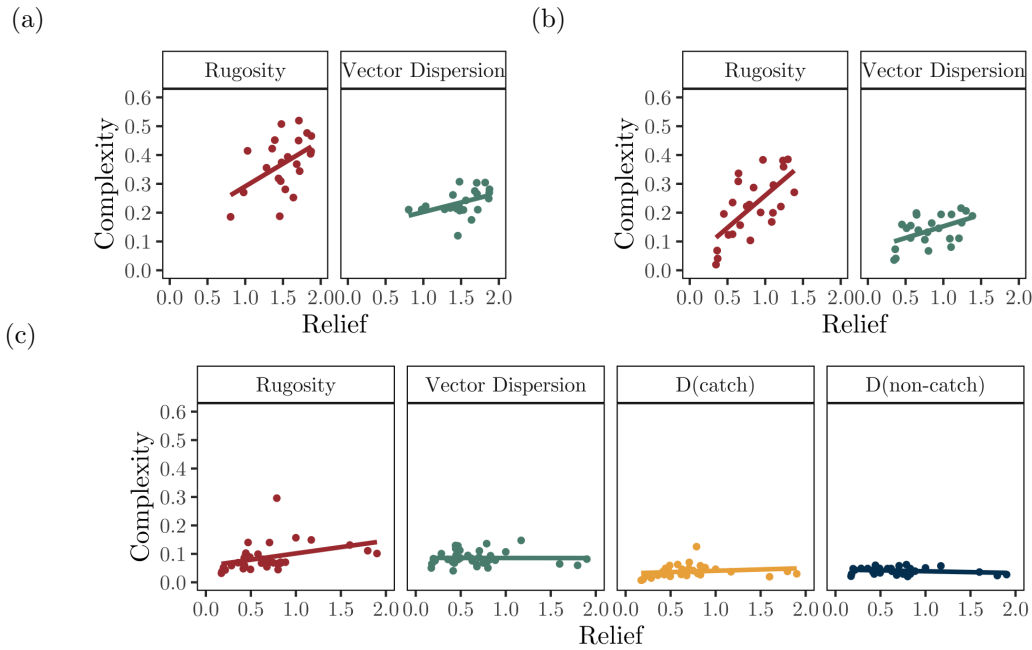


Figure 5.2: Linear correlations between relief and other complexity metrics (rugosity, vector dispersion, and fractal dimensions -  $D_{\text{catch}}$  for fractal dimension between 345-115 mm, and  $D_{\text{non-catch}}$  for fractal dimension between 115-28.75 mm) at (a) Pak Kasims and (b) Sampela coral reef sites, and (c) Cromer chalk reef. Fractal dimension is excluded from (a) and (b) as the size scales used were different from that for Cromer sites.

### 5.3.3 Relief and observed human impacts on chalk reefs

WS2 had more low severity damage than any other category (53), whereas ER had mostly high severity damage (48) (Fig. 5.3).

Due to the modelled complexity and species abundance data available, analysis of damage incidence was only carried out for first 100m of damage (Table 5.2).

Damage totals and severity did not vary between pot and control quadrats ( $p > 0.05$ ); however, control sites had more than double the incidence of abrasion than pot sites ( $t_{23,106} = 2.4676$ ,  $p < 0.05$ ). Damage did not correlate with crab abundance at either size category.

Damage incidence was different at each site ( $F_{2-27} = 6.453$ ,  $p < 0.01$ ), with WR having significantly less damage than both WS2 ( $p < 0.05$ ) and ER ( $p < 0.01$ ). High severity damage varied between sites ( $F_{2-27} = 6.205$ ,  $p < 0.01$ ), with significantly more at ER than WR ( $p < 0.005$ ).

This is similar to the variation in rubble ( $F_{2-27} = 8.789$ ,  $p < 0.005$ ), as ER had more than both WR ( $p < 0.01$ ) and WS2 ( $p < 0.01$ ) (Fig. 5.3). Medium severity damage was significantly greater ( $F_{2-27} = 4.778$ ,  $p < 0.05$ ) at ER than at WR ( $p < 0.05$ ). This can

Table 5.1: Correlations between crab abundance and fractal dimension, and crab abundance and relief at different size scales ( $n = 36$ ). Significant is indicated by bold text.

Metric	Abundance	$r$	$r^2$	t	$p$
$D_{\text{catch}}$	Total	0.0552	0.0030	0.2594	0.7977
	Adult	0.4499	0.2024	2.3629	<b>0.0274</b>
	Juvenile	-0.0280	0.0008	-0.1314	0.8967
$D_{\text{non-catch}}$	Total	-0.0492	0.0024	-0.2314	0.8191
	Adult	0.2676	0.0716	1.3027	0.2061
	Juvenile	-0.0975	0.0095	-0.4595	0.6504
Relief	Total	-0.0629	$3.9554e^{-3}$	-0.2956	0.7703
	Adult	0.1466	0.0215	0.6950	0.4943
	Juvenile	-0.0887	$7.8757e^{-3}$	-0.4179	0.6801

Table 5.2: Incidence of damage by severity level.

Site	All	High	Medium	Low
WS2	49	18	2	29
WR	18	8	1	9
ER	55	36	8	11

be attributed to strike damage as the only category at this severity level. There was more low severity damage ( $F_{2-27} = 5.953$ ,  $p < 0.01$ ) at WS2 than at WR ( $p < 0.01$ ) or at ER ( $p < 0.05$ ). This is reflective of the high incidence of abrasion ( $F_{2-27} = 7.122$ ,  $p < 0.005$ ) at WS2 versus that at WR ( $p < 0.005$ ) and ER ( $p < 0.05$ ).

When correlating damage incidence with complexity, no relationship was seen with  $R$ ,  $\frac{1}{k}$  or  $D_{\text{catch}}$ . Medium severity damage correlated with  $D_{\text{non-catch}}$  ( $r = 0.3751$ ,  $t_{28} = 2.1412$ ,  $p < 0.05$ ). Relief correlated with low severity damage ( $r = 0.3931$ ,  $t_{28} = 2.2625$ ,  $p < 0.05$ ), specifically with abrasions ( $r = 0.4109$ ,  $t_{28} = 2.3849$ ,  $p < 0.05$ ).

## 5.4 Discussion

### 5.4.1 Complexity and relief on chalk and coral reefs

Relief provides distinct information about rocky reef habitats. The relief metric was selected for the type of complexity seen in the environment itself, over the use of rugosity and vector dispersion, to detect medium-scale changes in structure compared to other common metrics used in other studies with similar aims [17, 66, 48].

Relief had a weak correlation with rugosity that is likely reflective of  $R$ 's ability to

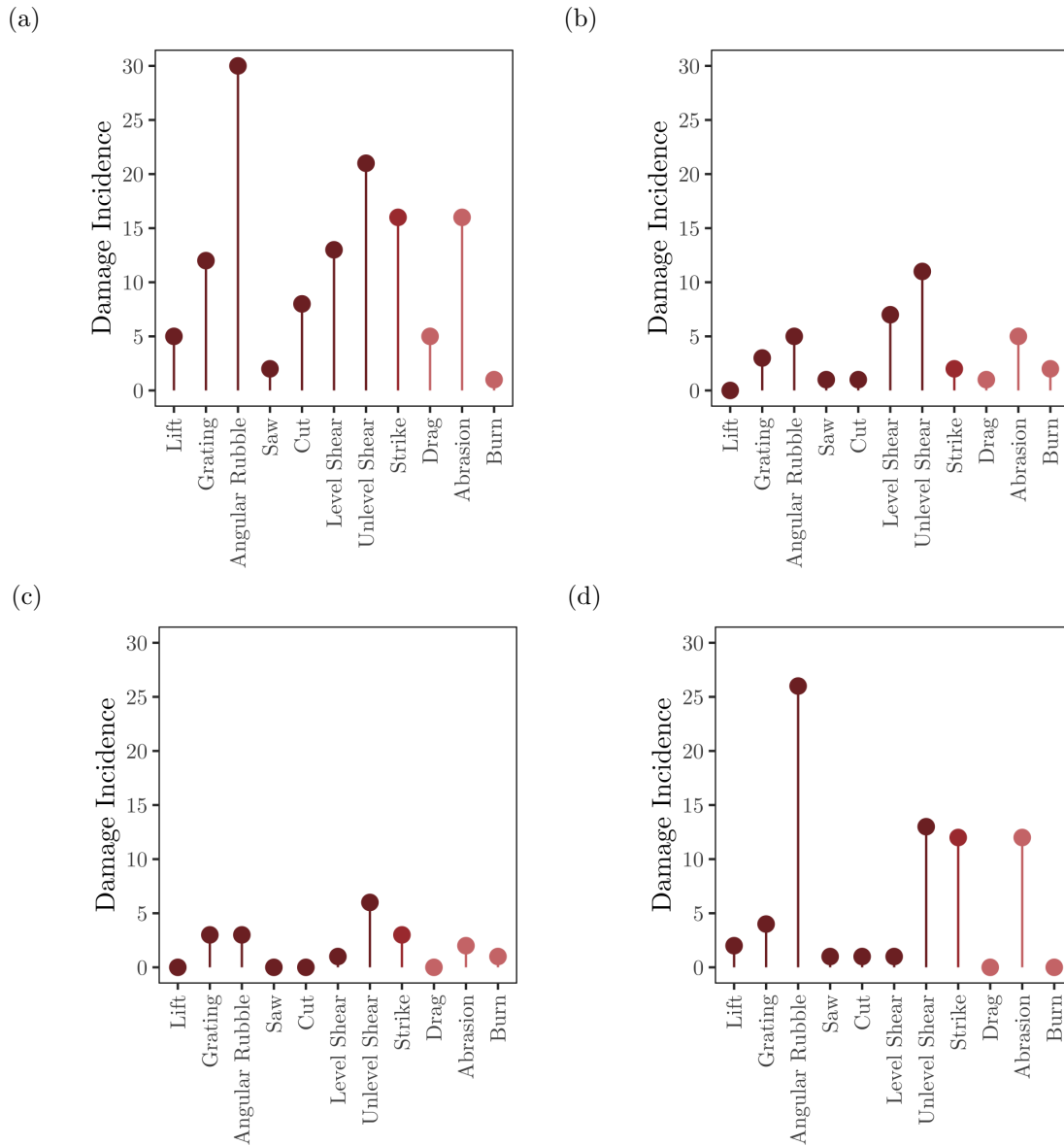


Figure 5.3: Incidence of high severity (dark red), medium severity (red), and low severity (pink) damage by category for (a) All sites, (b) WS2 ( $n = 83$ ), (c) WR ( $n = 37$ ), and (d) ER ( $n = 72$ ).

track changing height of the substrate if it is constant in one direction - i.e. an increase is not matched by a decrease in the same measurement. Rugosity likely captured the complexity of the gullies and ridges in some areas of the chalk reef. The lack of correlation with vector dispersion on the Cromer Shoal Chalk Bed showed that relief focuses on a different resolution and scale. Neither category of  $D$  correlated with relief, likely as the metrics are focused on entirely different factors of the ecosystem.

Cromer reef pot and control models showed no difference in complexity, potentially due to the similarity of conditions across each sample site and shanks being dropped in roughly, but not exactly, the same location repeatedly. This would spread any impact on

the reef across the entire fished area rather than in dedicated points. Cromer site variation suggested, as previously in Section 4.3, that WS1 was less complex than WS2 and WR. When considering relief, the greatest complexity was found at WS2, matching with *in-situ* visual observations. This indicates that the chalk substrate present along parts of the North Norfolk coast may be providing complexity to the region that cannot be attributed to sandy and stone covered substratum. ER was not dissimilar to any region, likely as its mixed substratum provided areas of elevated chalk and flat sand and stone grounds similar to other sites. For greater clarity and more definitive implications there is a need for a more extensive study of the chalk reef to increase the number of sites surveyed.

For rocky reefs, relief provides a different view to other common complexity metrics across a 3D area of reef, one that may better represent the complexity of other medium-scale rocky reef features, such as Kimmeridge ledges in the UK.<sup>1</sup> Here, the relief of chalk may also associate with the abundance of catchable crustaceans on the chalk reef with more data, as fishers often prefer to place their pots on “rough ground,” their term for complex chalk substrate.

At the coral reef sites, rugosity had moderate to strong correlations with relief, and vector dispersion had moderate correlations with relief. Pak Kasims was a sloping site with raised and settled substrate whereas Sampela had coral bommies, but both would provide elevation. Both sites’ relief, therefore, also led to more intricate complexities in rugosity and vector dispersion on the coral reefs. Coral reef relief could highlight areas providing both medium- and small-scale complexities, such as bommies and raised substrate that allow for more settlement of complex organisms.

#### 5.4.2 *C. pagurus* preferences in habitat complexity

Adapting the size categories of fractal dimension to suit the target species, *C. pagurus*, did not alter the overall findings of the original assessment (Section 4.4). Adult crab were again positively correlated with fractal dimension, in this case with  $D_{\text{catch}}$ , highlighting the importance of scale-associated complexity. Juvenile crab were not correlated to either fractal dimension scale, showing their dispersal across the reef system in contrast to the preference of adults for complex substrates. The distinction in complexity and species abundance with regards to fractal dimension was more reflective of real-world separation

---

<sup>1</sup>A example of the topography can be seen at: <https://skfb.ly/o6zt9> last accessed 8/9/2021

in *C. pagurus* individuals here than those in the previous tests (Section 4.3), that found correlations between the two only at scales above the minimum landing size (starting at 15 cm and upward). The adjusted metric connects the findings to the specific species targeted by fishing and may be a more viable foundation for policy changes and supporting research.

The increased  $D_{\text{catch}}$  at the more complex chalk sites indicates that these are preferred by catch-size *C. pagurus*. Higher *C. pagurus* abundance was not associated with flatter environments. This is supported by the correlation between  $D_{\text{catch}}$  and adult crab abundance, and the lack of correlation with  $D_{\text{non-catch}}$  or juvenile crab at either complexity. The lack of apparent habitat preference with juvenile crab could be due to all sites having the same  $D_{\text{non-catch}}$ , indicating that complexity preference for juvenile crabs was the same across the study, or because of the territorial nature of adults, particularly males, *C. pagurus* causing smaller individuals to be pushed out of their preferred environment [185]. Relief was also not correlated to species' abundance overall or by age/size. This is likely as the smaller intricacies of complexity favoured by *C. pagurus* are not detected by the medium-scale assessment of relief performed here.

### 5.4.3 Monitoring human impacts on chalk reefs

The difficulty in assessing chalk damage limits the conclusions that can be drawn. The number of damage types may be restrictive when analysing collected data and the number of distinct categories with indistinct classification may not be useful ecologically. Grouping damage by either severity or cause would provide fewer groups with greater incidence while also enabling managers of the chalk reef to have a clear indication into both the level of damage and the potential targets for further investigation.

When looking at damage in this manner, areas of higher relief showed increased levels of low severity damage and of abrasion damage. This could indicate that more elevated sites may be more susceptible to pots scraping down chalk to settle below, abrading the substrate, and to ropes dragging across them to scrape off surface algae and score into the chalk. The slight increase in  $D_{\text{non-catch}}$  with increased medium severity damage (and therefore strike damage) may be due to the loss of large chalk shattering into smaller sections, creating crevices that could provide areas only accessible to non-catch size crabs (those smaller than 115 mm in width). The correlation between metrics here and damage,

when compared to the lack of correlations seen in Chapter 4, highlight the need for tailoring complexity metrics to the environment.

The types and occurrences of damage at different sites, with different topographies, substrate and ecological functions need more surveying to explain (e.g., higher rates of damage at WS2 and ER compared to WR). Visual assessment at WR indicated an algae layer as with WS2 and this may offer protection from some impacts. For ER, when also considering its higher instances of rubble and strike damage, this could indicate a chalk composition and/or structure that is more susceptible to breaking than at the other sites. A more refined method for testing chalk hardness than used in the Natural England report [172] could be used. Greater incidence of low severity damage at WS2 than the other sites appears entirely reflective of abrasion damage (Fig. 5.3). This could be due to varied relief of the site as indicated in visual characterisation and in the changes measured. This supports the correlation of low severity damage, and specifically abrasion, with greater relief.

We know how human objects impact the substrate but not the extent across the site; partly because of the mixture of substrates and complexity and partly because fishing pressures are unevenly distributed across the MCZ due to the location of shore launching sites and nomadic fishing boats. Increasing the data collected may bring out patterns already appearing to emerge in the damage observations. The clustering of damage along the survey sites is a potential avenue for further investigation to determine if particular chalk features and characteristics are more at risk of certain types of damage. Further surveys along shanks, or alternatively reference areas of reef, could provide greater insight into this when combined with both complexity assessments, visual descriptions of the site and hardness measurements of the chalk itself.

#### **5.4.4 Limitations of the survey**

The extraction of relief data would benefit from vertical reference in each modelled area, such as a float [48]. As the models here used visually assessed alignments from video footage, the modelled substrate is at a “best guess” orientation that may not be entirely accurate to the *in-situ* substrate.

## 5.5 Summary

Capturing the complexity of the Cromer Shoal Chalk Bed MCZ in terms of relief provided a distinct view of the environment not shown by other metrics. Tailoring fractal dimension to commercially catchable *C. pagurus* demonstrated an association between the adult crab and complexity, highlighting the importance of scale when looking into relationships between fauna and habitat. Tailoring complexity metrics to target environments or species is a key step in gaining insight into community interactions with a habitat. The study of rocky reef environments that feature gullies, arches, stacks, and ledges would benefit from an analysis of relief and other adaptive complexity assessments (i.e. tailored fractal dimension where studies include benthic-associated species).

A larger and more comprehensive study into damage on the Cromer Shoal Chalk Bed is vital to understand the severity, frequency, and causes of human impacts on the habitat. A non-fished control area would be also beneficial more definitively compare human and naturally caused damage, as well as a site with ropeless potting technology to contrast pot/anchor and rope damage [179]. Most important, however, is a continuing narrative between the local community, the MCZ management, and researching academics involved with the chalk reef to protect both the habitat and its heritage.

The investigation into the human impacts on the Cromer Shoal Chalk Bed MCZ has highlighted the need for urgent action and more data is vital for accurate assessments of interactions between structural complexity and the species communities that make use of niches. Future work with Natural England, EIFCA, conservation groups, and the fishing industry aims to address these challenges through adaptive risk management.



# 6 | Automatic annotation of reef substrates

## 6.1 Introduction

Identification of coral reef substrate from video footage, images or directly while diving is a common assessment carried out in reef research and monitoring [186]. It is vital for grounding research into the wider reef system and for assessing and detecting changes in substrate composition. It is also, unavoidably, very time consuming. The constantly increasing volume of image and video data in ecology could be a vital resource in tracking ecosystem changes and trends locally, regionally, and globally, but the sheer quantity limits the usefulness as it is impractical if not impossible to annotate, tag, or label manually. Automatic annotation of benthic substrates from video stills or photographs would greatly increase the speed and scale of feasible coral reef monitoring, and could free up reef experts to focus on other areas to gain a wider view of shifting ecosystem dynamics.

The use of machine learning in ecology is becoming more prevalent following the popularity of image data collection in surveying and research [187]. The reduction in camera costs combined with the increasing quality and resolution of less expensive equipment enables a greater number of research teams to utilise image data in their research [47, 48, 122, and others]. Combined with the smaller size of equipment required (some action cameras no longer require housing to certain depths, whereas previous imaging required large cameras with lighting, buoyancy aids and intricate housings), this has widened the scope of *in-situ* imaging in marine monitoring globally.

These advancements required a new focus on utilising computer vision techniques for detection and classification of objects and images, which offers a valuable avenue into decreasing processing time and increasing the efficacy of digital image usage in ecological

research. This could reduce the need for more intensive forms of data collection and increase the information available from sites that are more difficult to access safely.

This chapter details the planning, development, and outcomes of the ImageCLEFcoral annual task from 2019 to 2021. ImageCLEFcoral is a recent addition to the ImageCLEF benchmarking campaign tasklist [188, 189, 190, 191] with an alternative marine focus, aiming to develop an accurate method of automatically annotating coral reef substrates. Developing an algorithm that is transferable to coral reef systems globally would be of great benefit to reef monitoring in general, but also when looking at global reef connectivity and changes in substrate bound fauna and flora.

## 6.2 ImageCLEFcoral tasks

ImageCLEFcoral was split into two subtasks of different difficulties and detail level:

### **Subtask 1** *Coral reef image annotation and localisation*

This subtask aimed to produce a bounding box around substrate fauna and flora, adding an associated semantic label identifying the substrate category. This is the simpler subtask of the two, but is less detailed.

### **Subtask 2** *Coral reef image pixel-wise parsing*

This subtask aimed to produce a polygon around substrate fauna and flora following their outline, adding an associated semantic label identifying the substrate category. This is a more complex task but provides a more detailed output.

Three metrics were used to assess the results produced in 2019:

**mAP 0.5 IoU** - Mean average precision (mAP), where intersection over union (IoU)  $\geq 50\%$  of each images ground truth, in predicting both semantic label and location.

**mAP 0 IoU** - Unlocalised mAP (IoU = 0%), wherein a semantic label is found within the image but it's location is irrelevant.

**R 0.5 IoU** - Mean recall, where IoU  $\geq 50\%$  of each images ground truth, when predicting both semantic label and location.

Precision is a calculation of the accuracy of correct predictions (i.e. where a substrate is found, is the class correct?), while recall calculates the ease of finding correct predictions

(i.e. how many substrates that exist were identified?). These values can then be plotted and mAP is calculated as the area under the curve, where both axes run from 0-1.

Mean recall was no longer used as an evaluation metric in 2020, as mAP provides a broader view of model performance and encompasses recall in its calculation. Agreement per class (Eq. 6.1) was added as a metric to the evaluation to provide further insights into the difficulty variance across each substrate type.

$$\text{agreement} = \frac{\text{number of true positives}}{\text{number of false positives} + \text{false negatives} + \text{true positives}} \quad (6.1)$$

In 2021, participants were encouraged to augment the dataset with that of the NOAA NCEI<sup>1</sup> and/or CoralNet<sup>2</sup>. For the NOAA images, a format conversion table was provided.

### 6.3 Coral reef image datasets

Images collected by the Marine Technology Research Unit at the University of Essex as part of a continuing data collection project were used. SJCam action cameras with external red filter attachments captured the images. These formed the ImageCLEFcoral dataset, but were originally for a monitoring project and as such many have a tape measure running through them. Images were collected from reefs across the globe, but the initial 2019 training ( $n = 240$ ) and test ( $n = 200$ ) set were both exclusively taken from the Wakatobi region of Indonesia.

The 2020 training data consisted of both the training and test set from 2019 ( $n = 440$ ). The test image dataset was expanded to include images from reef systems in four distinct regions. The provided test set contained 400 images from:

**Region 1 (Wakatobi)** - The training set location ( $n = 100$ ).

**Region 2 (Spermonde)** - Geographically and biologically similar ( $n = 100$ ).

**Region 3 (Seychelles)** - Geographically distinct but biologically similar ( $n = 100$ ).

**Region 4 (Dominica)** - Both geographically and biologically distinct ( $n = 100$ ).

The decision to include images from different reefs was to test the importance of geographical and ecological distinctness on the algorithms used. Spermonde archipelago is

---

<sup>1</sup><https://www.ncei.noaa.gov/access/metadata/landing-page/bin/iso?id=gov.noaa.nodc:0211063>

<sup>2</sup><https://coralnet.ucsd.edu/>

located on the opposite side of Sulawesi to the Wakatobi and was considered geographically and ecologically similar as it is within the Coral Triangle. The Seychelles are geographically distinct from the Wakatobi region, but were considered ecologically similar - both are a part of the Indo-Pacific biogeographical reef region [192]. The reefs of Dominica comprise of geographically and ecologically distinct rocky reef systems when compared to the Wakatobi due to their different biogeographical region [192] and species' differing evolutionary pathways and morphologies [193].

The 2021 training data consisted of both the training and test set from 2020 with some additional images added ( $n = 879$ ). The provided test set contained images from the same regions as in 2020 ( $n =$ ). The task images formed completed sets that could be used to generate 3D models of coral reef environments. In practice, this meant that each image would have several others containing at least two thirds of the same substrate, increasing the number of incidences of each substrates' occurrence.

### 6.3.1 Habitat feature classification

Determining the specific semantics used in annotation required an understanding of coral reef benthic fauna and flora with a focus on their morphology and function. To simplify the algorithm required where possible, labels were based on either functional groups or morphology rather than being genera specific (Table 6.1). The variations in reef fauna and flora morphology presents a challenge not regularly seen in automatic image annotation, and were predicted to cause issues with shape recognition and segmentation from the image's background [59, 194]. Even within the same semantic label, the shape and structure of benthos can vary greatly. Colour distinction is valuable when segmenting an image [195], but as corals, rocks, sponges, and other substrate and non-substrate bound organisms can appear very similar it adds another challenging aspect to the task.

Each substrate morphology can be indistinct from others due to the variation in that class' species. This is particularly true of classes that are not broken down into morphological groups, i.e. "soft coral," and less of an issue with classes that are split, i.e. each "hard coral" group. Difficulties can also arise from traits of the organisms within a group, such as in soft corals and some sponges which can appear fleshy and bulbous, and in some cases can have floating parts in the movement of the water column.

Table 6.1: Substrate morphological categories used to classify the reef benthos in ImageCLEFcoral images with a brief summary of the included organisms their appearance.

Classification	Organisms included	Description
Hard Coral - Branching	Branching sclerectinian corals.	Tree-like coral forms with long branches. Show secondary branching.
Hard Coral - Sub-Massive	Submassive sclerectinian corals.	Thick club or pillar shaped corals. Mostly primary branching.
Hard Coral - Boulder	Massive sclerectinian corals.	Spherical/hemispherical, robust corals.
Hard Coral - Encrusting	Encrusting sclerectinian corals.	Plate like sheets in a thick layer over existing substrate.
Hard Coral - Table	Tabulate sclerectinian corals.	Plate corals, often with a stalk. Plate appears most often as branching coral forming on one horizontal plane.
Hard Coral - Foliose	Foliose sclerectinian corals.	Thin, plate like structures. Structured similarly to lettuce or roses.
Hard Coral - Mushroom	Mushroom sclerectinian corals.	Circular or ovular. Solitary and unattached to substratum.
Soft Coral	All alcyonacean organisms, except those from the Gorgoniidae family.	Widely varying morphologies and colours, categorised overall by a fleshy appearance.
Gorgonian	All Gorgoniidae family organisms.	Can appear fan-, whip-, or feather-like, sometimes with a mesh-like connective structure. Often red/orange/yellow coloured.
Sponge	Organisms of Porifera phylum except those shaped as barrels or vases.	Greatly varied morphology and colour, can be fleshy. Pores range in size and are not always visible.
Barrel Sponge	Barrel and vase sponges.	Barrel or vase shaped sponges, varying in colour but often brown/red/purple. Can have ridges running from base to top.
Fire Coral - Millepora	All organisms from the genus <i>Millepora</i> .	Bright yellowish-brown calcified structures with white ends/tips. Often seen as branching structures.
Algae	Leafy macroalgae	Bushy or leafy plant-like organisms. Pale to vivid greens and browns.

### 6.3.2 Image annotation and validation

#### Annotator training

All images in the ImageCLEF coral task had to be accurately hand annotated to both train algorithms and test their accuracy. An online annotation tool was developed specifically for the task (Fig. 6.1), allowing polygons to be drawn and labelled by an initial annotator, then sent to an administrator for validation before being included in the final dataset. The scale of the image set required was large enough that the project benefited from a group of Tropical Marine Biology postgraduate students, who were trained in the expected benthos morphology and in the annotation process (see Appendix V for an example image of each substratum type). Administrators were a PhD student with experience in coral reef surveying and substrate identification within the Wakatobi region, and a marine technology academic with similar prior experience at a range of reef sites and with image annotation.

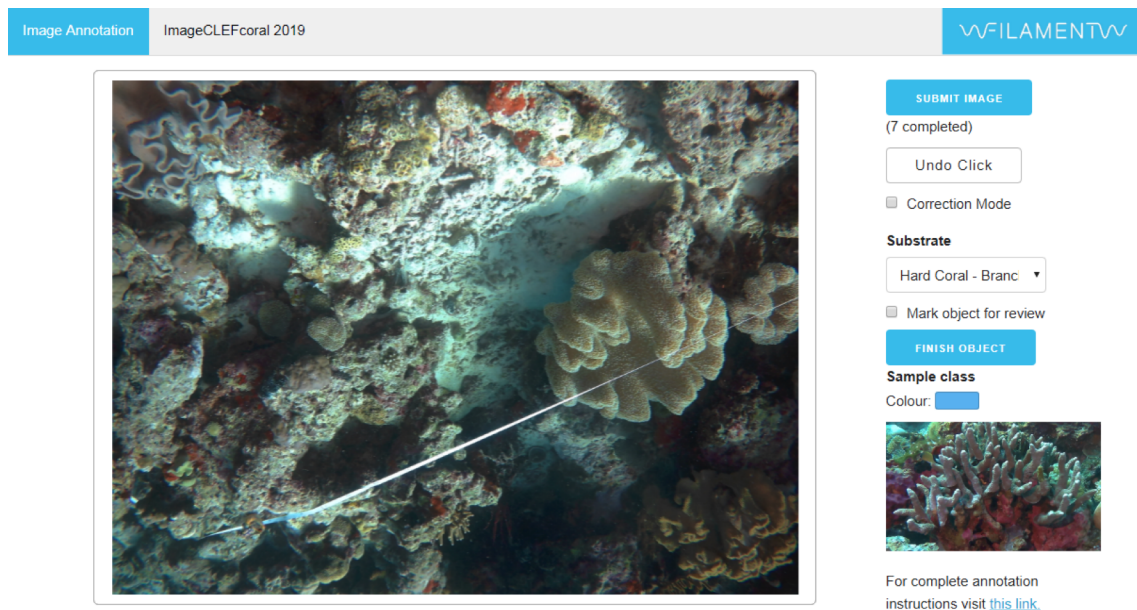


Figure 6.1: The custom annotation tool used when labelling images for the ImageCLEF-coral task. The larger image is the one to be annotated and can be zoomed in and out. The right hand side shows the options to (from top to bottom) “submit the image for validation,” “undo the previous label created,” “change the undo mode to remove individual points from a labels outline,” “select a semantic label from the drop down menu,” the option to “highlight a label to administrators to indicate uncertainty,” to “complete a specific polygon and associated label,” and shows the colour a polygon will appear, and an example of the current selected substratum type.

To use the annotation tool, the students were required to place points sequentially

within the boundaries of the selected organism/organisms (Fig. 6.2a). Adjacent organisms could be grouped together if the same semantic label would be applied (Fig. 6.2b). It was important that no polygon overlapped, so the foremost organism took precedence. To aid understanding, annotators were shown a presentation with relevant substratum types, given an annotation guide PDF, and all annotation was completed at scheduled times with at least one administrator present to verify selections.

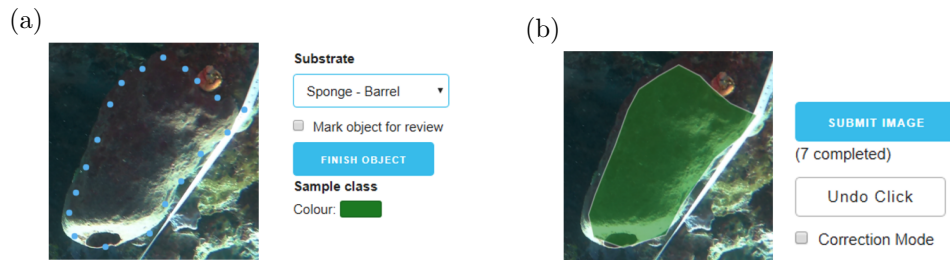


Figure 6.2: A vase sponge (a) outlined by selection dots just inside the objects boundary, and (b) the polygon created by connecting a semantic label to the dotted outline.

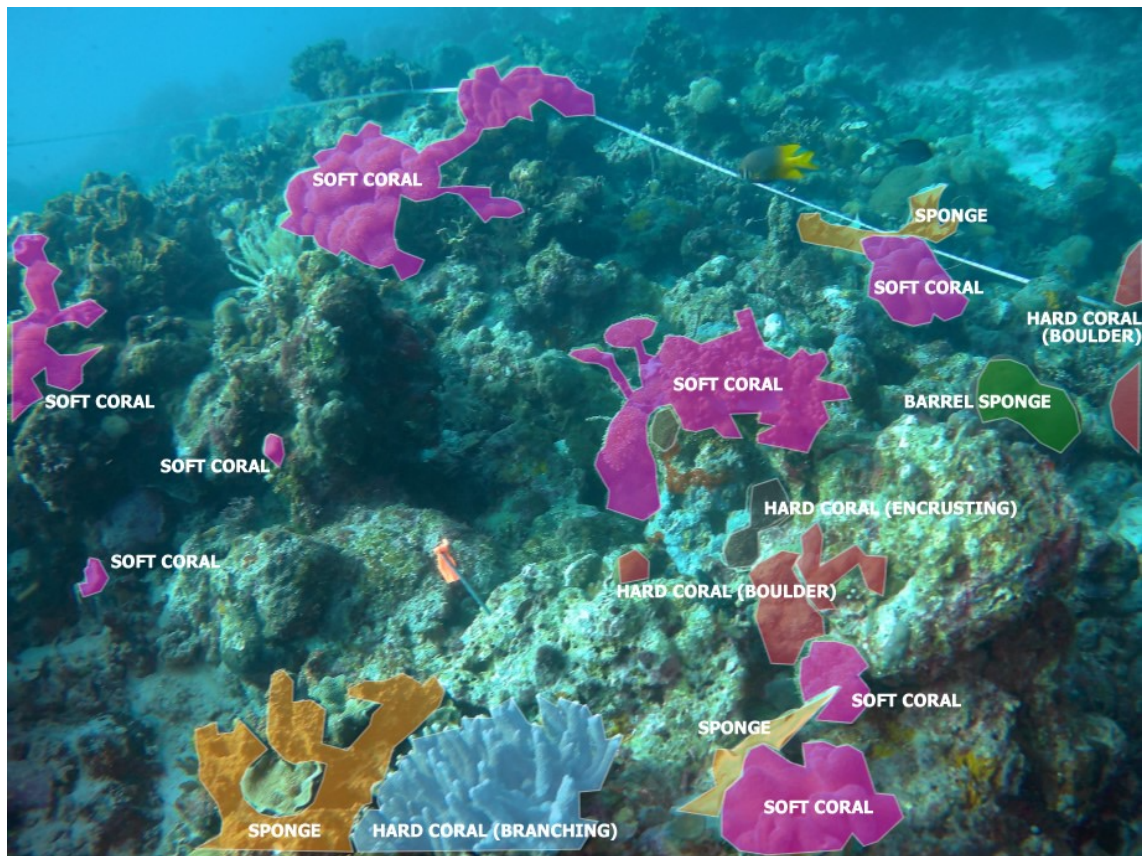


Figure 6.3: One of 5 training images used to test the accuracy and capabilities of prospective annotators to aid in the ImageCLEFcoral task.

## Image annotation

The initial task required 440 images to be annotated (Fig. 6.3). An training exercise assessed the capabilities of annotators to fulfil their task: five images were provided within the tool that demonstrated a range of substratum types that had been annotated previously by an administrator to pixel level accuracy (Fig. 6.3). Agreement per class was then calculated using IoU (Eq. 6.1) to identify any annotators who did not achieve sufficient accuracy ( $\text{IoU} < 15\%$ ) so that their images could be excluded.

Once images were annotated, administrators worked together to assess each one individually. Images were checked for accurate boundaries and semantics of labelled polygons, incorrectly placed polygons, missed substrates, and any polygons tagged for review. Any uncertainties were discussed before a decision was made to minimise errors as much as possible within the manual annotation.

### 6.3.3 Training image analysis

Within the 2019 training dataset, 76.44% of all pixels were considered background and had no substrate class annotations. The remaining 23.56% of pixels were represented across the substrate class semantic labels (Table 6.2). The large disparity in each substrate’s representation in the data set will likely skewed predictions to favour certain classes over others. Combining the small volume of images used for training with the variable quality of underwater imagery and the presence of foreign objects (tape measures and occasionally metal nails with tape can be seen throughout the image set), the task was challenging.

Table 6.2: Benthic substrate distribution, as a percentage of pixels with an associated substrate class (23.56% of all pixels) in the ImageCLEFcoral 2019 training set. Background pixels were not annotated (76.44% of all pixels).

Substrate class	Pixel representation %
Branching coral	13.7 %
Massive coral	22.9 %
Encrusting coral	3.3 %
Soft coral	49.3 %
Sponge	6.8 %
Barrel sponge	2.3 %
Remaining classes	1.7 %



In the 2020 dataset, 17.19 % of pixels were represented across the substrate class labels (Fig. 6.4). Soft corals represented 50.55 % of all classified pixels. Massive (boulder) corals were the next most prevalent (16.92 %), followed by branching corals (11.23 %). Sponges and encrusting corals were the next most common (8.26 % and 4.77 % respectively) with the remaining substrate classes collectively comprising the remaining 8.26 %. As in 2019, the skew towards certain substrates, particularly soft corals and branching corals, would likely skew participants algorithms in favour of more prevalent classes. Although the number of training images increased by over 80 %, there was little training data compared to a standard neural network designed to annotate images, which may hamper accuracy and reduce the mAP scores of submitted models.

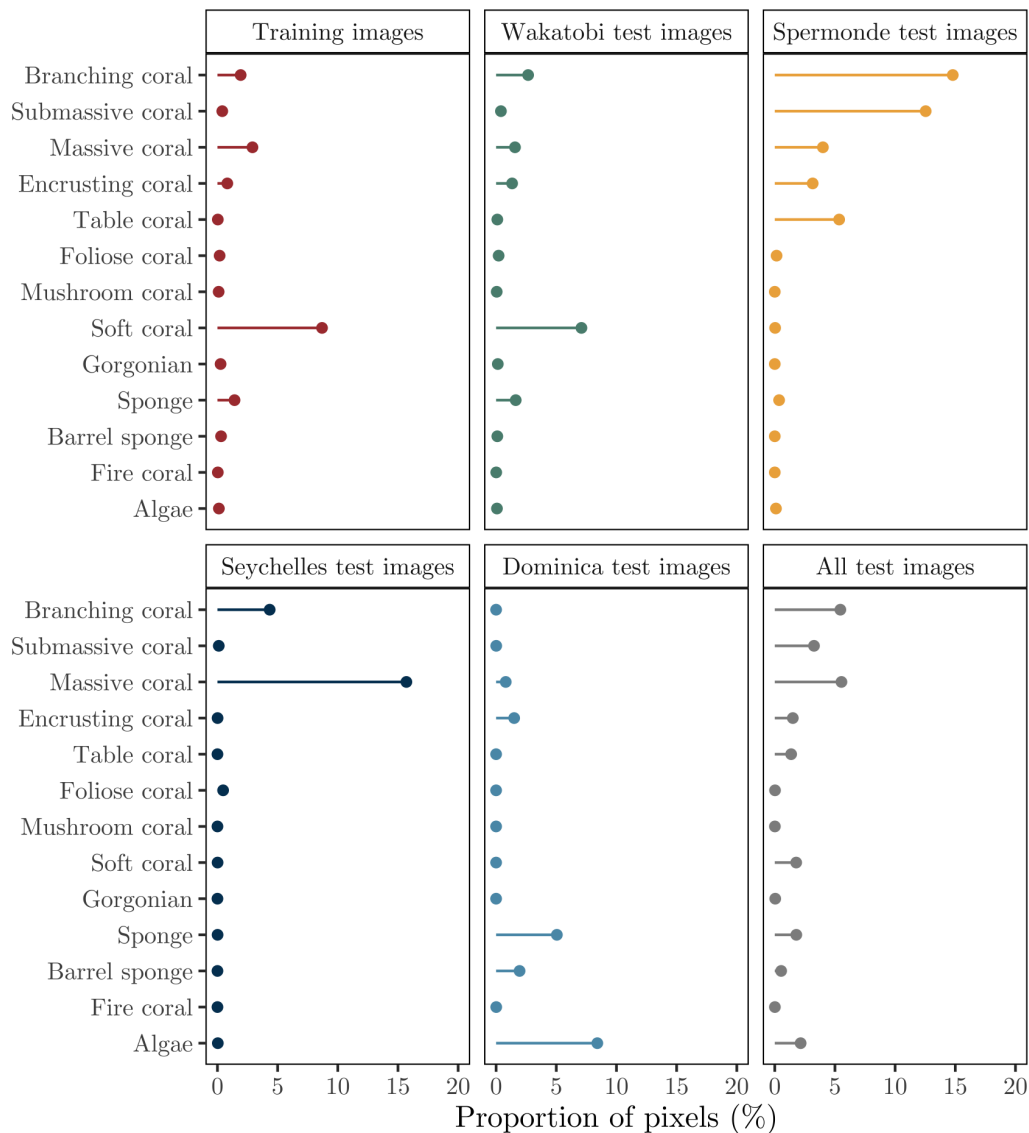


Figure 6.4: Analysis of the training and test data from the 2020 ImageCLEFcoral task showing classified benthic substrate pixel proportions (%) within the image set.

In the 2021 training dataset, classified pixels (20 % of total pixels) were predominantly composed of soft corals (27.84 % of classified pixels), massive corals (20.45 % of classified pixels), and branching corals (17.34 % of classified pixels). This reflects the patterns of substrate abundance from 2019 and 2020, and again will likely result in algorithms that are better at predicting these classes.

Table 6.3: Benthic substrate distribution, as a percentage of pixels with an associated substrate class (20 % of training image pixels; 23 % of test image pixels) in the ImageCLEFcoral 2021 image set. Background pixels were not annotated (80 % of test image pixels; 77 % of test image pixels).

Substrate class	Pixel representation %	
	Training images	Test images
Branching coral	17.34 %	24.28 %
Submassive coral	8.50 %	19.57 %
Massive coral	20.45 %	10.83 %
Encrusting coral	5.79 %	4.30 %
Table coral	3.16 %	9.81 %
Foliose coral	0.94 %	0.03 %
Mushroom coral	0.30 %	0.05 %
Soft coral	27.84 %	2.48 %
Gorgonian	0.71 %	0.14 %
Sponge	7.68 %	14.89 %
Barrel sponge	2.02 %	1.31 %
Fire corals	0.09 %	0.03 %
Algae	5.18 %	12.28 %

## 6.4 ImageCLEFcoral submissions

ImageCLEF tasks are open to submission from teams across the globe. For ImageCLEFcoral each team could submit up to 10 runs, where 1 run is one round of predictions generated by the network, per task (Table 6.4). In 2019, five teams produced results for one or both of the subtasks. In 2020, four teams produced results for one or both of the subtasks, with one team having also participated in the 2019 task. In 2021, three teams produced results for one or both of the subtasks, with two team having also participated in either the 2019 or 2020 editions of the task.

Table 6.4: Teams of the ImageCLEFcoral task

Year	Team	Institution	Number of runs	
			Subtask 1	Subtask 2
2019	ISEC [196]	Coimbra Institute of Engineering	1	0
	VIT [197]	Vellore Institute of Technology	5	0
	HHUD [198]	Heinrich Hein Universität Duesseldorf	9	1
	SOTON [NA]	University of Southampton	0	3
	MTRU [199]	University of Essex	0	1
2020	FZ PiVa [200]	University of West Bohemia	10	10
	FZ CV [201]	University of West Bohemia	2	1
	HHUD [202]	Heinrich Hein Universität Duesseldorf	10	0
	FHD [203]	Fachhochschule Dortmund	10	10
2021	Pilsen Eyes [204]	University of West Bohemia	2	1
	UAlbany [205]	University of Albany	1	0
	MTRU [206]	University of Essex	0	4

## 6.5 Results

### 6.5.1 Subtask 1 - annotation and localisation

#### 2019 annotation and localisation

When focusing on subtask 1, coral reef image annotation and localisation, teams were required to produce an annotated bounding box around each substrate in an image. HHUD, VIT, and ISEC each produced runs for this subtask, with the HHUD team being most successful in terms of mAP 0.5 IoU in 4 of their 9 runs (Table 6.5).

HHUD’s approach began by augmenting the dataset through noise and blur to maintain the bounding boxes within the training data, and generated a new data set from the bounding boxes themselves to triple the volume of images available to train their network on. They then increased the contrast of all images and sharpened each pixel according to neighbouring pixels. They used two methods in their runs, the first of which applied a You Only Look Once (YOLO) approach and the second that they developed independently. YOLO takes the entire image into account when predicting bounding boxes, rather than splitting it like R-CNN approaches, by dividing the image into square cells and predicting bounding boxes inside. The features of the entire image are therefore kept intact and inform the algorithm, reducing background errors by accounting for image context. The

Table 6.5: Results of ImageCLEFcoral 2019 subtask 1, from the top down showing the most successful per the mAP 0.5 IoU metric.

Run ID	Team	Approach	mAP 0.5 IoU	mAP 0 IoU	R 0.5 IoU
27417	HHUD	YOLO	0.243	0.488	0.131
27416	HHUD	YOLO	0.229	0.501	0.131
27419	HHUD	YOLO	0.220	0.442	0.122
27418	HHUD	YOLO	0.210	0.455	0.122
27349	VIT	R-CNN	0.140	0.431	0.068
27348	VIT	R-CNN	0.134	0.424	0.072
27115	VIT	R-CNN	0.085	0.424	0.046
27350	VIT	R-CNN	0.048	0.287	0.029
27347	VIT	R-CNN	0.041	0.272	0.027
27421	HHUD	Custom	0.003	0.205	0.004
27414	HHUD	Custom	0.003	0.228	0.004
27415	HHUD	Custom	0.003	0.291	0.005
27398	HHUD	Custom	0.003	0.272	0.004
27413	HHUD	Custom	0.002	0.203	0.003
27497	ISEC	Random Forest	0.001	0.001	0.001

strength of a predicted bounding box and the probability of its associated label are calculated across several steps throughout the YOLO algorithm. HHUD’s own method was based on the principle that the background across all images looks different to the labelling categories and looks similar across all images. From this, they split each image into “tiles” and extracted the tiles’ colour, texture, and shape features. These features were then used to train a binary classifier to distinguish areas of “coral” (or substrate classes) and non-coral (background) reef. After finding their bounding boxes, semantic labels were assigned using k-nearest neighbour ( $k = 15$ ) and by CNN with a simple and then deeper approach using a pre-trained VGG19 network with transfer learning, an already popular method.

The VIT team [197] was less successful than some of HHUD’s runs, but more successful than others and than the run of ISEC (Table 6.5). They augmented the dataset using horizontal and vertical flips of the images, as well as with  $90^\circ$  rotations and random contrast and brightness adjustments. VIT then used faster R-CNN variants. Faster R-CNNs expand on the capabilities of standard CNNs by applying the CNN algorithm to generate a feature map, but then utilise a separate network for localisation and a pooling layer to classify said localised position, whereas CNNs themselves cannot predict multiple instances of an object within one image. Three separate backbones were used (NasNet, Inception V2, and ResNet-101), all of which are pre-trained with 300,000 images across 80

categories. The VIT team further trained the networks with the provided training images.

The ISEC team had the poorest overall performance of any team in their single submitted run (Table 6.5). They calculated the mean, standard deviation, entropy of greyscale version of the image and hue ratio within a  $5 \times 5$  pixel neighbourhood around each pixel within an image and used a variety of models to test for classification accuracy. They determined that a random forest algorithm provided the best outcome, which uses decision trees to determine a substrate class for a particular region.

### **2020 annotation and localisation**

All teams produced runs for this subtask, with the FZ PiVa team being most successful in terms of mAP 0.5 IoU in four of their 10 runs (Table 6.6).

Ignoring location and focusing on substrate classification alone, no run performed better than others in all classes (Table V.3). Best performance in all classes except soft corals were found in runs by HHUD and FHD, which did not perform best overall (Table 6.6). The best soft coral performance was seen in the worst overall run from FZ PiVa (run ID 67857), which was also the highest overall IoU per benthic substrate class.

When adding in location as a factor, again no team outscored any other across all substrate classes in a run (Table V.4). Soft corals had the second best performance in any run with 0.5116, while branching corals had the highest score (0.5925) in a run with relatively poor performance in the other substrate categories. Unexpectedly, this high branching coral accuracy came from the Seychelles (the ecologically similar but geographically distinct) and not the Wakatobi (same) or Spermonde (similar ecologically and geographically). Most of the highest substrate scores were seen in the test data from the Wakatobi (same location as training set), with the runs from FHD and FZ PiVa each having 5 top scoring categories.

### **2021 annotation and localisation**

The Pilsen Eyes team was the most successful in terms of mAP 0.5 IoU in both of their runs for subtask 1 (Table 6.7).

Table 6.6: Results of ImageCLEFcoral 2020 subtask 1, from the top down showing the most successful per the mAP 0.5 IoU metric.

Run ID	Team	Approach	mAP 0.5 IoU	mAP 0 IoU
68143	FZ PiVa	R-CNN	0.582	0.853
67863	FZ PiVa	R-CNN	0.565	0.851
68094	FZ PiVa	R-CNN	0.530	0.825
68145	FZ PiVa	R-CNN	0.517	0.814
67539	FZ CV	SSD	0.490	0.822
68181	FHD	R-CNN	0.457	0.775
68188	FHD	R-CNN	0.440	0.725
67862	FZ PiVa	R-CNN	0.439	0.774
68187	FHD	R-CNN	0.424	0.729
68182	FHD	R-CNN	0.422	0.762
68146	FZ PiVa	R-CNN	0.415	0.747
68186	FHD	R-CNN	0.410	0.730
68183	FHD	R-CNN	0.405	0.759
68201	HHUD	RetinaNet & YOLO	0.392	0.806
67914	FHD	R-CNN	0.391	0.720
68184	FHD	R-CNN	0.388	0.707
67919	FHD	R-CNN	0.383	0.703
68138	FZ PiVa	R-CNN	0.377	0.721
68185	FHD	R-CNN	0.369	0.722
67858	FZ PiVa	R-CNN	0.357	0.712
68093	FZ PiVa	R-CNN	0.349	0.709
67857	FZ PiVa	R-CNN	0.347	0.728
68202	HHUD	Unknown	0.323	0.753
68198	HHUD	Unknown	0.313	0.702
68205	HHUD	RetinaNet & YOLO	0.303	0.727
68196	HHUD	Unknown	0.280	0.684
68212	HHUD	RetinaNet	0.263	0.663
68197	HHUD	Unknown	0.245	0.628
67558	FZ CV	R-CNN	0.243	0.664
68213	HHUD	Unknown	0.233	0.644
68178	HHUD	Unknown	0.010	0.206
68179	HHUD	Unknown	0.010	0.274

Table 6.7: Results of ImageCLEFcoral 2021 subtask 1, from the top down showing the most successful per the mAP 0.5 IoU metric.

Run ID	Team	Approach	mAP 0.5 IoU
138115	Pilsen Eyes	R-CNN	0.121
137821	Pilsen Eyes	R-CNN	0.105
139118	UAlbany	Wave-CLASS	0.001

## 6.5.2 Subtask 2 - pixelwise parsing

### 2019 pixelwise parsing

When focusing on subtask 2, coral reef image pixel-wise parsing, teams were required to produce an annotated polygon around outlining each substrate in an image. MTRU, SOTON, and HHUD each produced runs for this subtask, with the MTRU team being most successful in terms of mAP 0.5 IoU in their 1 run (Table 6.8).

Table 6.8: Results of ImageCLEFcoral 2019 subtask 2, from the top down showing the most successful per the maP 0.5 IoU metric.

Run ID	Team	Approach	mAP 0.5 IoU	mAP 0 IoU	R 0.5 IoU
27500	MTRU	DeeplabV3	0.042	0.240	0.049
27343	SOTON	DeeplabV3+	0.000	0.048	0.002
27324	SOTON	DeeplabV3+	0.000	0.090	0.000
27212	SOTON	DeeplabV3+	0.000	0.071	0.000
27505	HHUD	YOLO	0.000	0.000	0.000

The MTRU team augmented the image dataset primarily using random cropping, with 16 squares of varying sizes per image. All crops were then scaled to the same size and randomly flipped vertically and horizontally to further augment the data. This trained their network on a range of scales and orientations of the substrate classes in an attempt to combat the model overfitting utilising DeeplabV3, which avoids a separate post-processing model. MTRU used a ResNet-101 backbone for feature extraction (but noted that others could be used). To finalise their training, areas of images with poor network performance were cropped and removed, and the network was then retrained on the remaining image sections. Post-processing work included polygon approximation and other basic algorithms to adapt the data to the submission format.

The SOTON team submitted 3 runs, only one of which produced a positive mAP 0.5 IoU value, which used a pre-trained DeeplabV3+ network, further trained with the ImageCLEF coral training set using a one-versus-all pixel-wise classifier. This method trains binary classifiers to recognise one particular substrate category. As with several other teams, their pre-processing augmentation involved rotating, flipping, and shearing the training images. Their output utilised a conditional random field, which adds contextual information to the model using previously predicted semantic labels, to assign substrate categories to polygons.

The HHUD team used their previous approach (Section 6.5.1) in their run for this subtask, but did not produce a positive result in any evaluation metric (Table 6.8).

Both SOTON and HHUD submitted self-intersecting polygons, which were excluded from evaluation as they produce invalid geometry, where some sections with overlapping edges would be classed as both inside and outside of the polygon at the same time.

## 2020 pixelwise parsing

Three of the four teams produced runs for this subtask, with the FZ PiVa team once again being most successful in terms of mAP 0.5 IoU in 6 of their 10 runs (Table 6.9).

Table 6.9: Results of ImageCLEFcoral 2020 subtask 2, from the top down showing the most successful per the maP 0.5 IoU metric.

Run ID	Team	Approach	mAP 0.5 IoU	mAP 0 IoU
67864	FZ PiVa	R-CNN	0.678	0.845
68139	FZ PiVa	R-CNN	0.664	0.842
68095	FZ PiVa	R-CNN	0.629	0.817
68142	FZ PiVa	R-CNN	0.624	0.813
68144	FZ PiVa	R-CNN	0.617	0.807
68147	FZ PiVa	R-CNN	0.507	0.727
68190	FHD	R-CNN	0.474	0.715
68137	FZ PiVa	R-CNN	0.470	0.701
67968	FHD	R-CNN	0.469	0.708
67965	FHD	R-CNN	0.453	0.720
67964	FHD	R-CNN	0.449	0.717
67856	FZ PiVa	R-CNN	0.441	0.694
67967	FHD	R-CNN	0.435	0.695
68092	FZ PiVa	R-CNN	0.434	0.689
67963	FHD	R-CNN	0.433	0.694
68192	FHD	R-CNN	0.424	0.668
68191	FHD	R-CNN	0.416	0.692
68140	FZ PiVa	R-CNN	0.407	0.675
679669	FHD	R-CNN	0.376	0.629
68189	FHD	R-CNN	0.371	0.632
67620	FZ CV	R-CNN	0.304	0.602

When only considering substrate classification, similar to subtask 1 there was no clear run that excelled with predicting all classes and locations (Table V.5). FHD did have the highest scores in all substrates except submassive hard coral across all of their submitted runs, with the highest overall substrate prediction being 0.545 for soft coral. Submassive hard coral was best predicted by FZ PiVa at 0.026.

Taking location into account (Table V.6), FHD had the best run with the Wakatobi



test set (same location), predicting all classes except fire coral, branching hard coral, and submassive hard coral with greatest precision. Submassive corals were best predicted by FZ PiVa, also in the Wakatobi region. Fire coral were not predicted accurately in any location by any team, with scores of 0 in all runs, likely due to rare occurrence. Branching corals were predicted with a score of 0.718, the highest of any substrate class, by FHD in the Seychelles, the ecologically similar but geographically distinct location.

## 2021 pixelwise parsing

Chapter 7 details the 2021 edition of subtask 2 where, instead of organising, a series of participation runs were submitted. mAP 0.5 IoU scores are outlined in Table 6.10.

Table 6.10: Results of ImageCLEFcoral 2021 subtask 2, from the top down showing the most successful per the maP 0.5 IoU metric.

Run ID	Team	Approach	mAP 0.5 IoU
139084	Pilsen Eyes	R-CNN	0.075
138389	MTRU	DeeplabV3	0.021
138443	MTRU	DeeplabV3	0.018
138411	MTRU	DeeplabV3	0.017
138449	MTRU	DeeplabV3	0.011

## 6.6 Discussion

The first edition of the ImageCLEFcoral task confirmed the suspected challenges that marine environments pose to automatic annotation. The use of low-cost action cameras to collect images adds a dimension of difficulty that is highlighted by the results of the task in its first year. The varying accuracy of subtask runs overall (Tables 6.5 and 6.8) and per benthic substrate (Table V.1 and V.2) highlight the difficulties raised. The prevalence of self-intersecting polygons in subtask 2 and their subsequent exclusion from evaluation may have compounded the already demanding task and caused the low performance.

In 2020, the four highest mAP 0.5 IoU scores were over double that of 2019 when looking at subtask 1 (annotation and localisation). This drastic improvement demonstrates that annotation of lower quality substrate images is possible with moderate success. However, the lesser value of this task was highlighted by the FHD team, who were able to increase subtask 1 performance by redefining the bounding boxes themselves. The range

of non-normal shapes found in the substrate classes is clearly not best suited to this type of annotation and it may not be worthwhile to include in future versions of the task.

The best run in 2020 was submitted for subtask 2 (pixelwise parsing), the more challenging of the two subtasks. This run showed a large improvement from the best subtask 2 run of 2019 (2019 = 0.042, 2020 = 0.678). This improvement is likely due to the increased training data made available for model training, and again highlights that the pixelwise parsing task is likely the most viable for future years of ImageCLEFcoral. As such, there is a clear need for an increased volume of data, particularly for the rarer substrate classes as these were often the worse scoring in evaluation metrics.

In both subtasks in 2020, branching corals were predicted better than any other substrate class, both in the Seychelles region. This suggests that some substrate classes, potentially those with more distinct morphological structure, are more able to be recognised through transfer learning than others. The disparity in accuracy of predicting specific substrates and overall scores for FHD could show issues within their approach when detecting smaller polygons. Unexpectedly, the FZ CV team found that the models used for both subtasks had greater power when predicting test images than the training images they used for validation. This could be indicative of the capabilities of future algorithms to be used on global datasets, as is one of the aims of the ImageCLEFcoral challenge.

The drop in mAP 0.5 IoU scores in both subtasks in 2021 when compared to previous years is most likely due to the compounding difficulty when adding a variety of locations to an already complex training dataset. The variation in substrate morphology from geographically distinct reefs is well documented [207] and would hamper any algorithms ability to predict classes with accuracy due to the contradictory appearances being defined under the same semantic label. Even with an increased dataset it is likely that different algorithms would be needed for this task based on geographical location, but thus far the scale to which on algorithm could be relied upon is unknown.

### 6.6.1 Challenges of ImageCLEFcoral

Underwater imagery is often lower quality than that taken on land. Light attenuation distorts colour detection, water turbidity can reduce image quality and with all underwater imagery there is a greater chance for blurred or unfocused photographs. Taking steps to investigate, process and augment the provided data is expected to improve the data quality

and subsequent network results [200, 203]. There are several approaches to underwater image enhancement that can provide balanced colouring and contrast across large data sets without individually editing each photograph/still. Rayleigh enhancement is commonly used [202, 203, 208, 209] and is based upon image histogram stretching to balance colour input channels. Red-channel restoration has also been successful in improving the quality of a range of underwater imagery, including coral reef images [210]. Another method to balance the red channel commonly lost in marine imagery exploits the remaining colour input channels in an image for colour balance [195].

The number of images required to train a model to annotate regularly shaped objects (i.e. buildings, cars) is extensive. The added difficulty of indistinct, irregular geometry with a lack of colour differentiation requires even more images that were simply not available to the ImageCLEF task. Adding further data with external image sets was suggested to 2021 participants, but the difference in annotation and image styles was apparent when adding this dataset did not improve the accuracy of substrate classification, but instead reduced it greatly.

The time frame of the task may also be a limiting factor towards its success, though repeating teams have access to previous data and can continue to improve their algorithms throughout the year. The limited time may be a benefit in some cases, where teams are able to push for results in a Hackathon style and produce short but meaningful improvements each time they come together to work on their model.

The semantic labels selected for the ImageCLEFcoral task were chosen morphologically to simplify the challenge as much as possible. These labels may not link well enough to biological surveys to be useful as yet, but will be a good starting point to develop an algorithm to work from. Once this version of the task is a success, a collaboration with marine researchers may yield more beneficial semantic labelling to be used in further annotations.

## 6.7 Summary

The overarching aim of ImageCLEFcoral is to add substrate labelling to reconstructed 3D coral reef models and to create a globally applicable model to annotate coral reef substrate images. The first edition of the task in 2019 set the baseline with test and

training images from a single location, 2020 added test images from three other locations of varying similarities to the original region, and the 2021 edition of the task completed image sets that combine to generate 3D models of coral reef environments. Continuing the ImageCLEFcoral task with more image data should lead to improving results that may eventually be able to fulfil these aims. Whether this is by creating one global algorithm, or by creating a method for each biogeographical coral reef region, is yet to be determined.

The direct annotation of 3D models is highly complex, as the link between the dense cloud points and a specific reef substrate would be exceedingly challenging. It was then hypothesised that annotating 2D images before model construction and utilising the semantic labels in the photogrammetric pipeline would generate a 3D reconstructed reef system with associated substrate labels [211]. The data capture is directly linked to the 3D modelling aim, with action cameras set to video or time-lapse to collect images instead of using DSLR cameras. This does impact image quality in terms of blurring, contrast, and colour balance, but it is important as these cameras are commonly used in marine monitoring projects [48, 51, 52] and link this task to real world applications of coral reef conservation.

# 7 | Using global data for automatic annotation

## 7.1 Introduction

Deep learning algorithms may provide an answer to automatic annotation in marine environments [64]. The underlying architecture of most is the Convolutional Neural Network (CNN), often used for image and pattern recognition [212]. CNNs have been utilised in benthic annotation studies across a range of substrates with varying success. Focusing on object detection, CNNs have been successful in counting and identifying a range of benthic fauna [62, 213, 214, 215]. At a larger scale, CNNs have been used with satellite imagery to successfully (with 80-85% accuracy depending on the image source) identify coral, seagrass, sediment, and other coral reef associated substrate at a global scale [216].

There have been several examples of CNN use looking specifically at annotation within a coral reef environment [59, 194]. This type of task presents particular difficulties due to the nature of reef characteristics. Coral colonies of different species or genera can look highly similar, while coral colonies of the same species can look highly distinct due to a range of factors. Some benthic organisms are much more prevalent than others and image representation is often highly skewed towards these substrates [188, 189], so it is often challenging to provide adequate training data for certain classifications. Often, openly available annotated data sets focus on a combination of broad categories (i.e. “sand”, “rock”) and highly specific ones for those species/genera that are most prevalent (e.g. the EILAT dataset).

Attempts at classifying coral reef substrate from close-up imagery have been highly successful on some data sets [63], though this “zoomed-in” style of imagery would not necessarily translate to success in the annotation of larger regions that encompass many

different substrate classes within a single image. Where images of multiple substrate types are used, generally annotations are applied only to certain pixels instead of aiming to accurately annotate the entire visible substrate [154, 217], or focus entirely on specific scleractinian corals without annotating any other substrate features [194, 218].

This chapter details the work behind four submissions to the 2021 ImageCLEFcoral task attempting to improve upon the previous yearly results to automatically annotate coral reef substrates. An adaptation of the MTRU 2019 approach to ImageCLEFcoral task (Section 6.5.2) [199] was used to focus on merging the ImageCLEF data with an additional data set from NOAA NCEI, focusing on subtask 2 (pixelwise annotation; Section 6.2) as it was considered more valuable for practical use in monitoring reef systems accurately.

## 7.2 Methodology

### 7.2.1 Supplementing the ImageCLEF dataset

The ImageCLEFcoral 2021 task run provided 879 images with a combined 21,748 annotations as training data followed by 485 unannotated test images at a later date. As with previous years, the annotations were not evenly split across classes, likely as some are more prevalent than others in reef systems (Fig. 7.1). The NOAA data set had 15,019 available images, each with 10 single-pixel points annotated. Machine limitations allowed for 3,032 images to be downloaded; server timeout required restarting the download, which would begin from the first image instead of allowing for specific images to be selected, preventing further data being made available for the training set. Timeout limits could not be changed. The additional NOAA images then had to be further reduced to enable model training in a reasonable timeframe, again due to server timeout limitations.

To refine the NOAA images, five lesser represented substrate classes were selected for: Fire Coral - *Millepora*, Hard Coral - Foliose, Hard Coral - Table, Hard Coral - Sub-Massive, and Hard Coral - Encrusting. Though they also had few annotations, Soft Coral - Gorgonian, Hard Coral - Mushroom, and Sponge - Barrel were not chosen from the NOAA data set as they have more distinct morphologies than the selected classes, so were more likely to be predicted despite relatively few occurrences. Algae - Macro or Leaves were also not selected from the NOAA data set despite low incidence. Algae classification of the ImageCLEF set only accounted for large leaf macroalgae, whereas the NOAA data

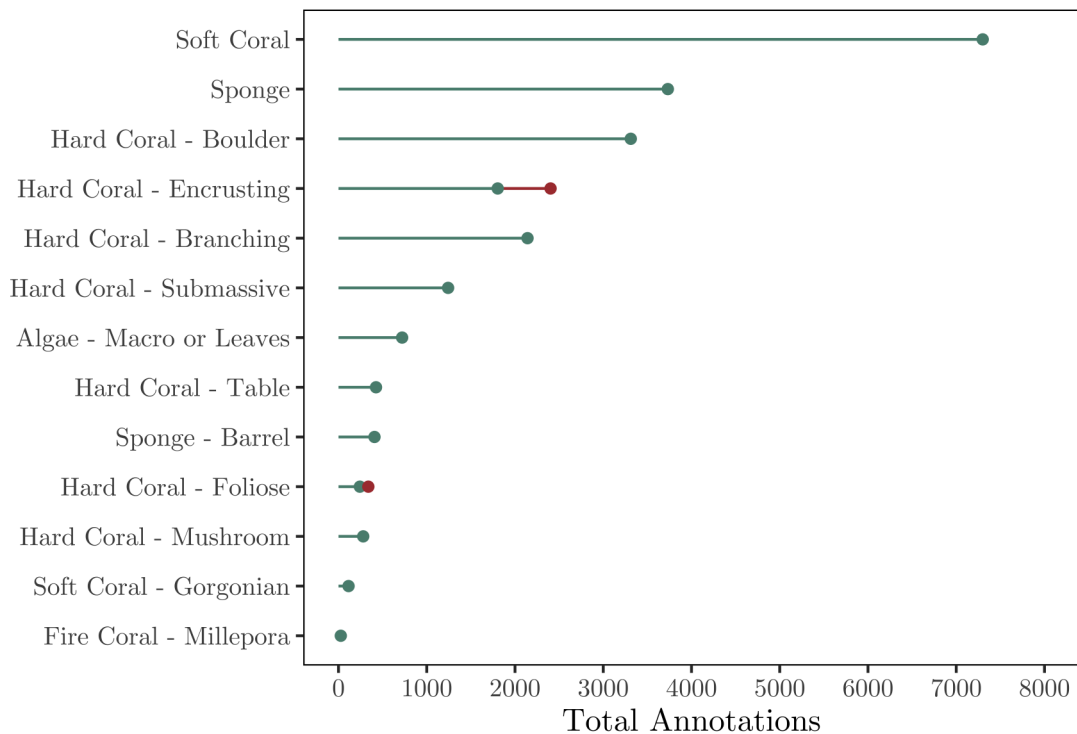


Figure 7.1: Substrate annotations in the ImageCLEF training set of 879 images ( $n = 21,748$ ; green), and the additional NOAA images added to the Hard Coral - Encrusting and Hard Coral - Foliose classes ( $n = 502$ ; red) to increase the total number of training images ( $n = 22,403$ ).

set also included other types such as turf and CCA, so conflicting annotations could have hampered the model predictions. 502 viable NOAA images were found, within which two of the five selected classes were found: Hard Coral - Encrusting and Hard Coral - Foliose. This almost doubled the processing time per epoch (wherein all training data is scanned by the network once), pushed the entire model training time from 10 hours to 17.5 hours (10 epochs total), and only increased the total number of substrate annotations from 21,748 to 22,403 (Fig. 7.1). The increased effort required for the additional data is unlikely to balance with significantly increased predictive power in the model at this scale, but the annotations were still utilised to test this process.

The NOAA data set contains a greater number of classification labels than the ImageCLEFcoral classes. These classifications are of a single pixel (10 pixels per image) so did not provide enough information for the image analysis and recognition algorithms used here. A NOAA Translation processor was used to capture the classification types within the data set and translate them via an expert defined translation matrix into the ImageCLEFcoral classes. The processor then created an adjustable Region Of Interest

(ROI) around the same pixel to provide an image patch, typically a 10x10 pixel area, that enabled the machine learning routines to adapt to the NOAA data sets.

### Editing and augmenting images

Following the premise that processing the images would improve the data quality and subsequent network results [200, 203], images were visually assessed and split into those with accurate colouring and contrast, those with a heavy green tint and those with a heavy blue tint. Colour accurate images were not altered in any way. Green and blue images were passed through an RGB histogram leveller followed by an RGB channel mixer, generalised to green or blue images for speed (Fig. 7.2). This would allow all the images to be processed easily but would not allow for image-specific editing.

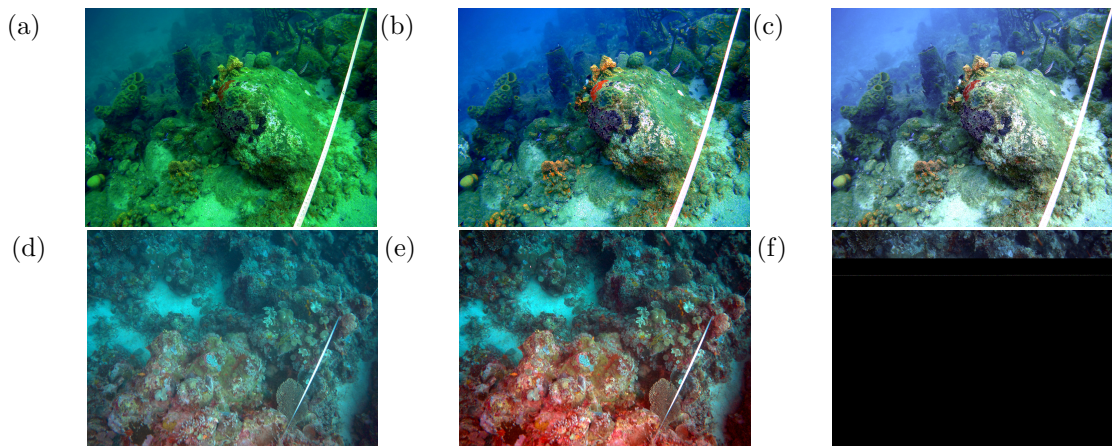


Figure 7.2: Transformation of (a) a green and (d) blue image through two stages to an image used in training. Each image had (b,e) balanced RGB levels, then (c,f) when through a generalised channel mixing process to balance the colours while maintaining image contrast. The leveling and mixing were selected to optimise substrate colour and contrast with less focus on the background and water colouring.

Before training the model, each image was cropped into 12 squares which were each then cropped at a random point to 480px<sup>2</sup>. Random horizontal flips were also utilized due to the limited amount of data. These pre-processing techniques present the model with different iterations of the same images, increasing the size of the data set available.

The test images were also cropped into 12 squares to match the training images used on the model. Each test image was then resized to a 520px square, which allowed us to predict all test images despite system limitations. The predicted pixel array of each test image was resized to its original dimensions before submission to match the ground truth annotation mask. This was carried out using spline interpolation through the zoom



function in SciPy<sup>1</sup>.

### 7.2.2 Submitted runs

#### The model

The base 2019 code utilised the DeepLabV3 model with a ResNet-101 backbone for feature extraction [199]. Atrous convolution was applied to increase the field of view of the final ResNet-101 layer with inserted 0-values in the network layer, followed by Atrous Spatial Pyramid Pooling (ASPP) for pixel labelling using the resulting atrous convolution rates. Evaluation of different crop and batch sizes found that a combination of 480 px<sup>2</sup> crops and batch size 4 to provide the greatest overall accuracy, in terms of mean average precision (mAP0.0 and mAP0.5), within system limitations.

Each team in the competition was allowed to submit up to 10 runs per task using the collaboration platform AICrowd<sup>2</sup>. We chose to submit four files to the pixelwise-parsing subtask only, representing four individual runs:

**MTRU1** - The “baseline” run, using the 2019 submission [199] that was rewritten and adapted by experimenting on crop  $\times$  batch size combinations. Batch size 4 with crop size 480 were found to give the best results and were used in this run.

**MTRU2** - The edited ImageCLEF run, using the same settings as MTRU1. Poorly coloured training images were enhanced to represent more accurate coloring of the coral reefs.

**MTRU3** - The NOAA run, using additional data from NOAA in three different substrates. The images were not enhanced or edited in any way, and the same settings from MTRU1 were used.

**MTRU4** - The fully edited run, using same settings as MTRU1, with both the additional NOAA data and image colour enhancements where needed.

All four runs predicted some images containing self-intersecting polygons. These polygons invalidate a run and are not permitted in the submission file so must be removed. The evaluation script was used to identify any images with self-intersecting polygons and

---

<sup>1</sup><https://docs.scipy.org/doc/scipy/reference/generated/scipy.ndimage.zoom.html>

<sup>2</sup><https://www.aicrowd.com>

the substrate type of the polygon. This process involved removing each polygon of the relevant substrate type one by one, re-running the evaluation script each time to check if the error was resolved.

Initial images were checked polygon by polygon in this manner to minimise any impact on model accuracy, but the time constraints of the challenge required faster processing of the latter runs. Images in these runs were checked in polygon “batches,” where several at a time would be deleted before running the evaluation script. While this did increase the speed of evaluation before submission, it is likely that a significant proportion of the deleted polygons were not self-intersecting and as such the mean average precision (mAP) of the runs would be both lower and less accurate.

Three of the four runs (2, 3 and 4) predicted images without any substrate class annotations. While clearly an error as all images were of coral reef substratum, these predictions were a part of our model outcome and therefore our submitted runs. The evaluation script used upon submission blocks these images and deem runs with them a failure so each had to be altered. As all images from the test set must be used, the blank images could not be removed. Our solution to this was to include a small square annotation in the center of the blank images and label it as Fire Coral - Millepora. This class was used as it had the lowest number of annotations and had no additional images added from NOAA images so was likely to be the least accurate class, limiting the effect on overall accuracy as much as possible. It could not be removed from analysis as all classes required predictions before submission, but any result for Fire Coral - Millepora should be considered invalid.

### 7.3 Results

Results provided by ImageCLEFcoral after submission used two metrics. mAP0.5 showed the localised mean average precision using intersection over union (IoU)  $\geq 0.5$ . Accuracy per substrate calculated the segmentation accuracy as the number of correctly labelled pixels of class over the number of pixels labelled with class in ground truth.

Overall results of the pixel-wise parsing subtask (Table 7.1) show that the MTRU runs were less accurate and precise than the Isoukup team. When considering the accuracy per class, however, there were some substrate categories that were better predicted by our

model.

Across the MTRU runs, we saw the highest accuracy of submassive coral, table coral and foliose coral predictions when images ran unedited and without additional NOAA data. The greatest prediction accuracy of boulder corals and algae across the subtask occurred when images were colour corrected, and of gorgonian soft corals occurred when unedited ImageCLEF data and NOAA data were used. MTRU3 was the only instance of gorgonian predictions with positive accuracy (0.002%) across all submissions. Similarly, MTRU1 was the only instance of positive accuracy in foliose coral prediction (0.097%). None of our runs predicted mushroom corals, sponges, barrel sponges, or fire coral accurately.

Of our runs, the greatest precision was seen in MTRU1 ( $\text{mAP}_{0.5} = 0.021$ ), though it did not have the highest accuracy (2.767%). MTRU4 was most accurate (2.951%) despite having the lowest overall precision ( $\text{mAP}_{0.5} = 0.011$ ).

Table 7.1: Overall precision ( $\text{mAP}_{0.5}$ ), average accuracy (%) and substrate class accuracy (%) of pixel-wise parsing subtask submissions to ImageCLEFcoral 2021. The best scores for each category are shown in red.

Category	MTRU1	MTRU2	MTRU3	MTRU4	Isoukup
mAP0.5	0.021	0.018	0.017	0.011	0.075
Average accuracy	2.767	2.531	1.942	2.951	6.147
Hard Coral - Branching	1.090	2.299	0.536	5.562	11.095
Hard Coral - Submassive	3.022	0.279	1.036	0.039	2.704
Hard Coral - Boulder	9.607	12.787	7.601	8.827	5.385
Hard Coral - Encrusting	0.017	2.595	0.729	2.429	2.615
Hard Coral - Table	0.353	0	0	0	0.008
Hard Coral - Foliose	0.097	0	0	0	0
Hard Coral - Mushroom	0	0	0	0	0
Soft Coral	0	0	0.228	0	50.433
Gorgonian	0	0	0.002	0	0
Sponge	0	0	0	0	1.625
Barrel Sponge	0	0	0	0	0.329
Fire Coral - Millepora	0	0	0	0	0
Algae	0	0.027	0	0	$1.0e^{-4}$

Overall precision and average accuracy were also lower than the 2019 run of this model [199], however we did show improvement in the prediction of submassive corals (MTRU1 = 3.022%, 2019 = 0%) and table corals (MTRU = 0.353%, 2019 = 0%), neither of which were predicted with any accuracy in 2019.

The colour adjustments made to the images increased the prediction accuracy of boul-

der corals, encrusting corals, and algae (Table 7.1). Submassive corals were less accurately predicted with image enhancement, as well as table corals, foliose corals, soft corals, and gorgonians.

Of the two categories with increased annotations from the NOAA data set, encrusting corals saw a greater accuracy while foliose corals had a lower prediction accuracy. Adding NOAA data had a detrimental effect on the accuracy of most other substrate categories. Where a prediction accuracy  $> 0$  without NOAA data (MTRU1 and MTRU2), adding NOAA annotations reduced the prediction accuracy of submassive, boulder, and table corals as well as algae. Accuracy also decreased for branching corals between MTRU1 and MTRU3 (unedited images), but increased between the colour enhanced runs (MTRU2 and MTRU4) by 5.026%. Predictions were also more accurate for soft coral (+0.228%) and gorgonians (+0.002%) when NOAA data was added but no colour enhancement was performed.

## 7.4 Discussion

Losses in predictive power in runs with image enhancement is likely due to the general nature of the colour correction performed. While some images would improve with the balancing and mixing at the levels set, others may have had colour blow outs or excessive input from one or more RGB channels [208]. This could have a blur-like effect, wherein neighbouring substrate categories look indistinct from each other due to a lack of colour definition [195].

For boulder corals, colour enhancement may have distinguished them from other reef substrates and enabled greater recognition of the coral over rocks and other substratum that they can easily resemble. Encrusting corals would benefit for the same reasons. Algae would likely show improvement with colour enhancement due to the removal of green image tints, which would allow the natural green of the algae to become more defined and clear [208]. Brown and red algae would also benefit from the red channel correction to make them more distinct from surrounding substrate [210].

The increased accuracy in predictions of branching corals, soft corals, and gorgonians in colour enhanced runs could be explained by the more distinct morphologies formed by these categories across all locations that may have become more distinguishable with an

increasingly balanced data set at the expense of the other classes. Although the soft coral category encompasses several distinct organisms with different morphologies, the abundance of annotations likely compensated by providing many examples of each structure.

The NOAA data used was from a different location than the ImageCLEF data which could greatly impact mAP0.5 and prediction accuracy as substrates from different geographic regions can show vastly different morphologies. Encrusting corals are very similar globally despite varying conditions, so increasing the number of annotations would likely improve the models predictive power by adding distinctive pixels to train on. This is not the case with foliose corals, which are more likely to show differing morphologies as they are not flat to the substrate. Foliose corals also have extensive structures that often appear layered and often appear to have many shadows that could hamper the training capabilities of the model. Any shadows would look like black regions of the image, probably with a flat texture [219]. These would provide no benefit to the model and may cause it to relate any dark spots to foliose corals or to fail to recognise them at all. The reduced accuracy across several categories with added NOAA data could occur if the additional NOAA annotations skewed the models perception of each category and altered the predictions made as a result.

#### **7.4.1 Limitations of the model**

The use of a dedicated GPU greatly increases the computational power of machine learning models. Training time can then be diminished and hyperparameters can be improved. The machine we used to run our model was affected by a lack of GPU memory, which can only be rectified by changing the graphics card to a more powerful one. The memory limitation heavily impacted batch sizes testing, limiting tests to batch size 4 at most. DeepLabV3 works best with a batch size of 16 (demonstrated on the PASCAL VOC data set [220]). Using a computer with a better GPU would allow for a greater batch size to be used which would improve the model parameters and strengthen the power of the predictions.

#### **7.4.2 Improving the approach**

In the future, including a greater volume of NOAA data may prove beneficial when training the model by increasing the number annotations per class across the training

data. More specific pixel expansion would also enable more precise training and may provided more pixels per class than otherwise achieved. A potential method could have different expansion shapes set by class (i.e. boulder coral expands as a circle) and a pixel selection/rejection threshold based on annotated pixel value.

Images and predictions would likely benefit from a more tailored colour correction approach. This could be performed with the commonly used Rayleigh distribution [203, 208, 209] or with a different approach such as red channel weighted compensations [195] that leverage the other colour input channels to colour balance an image with accuracy. The addition of fluorescence imagery to accompany the standard pictures captured may reduce prediction errors [61], though is likely impossible to procure for the already captured areas. Newly added data would enable this type of image to be included, though it would require more specialist equipment that would impede the low-cost and repeatable premise of the ImageCLEFcoral task.

Using the results from this approach, developing a staggered pipeline may improve prediction accuracy in the future. A bounding box approach to gain a generalised location of each substrate could be used to then send images through different processing steps, such as colour correction, blur reduction, contrast changes, etc, based on the class found. This could then feed into a pixel-wise prediction model to find precise location of substrate classes within an image.

## 7.5 Summary

Image colour enhancements can increase the accuracy of coral reef substrate predictions when those substrates are otherwise difficult to distinguish from the surrounding environment. It can also be detrimental when the editing performed is generalised instead of image specific. Similarly, augmenting the training data set with annotations from other sources can improve the predictions of substrates that are either morphologically general across different geographical regions or those that form distinct structures despite changing geography. Large increases in the number of annotations should be reflected in a subsequent increase of accuracy in the represented classes. When this does not occur, the abundance of data can impair the predictive power of the model by blurring the line between substrate categories through incorrect annotation or by skewing the predictions

made as a result of an imbalanced data set.

A combination of an augmented data set with distinct image enhancement pathways for either different geographic locations or substrate categories may provide a more accurate and precise prediction array. Combining these steps with improved hyperparameters would enhance model performance and provide a coral reef substrate prediction tool that would be applicable to reefs across the globe.

# 8 | Discussion

## 8.1 Key findings

The work throughout this thesis primarily aimed to trial and improve upon computational approaches used in the monitoring of marine reef systems. To do this, three questions were defined:

- Can multiple cameras be used to the same accuracy of single cameras in Structure from Motion photogrammetry in less time?
- Are coral reef complexity metrics developed for tropical systems of use to temperate habitats?
- Can coral reef substrates be automatically annotated from 2D images accurately?

Here, the outcomes of each area of work are discussed and interlinked to contextualise the efficacy, benefits, and limitations of this type of methodology.

### 8.1.1 Multi-camera arrays for coral reef surveying

To begin a comparison of modelled complexity, 3D models of the coral reef environment must be created. Despite SfM becoming a regularly used approach [48, 3], the parameters used for model processing are often stated without explanation or not at all [47, 49]. This raises the question of how impactful SfM processing quality could be on a model and subsequently extracted data.

All data collected here relied upon action cameras of similar quality so the effect of varying equipment could not be investigated. However, this did enable a clear view on the impact of quality at each build stage relative to two coral reef environments (one relatively pristine and one highly degraded). Results showed that low quality image alignment performed as well as higher quality settings on the small scale ( $\approx 4\text{m}^2$ ) models created,



but that later build stages had increasing quality with each improved setting selection. With higher quality dense cloud settings a more concentrated point cloud was produced, as could be expected. From a model's dense cloud, a mesh is generated to form a single connected surface over the model by connecting adjacent dense cloud points into "faces". As such, the face count setting will create more polygons from connected points at higher quality settings to form a more detailed mesh. This mesh is often what is used to extract data from the model itself. Unexpectedly, increasing face count had no impact on mesh quality. In practical terms, this implies that the quality of a model's dense cloud is likely to impact the accuracy of extracted data more so than the mesh. Mesh quality was the only setting effected by site, though further investigations would be needed to determine the cause of this difference. The overarching conclusions to be drawn here are that, when processing images to create a model, the selection of appropriate settings is a balance between computational power, time, and desired quality. Further testing comparing a combination of settings with complexity metrics extracted from models may reveal the need for a minimum standard of build quality and should be carried out when using new equipment or when in new environments. Larger image sets/models should also be investigated to evaluate any changes in setting requirements to render an accurate model that can be used in complexity assessments.

Once model processing settings were determined, a comparison of captured complexity from 3D models could take place. Comparing a group of metrics through a single camera technique that has been previously evaluated [48] allowed the multi-camera array to be tested against a precise method. When comparing the captured complexity of single versus multi-camera image capture, exact data extraction proved challenging. The placement of associated reef complexity helper files on models of different scales was challenging, mainly when locating the exact positioning of the 2×2 m quadrats within the larger 4×6 m quadrat. Any shift in the position of these helper files would change the output complexity, nullifying the power of the comparison. Instead, specific ground-truthing relevant to the multi-camera array (with each common number of cameras) should be carried out *in-* and *ex-situ* to determine the exact discrepancies in real to modelled complexity for the array alone, without the need to compare it to already established metrics.

Testing the multi-camera array against a single camera showed that site set-up and image capture could be performed more rapidly at a greater scale (Fig. 8.1). Visual

assessment of models also showed good rendering capabilities (Fig. 8.2). Though they did take longer to reconstruct on a per-model basis, likely due to the larger volume of images involved, processing for one larger model was faster than that of six smaller models. When using a multi-camera array to capture a substrate, the number of cameras used should reflect the structure of the substrate. Flat areas with no overhangs or bommies would require fewer cameras than a widely varying substrate that has overhangs and cave-like areas. Ensuring that only required cameras are used restricts the number of images captured to only those focused on the desired area, removing views that would capture unnecessary views (i.e. cameras facing water) that increase model processing time.

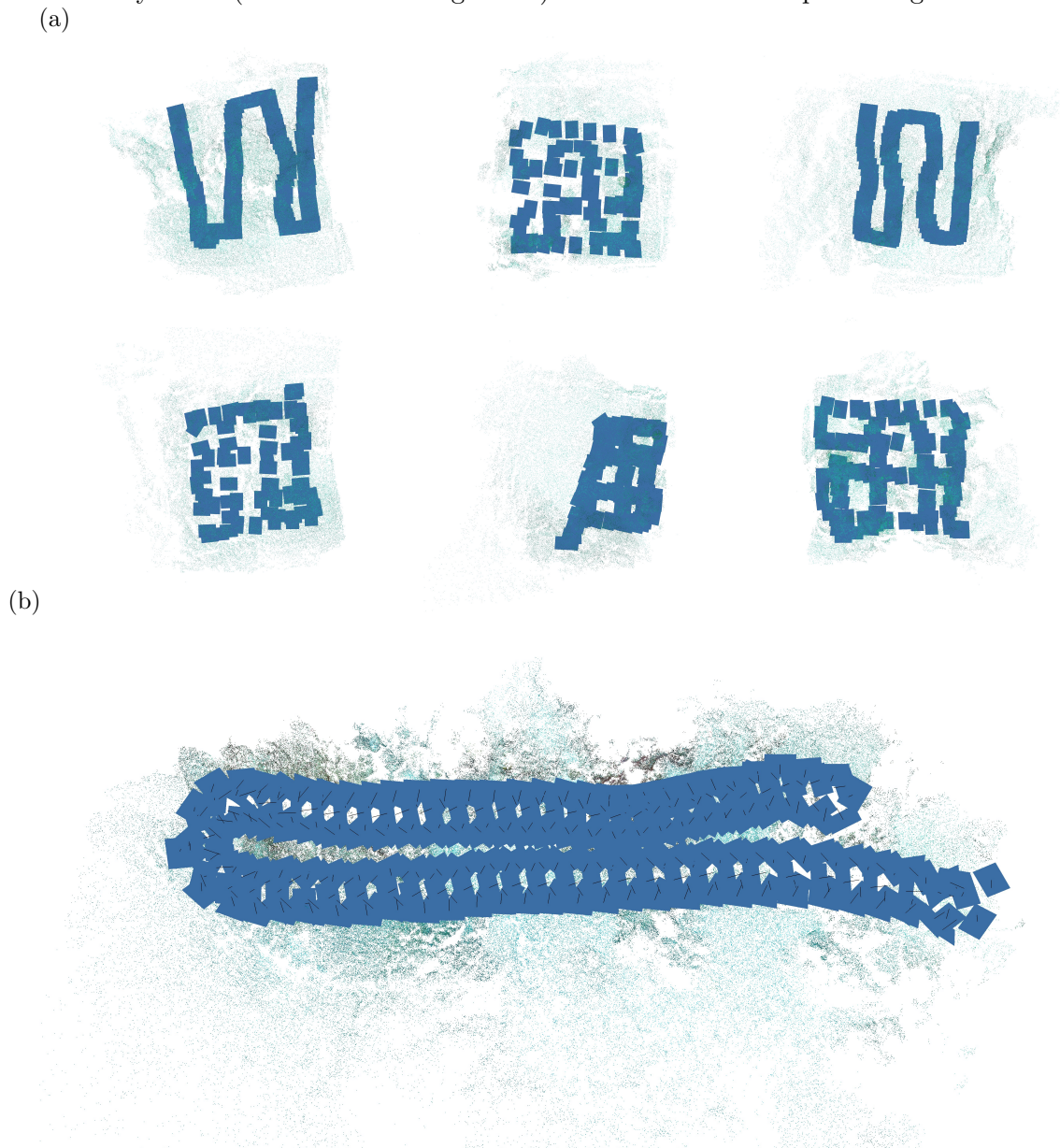


Figure 8.1: Aligned substrate images and common points showing the pathway used when generating (a) six  $2 \times 2$  m quadrats with a single camera, and (b) the associated  $4 \times 6$  m quadrat of the same reef area captured using a multi-camera array.

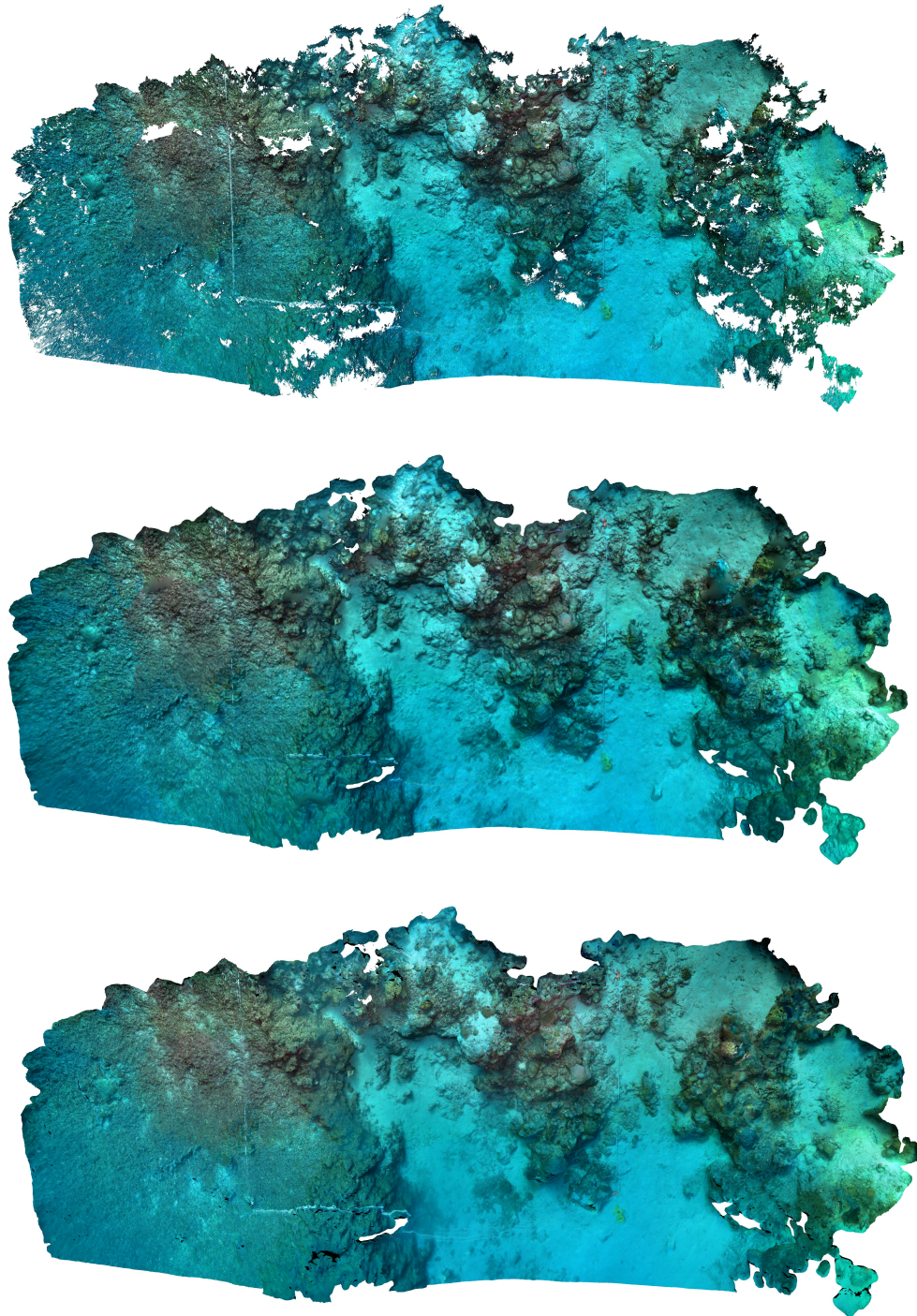


Figure 8.2: Processing of a coral reef 3D model generated using images captured with a multi-camera array, showing the creation of (b) the dense cloud, (c) mesh, and (b) texture.

When considering substrate complexity, only fractal dimension matched up between models. This highlights the difficulty in replication when using certain methods to find rugosity and vector dispersion [48], in contrast to the supposed benefits of 3D modelled substrates in terms of repeated data extraction [121]. Other approaches to these metrics may remove these difficulties and allow for a more general positioning of helper files, or

remove the need for these additional files entirely [125].

There is also the potential that the mesh, which the helper file uses, differed enough to prevent the same values of complexity to be found despite positioning accuracy, though this was not tested. A future examination of the models could be performed by rebuilding the single camera models in one combined process, collating the images from all six  $2 \times 2$  m quadrats into one 3D model. Then, after cropping the models to the study area and excluding uneven edges to ensure the scale was equal, this would allow for cloud-to-cloud and mesh-to-mesh comparisons between the single and multi-camera methods to either confirm or exclude one potential source of discrepancy in the extracted complexity.

Chapter 3 demonstrated the successful trial of a rapid, multi-camera approach to coral reef image data collection and subsequent 3D modelling. This method then acted as the foundation for the data collection undertaken in Chapter 4.

### 8.1.2 Expanding the cases for computational complexity measurements

Through a collaborative project with Natural England, the Cromer Shoal Chalk Bed Marine Conservation Zone was used as a secondary testing site for the multi-camera array developed in Chapter 3. This work was primarily undertaken for the Eastern Inshore Fisheries and Conservation Agency (EIFCA) and provided a habitat with distinct topography and challenges to contrast the coral reef ecosystems previously assessed.

There are few studies looking into fisheries or potting effort in MCZs and there is not enough data or research currently to comprehensively assess habitat vulnerabilities [170]. Prior research into crustacean fisheries investigated the effects on epifauna rather than the structure of the system itself [?, 221]. Understanding the impact of the fishery on habitat features is crucial for the management and conservation of reef systems. The management of small-scale fisheries must incorporate conservation of ecosystems and socio-economic factors into policies for the betterment of the environment and those that rely on it for food and income [222].

The preliminary report into the state of the Cromer Shoal Chalk Bed [172] utilised well-known complexity metrics [48, 65, 45, 56], scaled and defined in terms of coral reef systems [48], simply because no metrics had yet been fully specified for rocky chalk reef environments. The outcome of the assessment showed a great disparity in computational complexity and *in-situ* visual assessments, so further testing was performed to investigate

the type of complexity applicable to the environment.

In Chapter 5, when considering the species' counts and commercial value, fractal dimension was scaled to *C. pagurus* minimum catch size and maximum overall size. This was an essential step in relating the metric to the environment being assessed and would allow far more valid connections to be drawn between the species and its habitat, particularly with larger scale studies. Fractal dimension is easily adaptable and could be tailored to each organism in a study on the Cromer reef as there are a limited array of fauna, and very few considered of interest commercially and therefore relevant to the fishery on the chalk reef [29]. Rugosity and vector dispersion were disregarded entirely. The relatively small scale changes detected were not applicable to the sweeping shifts in topography seen on the chalk reef and they were considered to provide little value to further analysis and future assessments. Instead, a novel approach to calculating relief was developed to be applicable at any model scale. Removing the dimensional restrictions from the complexity assessment opens up surveying to fewer scale-based restrictions and, when combined with multi-camera imaging, could vastly increase the area that can be assessed at any one time.

Utilising the camera array in a distinct rocky reef environment with challenging surveying restrictions and conditions demonstrated the advantages of rapid surveying. Large areas of the chalk reef could be surveyed in a single dive, despite restricted dive time, environmental hazards (i.e. the shank lines, fishing boats, etc.), and the requirement for *in-situ* training with the equipment and surveying method itself. The array's design allowed for an additional camera attachment, vital for the collection of video footage of the transects without the need for additional divers. The use of computational methods generally also proved essential. When the need for different complexity metrics became clear, 3D models could simply be re-evaluated without requiring another complex and expensive survey. This allowed the metrics used in Chapter 5 to be developed and used quickly and effectively.

Where Chapter 4 further demonstrated the benefits of multi-camera array in image data collection, Chapter 5 highlighted the value of tailoring experimental approach to the target habitat. Both chapters underscore the benefits of computational analysis in marine environments, particularly where data collection is challenging to replicate regularly. Assessment of the Cromer Shoal Chalk Bed MCZ is ongoing, utilising the work undertaken here.

### 8.1.3 Automatic analysis of coral reef imagery

Where Chapters 4 and 5 demonstrate the use of computational methods in conjunction with human assessment of species counts and other variables, Chapters 6 and 7 move further towards fully computational approaches by leveraging the ImageCLEF initiative to evaluate and advanced the capabilities of automatic annotation of coral reef substrates.

The development of ImageCLEFcoral leveraged the expertise of people outside of the research group to create and improve upon algorithms to annotate coral reef substrates. Enhancing image quality through colour adjustments was a clear thread through which some teams began their task runs [203, 202] and is important to pursue in both this task [208, 209] and in 3D modelling in general. Continuing the use of action cameras to provide data allows for reef systems to be surveyed by monitoring teams with a range of budgets and through images captured by non-researchers, either from citizen scientists or SCUBA hobbyists and holidaymakers, but does stress the need for image enhancement prior to annotation as the quality of images is less than that of high-end camera equipment and more prone to blurring (often action cameras are used to capture video instead of images, so a static position is not held while capturing the substrate).

While the initial 2019 ImageCLEFcoral task showed little success, the 2020 edition of the task showed an unexpectedly large jump in performance: pixelwise parsing, considered the more valuable task for future work, showed a in improvement from  $\approx 4\%$  success to  $\approx 68\%$  success in a single year. The increase in training data likely provided some advantages over the 2019 task, but the inclusion of coral reef images from other regions in the test data was expected to nullify some of the predicting power. Though this didn't appear to be the case in 2020, when the 2021 training dataset included these distinct coral reefs the results of both localisation and pixelwise parsing steeply declined; though, the most successful pixelwise parsing run was still an improvement on the 2019 task. The success rate of ImageCLEFcoral is not yet high enough to produce a reliable and accurate annotation network but annual cycle of expanding datasets and using a competitive campaign to progress has produced more insights into successful approaches (see Chapter 6 for detail) than could have otherwise been developed, tested and compared independently in the same timeframe.

The overarching aim of ImageCLEFcoral is to integrate semantic annotations into the

3D models of coral reef systems before the reconstruction pipeline. This has not thus far been attempted for coral reef environments, though post-modelling annotation has been investigated. Hopkinson et al. [156] created SfM 3D models using Photoscan (now Metashape) and re-projected mesh triangles back to the original image set. A subset of these elements used for training were then manually annotated, with up to six associated images with a clear view of the mesh area used to determine its associated annotation label (from 11.9 images per mesh triangle on average). Ten labels were used, with four specific species, one genus, three functional groups (one of which was macroalgae/dense turf algae), rubble, and sand used as semantic labels. Pierce et al. [223] have similarly generated a post-modelling approach, though with fewer classes than Hopkinson et al.: seven categories, only four of which were biological to classify fish, algae, massive corals, and branching soft and hard corals. Not all labels were relevant to 3D modelling (i.e. fish and water cannot be modelled with SfM as they are moving “objects”). Classes were selected based on prevalence in their image dataset. Here, they produce a 3D reconstruction and subsequently swap the original images with an automatically annotated set that then allows them to independently generate the dense cloud, mesh, and texture.

The network from Hopkinson et al. [156] found 93% average accuracy across individual classes, while Pierce et al. [223] had a high of 91% pixel accuracy. The use of reef-specific labelling likely increases the accuracy of the model output, as relevant substrates are both trained and tested on from the same reef, but this minimises its application to other ecosystems. The restricted labels also limit the usefulness of this methodology to other studies within this reef area. The merit of these studies cannot be understated, but the restrictions they face through their annotation methodology limit their power in wide-ranging monitoring and research. Pixel point annotation presents the same challenges of *in-situ* point transects, where rarer or smaller organisms are more likely to be missed simply due to the sampling selection. Reef or study specific labelling prevents the application of the model in other research and would require subsequent studies to apply the methodology to their own training before it can be used. Though ImageCLEFcoral has thus far had limited accuracy, the overarching global or biogeographical applications provide an advantage over reef specific algorithms as they would not require every reef, or indeed every study, to train and test their own network prior to use.

Chapter 6 outlined the work in creating the dataset for the ImageCLEFcoral task, the

changes made to the task annually, and the results from 2019 – 2021, while Chapter 7 detailed the submission made to the 2021 edition of ImageCLEFcoral undertaken in place of organising the task. Throughout these chapters, the challenge of automatically annotation images of wider coral reef areas to a high level of detail is clear. With the continuation of the annual task and advancements in automatic annotation, further improvements can be expected in the future, hopefully leading to a fully annotated, 3D translatable, widespread and more generic approach to annotations. While much more challenging and time-consuming to develop when considering the wide ranging morphologies of coral reef substrates from region to region, this would fill a clear gap in the furthering of automatic annotation in coral reef research.

## 8.2 Limitations of the work

### 8.2.1 Data collection

The videos and stills used throughout this thesis were captured through SCUBA diving surveys and faced the challenges commonly associated with this type of *in-situ* work (i.e. time limits, depth limits, air limits). Varying day-to-day conditions on the coral reef led to quality differences between repeatedly dived sites. Changes to turbidity, light attenuation, current strength and direction, and even the work of other divers all compound to create a complex working environment even before the complexities of SCUBA itself are considered. Locating the sites themselves was also impacted by these factors, and though metal pins were placed into non-living substrate, the transect tapes used to outline the 4×6 m area and the 2×2 m quadrats within this area were laid by hand each day and likely shifted slightly each time.

One avenue through which to minimise the challenges of SCUBA surveying may be to use remotely operated vehicles (ROVs) or for data collection. Though this would still require a human operator and a boat team, an ROV would likely be more stable in strong currents and would negate dive-time limits, potentially allowing for a full site to be surveyed in each data collection session depending on scale [224]. Concerning visibility, lights could be fitted to the camera arrays to combat low light conditions, though their strength would have to be balanced against a site’s turbidity to prevent backscattering from impacting image quality from turbid water.



### 8.2.2 3D reconstruction

The greatest limiting factor in 3D reconstruction is the computer itself. The larger the dataset and the more accurate the 3D model, the more processing time and power required. An ideal scenario would be to model an entire reef as one to the highest quality possible, but the sheer expense monetarily and temporally may outweigh the usefulness of such a model in many cases. In balance, the cost of the computer (as a whole or as upgraded components) must be weighed against the reconstruction's quality and scale to provide a useful output quickly enough for monitoring use.

Testing a few representative models to assess the build quality required for data extraction would be useful at the start of any survey, but this would require every research team to perform ground truth testing and corresponding metric testing for each survey carried out. In practical terms, the use of accessible software is a middle ground to a still somewhat inaccessible field.

### 8.2.3 Automatic annotation

The number of images required to train a neural network to annotate regularly shaped objects (i.e. buildings, cars) is extensive. The added difficulty of indistinct, irregular geometry with a lack of colour differentiation (as with coral reef substrates) requires even more images that were simply not available to the ImageCLEF task. Adding further data with external image sets was suggested to 2021 participants, but the difference in annotation and image styles was apparent when adding to this dataset did not improve the accuracy of substrate classification, and instead reduced it greatly [204, 206].

Utilising a larger team of experienced annotators and administrators (annotators to define the objects within images and administrators to assign a semantic label to these objects) would enable a larger dataset to be trialled with less margin for error in the groundtruth data. This would be particularly beneficial if more specific semantic labels were used to better link a model's results to biologically useful outputs.

## 8.3 Future directions for research

The research objectives tackled within this thesis provide a basis for further in-depth study into the role of computation analysis in benthic monitoring and assessment.

### 8.3.1 Reef-wide surveying of the Cromer Shoal Chalk Bed MCZ

The surveying carried out in Chapter 4 was a preliminary assessment into the area, intended to indicate if further research was needed rather than to provide broad implications into the ecosystem's overall health. As such, the state of the chalk reef is still relatively unknown in terms of damage and complexity. Capturing video surveys of the entire reef would be an extremely intensive project, and simultaneously one of high value. These videos would not only allow the chalk reef to be modelled for further assessments, but would provide a record of the current condition of the ecosystem for future comparison.

This could be performed concurrently by citizen scientists (such as SeaSearch East, an experienced group of local divers with an interest in the ecology of the system) and by ROV and/or dive surveys from relevant bodies (i.e. the EIFCA, Natural England) for sites not as accessible. The collating of data and subsequent analysis would likely require a small team, but would allow for fully reasoned insights to be reached with less obscurity in the data.

A full study into the impact of damage on the local ecosystem could also be instigated with a temporary "no-take zone" and a ropeless potting area, with an initial damage and stock survey followed by several more repeated assessments over a set time period to look into the effect of human activity on the reef with more robust certainty.

### 8.3.2 Automatically annotating other substrate features

As highlighted throughout this thesis, coral reef systems are not the only important marine reef environment. The use of automatic annotation on reef substrates focused on coral reef ecosystems predominantly because of the scale of the available dataset, but other environments would benefit from similar technology in their monitoring and conservation.

The chalk reef damage assessment proposed in Chapter 4 was challenging to action in part due to video quality and its novelty, but also due to the need for continual discussion between annotators before an agreement on category could be reached in a considerable number of instances. Automating this processes, even to the point of simply tagging damaged versus not damaged areas, has the potential to increase data processing time and aid in reef-wide research on the Cromer Shoal Chalk Bed and other similar environments.

### 8.3.3 Computational habitat-wide assessments

Utilising computational analysis with outdated or oversimplified structural complexity assessments limits the capabilities of modern techniques. Developing a tool set of the most useful marine habitat metrics, where useful is classed as both relevant to a wide range of assessments and not providing the same information as another metric without a different context, for use on 3D reconstructions of reef ecosystems is an essential step forward in modern research. Creating a globally accessible resource for use in common software would allow researchers to select their desired metrics while also maintaining a standard of assessment that in turn allows for cross-research analysis to take place without differences in methodologies limiting comparisons.

### 8.3.4 3D printing in coral reef research

With repeated imaging surveys to provide a guide on historical reef structure and composition, loss of coral colonies through bleaching and rubbleisation, storms, blast fishing, or other harmful action could be tracked. One possibility for combating the subsequent complexity losses that lead to ecosystem decline is to 3D print lost structures in reef friendly materials to replace and fill “gaps” in the reef [225]. This would counteract the immediate topographical decline that often signals the beginning of reef fauna loss, which can spiral to extremes of entire reef decline or phase shifts when it occurs on a reef-wide scale [101].

Another use of 3D printing in reef research is for the creation of artificial reef systems [226]. These environments are becoming more commonplace, either with wrecked objects or deliberately placed structures forming the base [227]. The challenge with deliberate structures is often the lack of initial complexity, which fails to entice reef organisms to migrate and colonise the new environment. 3D printing coral-like, complex structures which interlink to form an artificial reef would provide an immediately topologically intricate ecosystem that would provide the desired habitat for reef-associated organisms while also introducing a range of settlement areas for reef benthic organisms.

## 8.4 Concluding remarks

Marine monitoring and surveying is an essential and invaluable tool in a world with drastically shifting oceanic conditions. The range of tools available to researchers is expanding with modern technological advancements, but often the measures and metrics utilised are those used decades ago. These assessments were often developed for analogue *in-situ* research that is subject to varied challenges and limitations that can impact the outputs and results gathered, and therefore impact the conclusions drawn.

This thesis aimed to further the use of 3D reconstruction and other computational tools in marine substrate monitoring. To that end, a multi-camera array demonstrated the speed at which data can be collected with varying angles to minimise reconstructed data loss. While comparisons to single camera methods were challenging, the use of multi-camera arrays was proved beneficial in terms of speed and scale in both tropical coral and temperate chalk reef environments. Using the multi-camera array on the chalk environment, structural complexity, species abundance, and substrate damage were investigated. A set of tailored complexity metrics were computationally developed to better represent the non-coral system, with the characteristics of the environment leading the determination of appropriate assessments over those commonly used in other reef types. Following this, the viability of automatic annotation for coral reef substrates was tested, looking to both increase the volume of analysed coral reef data and decrease the necessary time-input of researchers. Though a challenging problem to navigate, there is clear promise in incorporating this type of technology into coral reef substrate monitoring, though there is still a vital need for further refinement and scale before a usable algorithm can be relied upon for research.

The outcomes of these areas of work demonstrate the wide-ranging usefulness of modern techniques in ecosystem surveying. These tools can provide a myriad of tailored assessments to researchers when used appropriately and could aid marine substrate research in becoming a globally interlinked effort instead of a series of distinct and isolated projects. Despite the challenges to computational research, the potential for mass data analysis and comparable results is an essential step in the worldwide effort to conserve marine ecosystems.

# References

- [1] F. Moberg and C. Folke, “Ecological goods and services of coral reef systems,” *Ecological Economics*, vol. 29, pp. 215–233, 1999.
- [2] B. Bowen, L. Rocha, R. Toonen, S. Karl, and the Tobo Laboratory, “The origins of tropical marine biodiversity,” *Trends in Ecology and Evolution*, vol. 28, no. 6, pp. 359–366, 2013.
- [3] J. Burns, D. Delparte, L. Kapon, M. Belt, R. Gates, and M. Takabayashi, “Assessing the impact of acute disturbances on the structure and composition of a coral community using innovative 3d reconstruction techniques,” *Methods in Oceanography*, vol. 15, pp. 49–59, 2016.
- [4] B. Gratwicke and M. Speight, “The relationship between fish species richness, abundance and habitat complexity in a range of shallow tropical marine habitats,” *Journal of Fish Biology*, vol. 66, no. 3, pp. 650–667, 2005.
- [5] P. Sale, W. Douglas, and P. Doherty, “Choice of microhabitats by coral reef fishes at settlement,” *Coral Reefs*, vol. 3, pp. 91–99, 1984.
- [6] W. Reid and C. Raudsepp-Hearne, “The Millenium Ecosystem Assessment: Ecosystems and human well-being,” 2005.
- [7] A. Woodhead, C. Hicks, A. Norström, G. Williams, and N. Graham, “Coral reef ecosystem services in the anthropocene,” *Functional Ecology*, vol. 33, pp. 1023–1034, 2019.
- [8] A. Rogers, A. Harborne, C. Brown, Y.-M. Bozec, C. Castro, I. Chollett, K. Hock, C. Knowland, A. Marshall, J. Ortiz, T. Razak, G. Roff, J. Samper-Villarreal, M. Saunders, N. Wolff, and P. Mumby, “Anticipative management for coral reef ecosystem services in the 21st century,” *Global Change Biology*, vol. 21, no. 2, pp. 504–514, 2015.
- [9] L. Burke, K. Reytar, M. Spalding, and A. Perry, “Threats to the World’s Reef,” in *Reefs at Risk Revisited*, 1st ed. Washington DC, USA: World Resources Institute, 2011.
- [10] M. Weijerman, J. Gove, I. Williams, W. Walsh, D. Minton, and J. Polovina, “Evaluating managemet strategies to optimise coral reef ecosystem services,” *Journal of Applied Ecology*, vol. 55, no. 4, pp. 1823–1833, 2018.
- [11] E. Darling and S. D’agata, “Coral reefs: Fishing for sustainability,” *Current Biology*, vol. 27, no. 2, pp. R65–R68, 2017.
- [12] C. Shuman, G. Hodgson, and R. Ambrose, “Managing the marine aquarium trade: is eco-certification the answer?” *Environmental Conservation*, vol. 31, no. 4, pp. 339–348, 2004.

- [13] A. Wali, S. Majid, S. Rasool, S. Shehada, S. Abdulkareem, A. Firdous, S. Beigh, S. Shakeel, S. Mushtaq, I. Akbar, H. Madhkali, and M. Rehman, “Natural products against cancer: Review on phytochemicals from marine sources preventing cancer,” *Saudi Pharmaceutical Journal*, vol. 27, no. 6, pp. 767–777, 2019.
- [14] B. Hunt and A. Vincent, “The Use of Marine Organisms in Traditional and Allopathic Medicine” in *Conserving Medicinal Species: securing a healthy future*, 1st ed. Sri Lanka: IUCN: Ecosystems and Livelihoods Group, Asia, 2006.
- [15] E. Cooper, K. Hirabayashi, K. Strychar, and P. Sammarco, “Corals and their potential applications to integrative medicine,” *Evidence-Based Complementary and Alternative Medicine*, vol. 2014, no. 184959, pp. 1–9, 2014.
- [16] F. Ferrario, M. Beck, C. Storlazzi, F. Micheli, C. Shepard, and L. Airoidi, “The effectiveness of coral reefs for coastal hazard risk reduction and adaptation,” *Nature Communications*, vol. 5, p. 3794, 2014.
- [17] A. Oakley-Cogan, S. Tebbett, and D. Bellwood, “Habitat zonation on coral reefs: Structural complexity, nutritional resources and herbivorous fish distributions,” *PLoS ONE*, vol. 15, no. 6, p. e0233498, 2020.
- [18] M. Beck, I. Losada, P. Menéndez, B. Reguero, P. Díaz-Simal, and F. Fernández, “The global flood protection savings provided by coral reefs,” *Nature Communications*, vol. 9, p. 2186, 2018.
- [19] H. Cesar, L. Burke, and L. Pet-Soede, *The Economics of Worldwide Coral Reef Degradation*, 3rd ed. Arnhem, The Netherlands: Cesar Environmental Economics Consulting (CEEC), 2013.
- [20] A. Abelson, “Are we sacrificing the future of coral reefs on the alter of the “climate change” narrative?” *ICES Journal of Marine Science*, vol. 77, no. 1, pp. 40–45, 2020.
- [21] G. De’ath, K. Fabricius, H. Sweatman, and M. Puotinen, “The 27-year decline of coral cover on the great barrier reef and its causes,” *PNAS*, vol. 109, no. 44, pp. 17995–17999, 2012.
- [22] J. Pandolfi, R. Bradbury, E. Sala, T. Hughes, K. Bjorndal, R. Cooke, D. McArdle, L. McClenachan, M. Newman, G. Parades, R. Warner, and J. Jackson, “Global trajectories of the long-term decline of coral reef ecosystems,” *Science*, vol. 301, no. 5635, pp. 955–958, 2003.
- [23] T. Hughes, J. Kerry, A. Baird, S. Connolly, A. Dietzel, C. Eakin, S. Heron, A. Hoey, M. Hoogenboom, G. Liu, M. McWilliam, R. Pears, M. Pratchett, W. Skirving, J. Stella, and G. Torda, “Global warming transforms coral reef assemblages,” *Nature*, vol. 556, pp. 492–496, 2018.
- [24] S. Heron, R. van Hooidonk, J. Maynard, K. Anderson, J. Day, E. Geiger, O. Hoegh-Guldberg, T. Hughes, P. Marshall, D. Obura, and C. Eakin, “Impacts of climate change on world heritage coral reefs: Update to the first global scientific assessment,” *UNESCO World Heritage Centre*, 2018.
- [25] N. Phongsuwan and H. Chansang, “Repeated coral bleaching in the andaman sea, thailand, during the last two decades,” *Phuket Marine Biological Center Research Bulletin*, vol. 17, pp. 19–41, 2012.

- [26] J. Morais, R. Morais, S. Tebbett, M. Pratchett, and D. Bellwood, “Dangerous demographics in post-bleach corals reveal boom-bust versus protracted declines,” *Scientific Reports*, vol. 11, no. 18787, 2021.
- [27] G. Bravo, J. Livore, and G. Bigatti, “The importance of surface orientation in biodiversity monitoring protocols: The case of Patagonian rocky reefs,” *Frontiers in Marine Science*, vol. 7, p. 578595, 2020.
- [28] S. Gaylard, M. Waycott, and P. Lavery, “Review of coast and marine ecosystems in temperate australia demonstrates a wealth of ecosystem services,” *Frontiers in Marine Science*, vol. 7, p. 453, 2020.
- [29] T. Bridges, “Crab and lobster stock assessment,” Eastern Inshore Fisheries and Conservation, Tech. Rep., 2018.
- [30] S. Bennett, T. Wernberg, S. Connell, A. H. amd CR Johnson, and E. Poloczanska, “The ‘Great Southern Reef’: social, ecological and economic value of Australia’s neglected kelp forests,” *Marine and Freshwater Research*, vol. 67, no. 1, pp. 47–56, 2016.
- [31] J. García Charton and A. Pérez Ruzafa, “Correlation between habitat structure and a rocky reef fish assemblage in the Southwest Mediterranean,” *Marine Ecology*, vol. 19, no. 2, pp. 111–128, 1998.
- [32] E. Sala, E. Ballesteros, P. Dendrinis, A. Di Franco, F. Ferretti, D. Foley, S. Frascchetti, A. Friedlander, J. Garrabou, H. Güçüsoy, P. Guidetti, B. Halpern, B. Hereu, A. Karamanlidis, Z. Kizilkaya, E. Macpherson, L. Mangialajo, S. Mariani, F. Micheli, A. Pais, K. Riser, A. Rosenberg, M. Sales, K. Selkoe, R. Starr, F. Tomas, and M. Zabala, “The structure of Mediterranean rocky reef ecosystems across environmental and human gradients,” *PLoS ONE*, vol. 7, no. 2, p. e32742, 2012.
- [33] F. Enrichetti, G. Bavestrello, V. Cappanera, M. Mariotti, L. Merotto, P. Povero, I. Rigo, M. Toma, L. Tunesi, S. Venturini, and M. Bo, “High megabenthic complexity and vulnerability of a mesophotic rocky shoal support its inclusion in a mediterranean MPA,” *Diversity*, vol. 15, no. 8, p. 933, 2023.
- [34] S. Bevilacqua, L. Airoidi, E. Ballesteros, L. Benedetti-Cecchi, F. Boero, F. Bulleri, E. Cebrian, C. Cerrano, J. Claudet, F. Colloca, M. Coppari, A. Di Franco, S. Frascchetti, J. Garrabou, G. Guarnieri, C. Guerranti, P. Guietti, B. Halpern, S. Katsanevakis, M. Mangano, F. Micheli, M. Milazzo, A. Pusceddu, M. Renzi, G. Rilov, G. Sará, and A. Terlizzi, “Mediterranean rocky reefs in the Anthropocene: Present status and future concerns,” *Advances in Marine Biology*, vol. 89, pp. 1–51, 2021.
- [35] R. Treblico, N. Dulvy, H. Stewart, and A. Salomon, “The role of habitat complexity in shaping the size structure of a temperate reef fish community,” *Marine Ecology Progress Series*, vol. 532, pp. 197–211, 2015.
- [36] Norfolk Wildlife Trust. Sponge confirmed as new to science. [Online]. Available: <https://www.norfolkwildlifetrust.org.uk/news-and-articles/news/all-news/2011-10-10-sponge-confirmed-as-new-to-sci>
- [37] E. Sheehan, D. Bridger, and M. Attrill, “The ecosystem service value of living versus dead biogenic reef,” *Estuarine, Coastal and Shelf Science*, vol. 154, pp. 248–254, 2015.

- [38] E. Di Franco, A. Di Franco, A. Caló, M. Di Lorenzo, L. Mangialajo, S. Bussotti, C. Bianchi, and P. Guidetti, “Inconsistent relationships among protection, benthic assemblage, habitat complexity and fish biomass in Mediterranean temperate rocky reefs,” *Ecological Indicators*, vol. 128, p. 107850, 2021.
- [39] I. Tittley, “Background document for littoral chalk communities,” OSPAR Commission, Tech. Rep., 2009.
- [40] D. Aldiss, A. Farrant, and P. Hopson, “Geological mapping of the Late Cretaceous Chalk Group of southern England: a specialised application of landform interpretation,” *Proceedings of the Geologists’ Association*, vol. 123, no. 5, pp. 728–741, 2012.
- [41] I. Tittley, C. Spurrier, P. Chimonides, J. George, J. Moore, N. Evans, and A. Muir, “Survey of chalk cave, cliff, intertidal and subtidal reef biotopes in the Thanet coast cSAC,” English Nature Research Reports, Tech. Rep., 1998.
- [42] C. Moffat, H. Richardson, and G. Roberts, “Natural England marine chalk characterisation project,” Natural England, Tech. Rep., 2019.
- [43] T. Eddy, V. Lam, G. Reygondeau, A. Cisneros-Montemayor, K. Greer, M. Palomares, J. Bruno, Y. Ota, and W. Cheung, “Global decline in capacity of coral reefs to provide ecosystem services,” *One Earth*, vol. 4, no. 9, pp. 1278–1285, 2021.
- [44] M. Crabbe and D. Smith, “Comparison of two reef sites in wakatobi marine national park (se sulawesi, indonesia) using digital image analysis,” *Coral Reefs*, vol. 21, no. 3, pp. 242–244, 2002.
- [45] S. Pittman, B. Costa, and T. Battista, “Using Lidar bathymetry and boosted regression trees to predict the diversity and abundance of fish and corals,” *Journal of Coastal Research*, vol. 53, pp. 27–38, 2009.
- [46] M. Risk, “Fish diversity on a coral reef in the virgin islands,” *Atoll Research Bulletin*, vol. 153, pp. 1–6, 1972.
- [47] D. Bayley, A. Mogg, H. Koldewey, and A. Purvis, “Capturing complexity: field-testing the use of ‘structure from motion’ derived virtual models to replicate standard measures of reef physical structure,” *PeerJ*, vol. 7:e6540, 2019.
- [48] G. Young, S. Dey, A. Rogers, and D. Exton, “Cost and time-effective method for multi-scale measures of rugosity, fractal dimension and vector dispersion from coral reef 3d models,” *PLoS ONE*, vol. 12, no. 4, p. e0175341, 2017.
- [49] J. Burns, D. Delparte, R. Gates, and M. Takabayashi, “Integrating structure-from-motion photogrammetry with geospatial software as a novel technique for quantifying 3d ecological characteristics of coral reefs,” *PeerJ*, vol. 3:e1077, 2015.
- [50] V. Raoult, P. David, S. Dupont, C. Mathewson, S. O’Neill, N. Powell, and J. Williamson, “Gopros™ as an underwater photogrammetry tool for citizen science,” *PeerJ*, vol. 4, p. e1960, 2016.
- [51] V. Raoult, S. Reid-Anderson, A. Ferri, and J. Williamson, “How reliable is structure from motion (sfm) over time and between observers? a case study using coral reef bommies,” *Remote Sensing*, vol. 9, no. 740, pp. 740–755, 2017.



- [52] J. Carlot, A. Rovère, E. Casella, D. Harris, C. Grellet-Muñoz, Y. Chancerelle, E. Dormy, L. Hedounin, and V. Parravicini, “Community composition predicts photogrammetry-based structural complexity on coral reefs,” *Coral Reefs*, vol. 39, no. 4, pp. 967–975, 2020.
- [53] J. Magel, J. Burns, R. Gates, and J. Baum, “Effects of bleaching-associated mass coral mortality on reef structural complexity across a gradient of local disturbance,” *Scientific Reports*, vol. 9, no. 2512, p. 2512, 2019.
- [54] A. Fukunaga, J. Burns, B. Craig, and R. Kosaki, “Integrating three-dimensional benthic habitat characterization techniques into ecological monitoring of coral reefs,” *Journal of Marine Science and Engineering*, vol. 7, no. 2, pp. 27–40, 2019.
- [55] D. Bayley, A. Mogg, A. Purvis, and H. Koldewey, “Evaluating the efficacy of small-scale marine protected areas for preserving reef health: A case study applying emerging monitoring technology,” *Aquatic Conservation: Marine and Freshwater Ecosystems*, pp. 1–19, 2019.
- [56] M. Kalacska, O. Lucanus, L. Sousa, T. Vieira, and J. Arroyo-Mora, “Freshwater fish habitat complexity mapping using above and underwater structure-from-motion photogrammetry,” *Remote Sensing*, vol. 10, no. 12, pp. 1912–1940, 2018.
- [57] A. Fukunaga, J. Burns, K. Pascoe, and R. Kosaki, “Associations between benthic cover and habitat complexity metrics obtained from 3d reconstruction of coral reefs at different resolutions,” *Remote Sensing*, vol. 12, no. 6, pp. 1011–1026, 2020.
- [58] M. Bryson, F. R. W. Figueira, O. Pizarro, J. Madin, S. Williams, and M. Byrne, “Characterization of measurement errors using structure-from-motion and photogrammetry to measure marine habitat structural complexity,” *Ecology and Evolution*, vol. 7, no. 15, pp. 5669–5681, 2017.
- [59] A. Raphael, Z. Dubinsky, D. Iluz, and N. Nethanyahu, “Neural network recognition of marine benthos and corals,” *Diversity*, vol. 12, no. 1, p. 29, 2020.
- [60] A. Bahrani, B. Majidi, and M. Eshghi, “Coral reef management in persian gulf using deep convolutional neural networks,” in *4th International Conference on Pattern Recognition and Image Analysis (IPRIA)*, 2019, pp. 200–204.
- [61] O. Beijbom, T. Treibitz, D. Kline, G. Eyal, A. Khen, B. Neal, Y. Loya, B. Mitchell, and D. Kriegman, “Improving automated annotation of benthic survey images using wide-band fluorescence,” *Scientific Reports*, vol. 6, no. 1, p. 23166, 2016.
- [62] J. Durden, B. Hosking, B. Bett, D. Cline, and H. Ruhl, “Automated classification of fauna in seabed photographs: The impact of training and validation dataset size, with considerations for the class imbalance,” *Progress in Oceanography*, vol. 196, p. 102612, 2021.
- [63] A. Gómez-Ríos, S. Tabik, J. Luengo, A. Shihavuddin, B. Krawczyk, and F. Herrera, “Towards highly accurate coral texture images classification using deep convolutional neural networks and data augmentation,” *Expert Systems with Applications*, vol. 118, pp. 318–328, 2019.
- [64] A. Mahmood, M. Bennamoun, S. An, F. Sohel, F. Boussaid, R. Hovey, G. Kendrick, and R. Fisher, “Automatic annotation of coral reefs using deep learning,” in *Oceans 2016 mts/IEEE Monterey*, 2016, pp. 1–5.

- [65] N. Graham and K. Nash, “The importance of structural complexity in coral reef ecosystems,” *Coral Reefs*, vol. 32, no. 2, pp. 315–326, 2013.
- [66] M. McCormick, “Comparison of field methods for measuring surface topography and their associations with a tropical reef fish assemblage,” *Marine Ecology Progress Series*, vol. 112, pp. 87–96, 1994.
- [67] L. Richardson, N. Graham, M. Pratchett, and A. Hoey, “Structural complexity mediates functional structure of reef fish assemblages among coral habitats,” *Environmental Biology of Fishes*, vol. 100, no. 3, pp. 193–207, 2017.
- [68] R. MacArthur and J. MacArthur, “On bird species diversity,” *Ecology*, vol. 42, no. 3, pp. 594–598, 1961.
- [69] C. Badgley, T. Smiley, R. Terry, E. Davis, L. DeSantis, D. Fox, S. Hopkins, T. Jezkova, M. Matocq, N. Matzke, J. McGuire, A. Mulch, B. Riddle, V. Roth, J. Samuels, C. Strömberg, and B. Yanites, “Biodiversity and topographic complexity: Modern and geohistorical perspectives,” *Trends in Ecology and Evolution*, vol. 32, no. 3, pp. 211–226, 2017.
- [70] C. Gough, J. Atkins, R. Fahey, and B. Hardiman, “High rates of primary production in structurally complex forests,” *Ecology*, vol. 100, no. 10, 2019.
- [71] B. Luckhurst and K. Luckhurst, “Analysis of the influence of substrate variables on coral reef fish communities,” *Marine Biology*, vol. 49, pp. 317–323, 1978.
- [72] P. J. Mumby and A. Hastings, “The impact of ecosystem connectivity on coral reef resilience,” *Journal of Applied Ecology*, vol. 45, no. 3, pp. 854–862, 2008.
- [73] C. Lønborg, M. L. Calleja, K. E. Fabricius, J. N. Smith, and E. P. Achterberg, “The great barrier reef: A source of CO<sub>2</sub> to the atmosphere,” *Marine Chemistry*, vol. 210, pp. 24–33, 2019.
- [74] R. K. F. Unsworth, C. J. Collier, G. M. Henderson, and L. J. McKenzie, “Tropical seagrass meadows modify seawater carbon chemistry: implications for coral reefs impacted by ocean acidification,” *Environmental Research Letters*, vol. 7, no. 2, 2012.
- [75] R. Hiatt, D. Strasburg, S. Monographs, and N. Jan, “Ecological relationships of the fish fauna on coral reefs of the marshall islands,” *Ecological Monographs*, vol. 30, no. 1, pp. 65–127, 1960.
- [76] G. Almany, “Differential effects of habitat complexity, predators and competitors on abundance of juvenile and adult coral reef fishes,” *Oecologia*, vol. 141, pp. 105–113, 2004.
- [77] L. Alvarez-Filip, N. Dulvy, I. Côté, A. Watkinson, and J. Gill, “Coral identity underpins architectural complexity on caribbean reefs,” *Ecological Applications*, vol. 21, no. 6, pp. 2223–2231, 2011.
- [78] A. Rogers, J. Blanchard, and P. Mumby, “Fisheries productivity under progressive coral reef degradation,” *Journal of Applied Ecology*, vol. 55, pp. 1041–1049, 2018.
- [79] S. Fraser and G. Sedberry, “Reef morphology and invertebrate distribution at the continental shelf edge reefs in the South Atlantic Bight,” *Southeastern Naturalist*, vol. 7, no. 2, pp. 191–206, 2008.

- [80] C. Rosenzweig, D. Karoly, M. Vicarelli, P. Neofotis, Q. Wu, G. Casassa, A. Menzel, T. Root, N. Estrella, B. Seguin, P. Tryjanowski, C. Liu, S. Rawlins, and A. Imeson, “Attributing physical and biological impacts to anthropogenic climate change,” *Nature*, vol. 453, no. 7193, pp. 353–357, 2008.
- [81] D. Stern and R. Kaufmann, “Anthropogenic and natural causes of climate change,” *Climatic Change*, vol. 122, pp. 257–269, 2014.
- [82] S. Heron, J. Maynard, R. van Hooidonk, and C. Eakin, “Warming trends and bleaching stress of the world’s coral reefs 1985–2012,” *Scientific Reports*, vol. 6, no. 38402, 2016.
- [83] O. Hoegh-Guldberg, P. Mumby, A. Hooten, R. Steneck, P. Greenfield, E. Gomez, C. Harvell, P. Sale, A. Edwards, K. Caldeira, N. Knowlton, C. Eakin, R. Iglesias-Prieto, N. Muthiga, R. Bradbury, A. Dubi, and M. Hatzio, “Coral reefs under rapid climate change and ocean acidification,” *Science*, vol. 318, no. 1737, 2007.
- [84] B. Brown, “Coral bleaching: causes and consequences,” *Coral Reefs*, vol. 16, pp. S129–S138, 1997.
- [85] O. Hoegh-Guldberg, “Climate change, coral bleaching and the future of the world’s coral reefs,” *Marine and Freshwater Research*, vol. 50, pp. 839–866, 1997.
- [86] IPCC, “Climate change 2021: The physical science basis, contribution of working group i to the sixth assessment report of the intergovernmental panel on climate change,” *Cambridge University Press*, 2021.
- [87] N. Mollica, W. Guo, A. Cohen, K.-F. Huang, G. Foster, H. Donald, and A. Solow, “Ocean acidification affects coral growth by reducing skeletal density,” *PNAS*, vol. 115, no. 8, pp. 1754–1759, 2018.
- [88] C. Rogers, “The effect of shading on coral reef structure and function,” *Journal of Experimental Marine Biology and Ecology*, vol. 41, no. 3, pp. 269–288, 1979.
- [89] S. Andréfouët, P. Mumby, M. McField, C. Hu, and F. Muller-Karger, “Revisiting coral reef connectivity,” *Coral Reefs*, vol. 21, no. 1, pp. 43–48, 2002.
- [90] S. Wear and R. Vega Thurber, “Sewage pollution: mitigation is key for coral reef stewardship,” *Annals of the New York Academy of Sciences*, vol. 1355, no. 1, pp. 15–30, 2015.
- [91] A. Bauman, J. Burt, D. Feary, E. Marquis, and P. Usseglio, “Tropical harmful algal blooms: An emerging threat to coral reef communities?” *Marine Pollution Bulletin*, vol. 60, no. 11, pp. 2117–2233, 2010.
- [92] J. Martinez, C. Smith, and R. Richmond, “Invasive algal mats degrade coral reef physical habitat quality,” *Estuarine, Coastal and Shelf Science*, vol. 99, pp. 42–49, 2012.
- [93] M. Harmelin-Vivien, “The effects of storms and cyclones on coral reefs: A review,” *Journal of Coastal Research Special Issue No. 12*, pp. 211–231, 1994.
- [94] A. Bruckner, “Tracking the trade in ornamental coral reef organisms: The importance of CITES and its limitations,” *Aquarium Science and Conservation*, vol. 3, no. 3, pp. 79–94, 2001.

- [95] P. Sale, “Coral reef conservation and political will,” *Environmental Conservation*, vol. 42, no. 2, pp. 97–101, 2015.
- [96] A. Contreras-Silva, A. Tilstra, V. Migani, A. Thiel, E. Pérez-Cervantes, N. Estrada-Saldívar, X. E. Ilosvay, C. Mott, L. Alvarez-Filip, and C. Wild, “A meta-analysis to assess long-term spatiotemporal changes of benthic coral and macroalgae cover in the Mexican Caribbean,” *Scientific Reports*, vol. 10, no. 1, pp. 1–12, 2020.
- [97] B. Riegl, A. Bruckner, S. Coles, P. Renaud, and R. Dodge, “Coral reefs: threats and conservation in an era of global change,” *Annals of the New York Academy of Sciences*, vol. 1162, no. 1, pp. 136–186, 2009.
- [98] J. Maragos, “Impact of coastal construction on coral reefs in the U.S.-affiliated Pacific Islands,” *Coastal Management*, vol. 21, no. 4, pp. 235–269, 1993.
- [99] J. Bell, S. Davy, T. Jones, M. Taylor, and N. Webster, “Could some coral reefs become sponge reefs as our climate changes?” *Global Change Biology*, vol. 19, pp. 2613–2624, 2013.
- [100] A. Norström, M. Nyström, J. Lokrantz, and C. Folke, “Alternative states on coral reefs: beyond coral-macroalgal phase shifts,” *Marine Ecology Progress Series*, vol. 376, pp. 295–306, 2009.
- [101] S. Crisp, S. Tebbett, and D. Bellwood, “A critical evaluation of benthic phase shift studies on coral reefs,” *Marine Environmental Research*, vol. 178, p. 105667, 2022.
- [102] T. Gardner, I. Côté, J. Gill, A. Grant, and A. Watkinson, “Long-term region-wide declines in Caribbean corals,” *Science*, vol. 301, pp. 952–960, 2003.
- [103] J. Arias-González, T. Fung, R. Seymour, J. Garza-Pérez, G. Acosta-González, Y. Bozec, and C. Johnson, “A coral-algal phase shift in Mesoamerica not driven by changes in herbivorous fish abundance,” *PLoS ONE*, vol. 12, no. 4, p. e0174855, 2017.
- [104] J. Idjadi, S. Lee, J. Bruno, W. Precht, L. Allen-Requa, and P. Edmunds, “Rapid phase-shift reversal on a Jamaican coral reef,” *Coral Reefs*, vol. 25, pp. 209–211, 2006.
- [105] J. Bechtel, P. Gayle, and L. Kaufman, “The return of *Diadema antillarum* to Discovery Bay: Patterns of distribution and abundance,” in *Proceedings of the 10th International Coral Reef Symposium*, 2006, pp. 367–375.
- [106] A. Spadaro and M. Butler IV, “Herbivorous crabs reverse the seaweed dilemma on coral reefs,” *Current Biology*, vol. 31, no. 4, pp. R188–R190, 2021.
- [107] C. Jones, J. Lawton, and M. Shachak, “Positive and negative effects of organisms as physical ecosystem engineers,” *Ecology*, vol. 78, no. 7, pp. 1946–1957, 1997.
- [108] P. Hutchings, “Biological destruction of coral reefs,” *Coral Reefs*, vol. 4, no. 4, pp. 239–252, 1986.
- [109] A. Margiotta, V. Shervette, N. Hadley, C. Plante, and D. Wilber, “Species-specific responses of resident crabs to vertical habitat complexity on intertidal oyster reefs,” *Journal of Experimental Marine Biology and Ecology*, vol. 477, pp. 7–13, 2016.
- [110] D. Parsons, I. Suthers, D. Cruz, and J. Smith, “Effects of habitat on fish abundance and species composition on temperate rocky reefs,” *Marine Ecology Progress Series*, vol. 561, pp. 155–171, 2016.

- [111] H. Dierssen and A. Theberge Jr., “Bathymetry: History of seafloor mapping,” *Encyclopedia of Natural Resources*, vol. 2, p. 564, 2014.
- [112] L. Mayer, “Frontiers in seafloor mapping and visualization,” *Marine Geophysical Researches*, vol. 27, no. 1, pp. 7–17, 2006.
- [113] G. Konecny, “Photogrammetry” in *Geoinformation: Remote sensing, photogrammetry and geographic information systems*, 1st ed. London, UK: Taylor & Francis, 2003.
- [114] F. Doyle, “The historical development of analytical photogrammetry,” *Photogrammetric Engineering*, pp. 259–265, 1964.
- [115] G. Konecny, “The International Society for Photogrammetry and Remote Sensing: 75 years old, or 75 years young?” *Photogrammetric Engineering and Remote Sensing*, vol. 51, no. 7, pp. 919–933, 1985.
- [116] P. Wolf, B. Dewitt, and B. Wilkinson, *Elements of Photogrammetry with Applications in GIS*, 4th ed. McGraw-Hill Education, 2014.
- [117] B. Wu, “Photogrammetry,” *International Encyclopedia of Geography*, pp. 1–13, 2017.
- [118] R. Batson, “Status and future of extraterrestrial mapping programs,” NASA, Tech. Rep., 1981.
- [119] T. Schenk, *Digital photogrammetry*, 1st ed. TerraScience, 1999.
- [120] P. Rossi, C. Castagnetti, A. Capra, A. Brooks, and F. Mancini, “Detecting change in coral reef 3D structure using underwater photogrammetry: critical issues and performance metrics,” *Applied Geomatics*, vol. 12, pp. 3–17, 2020.
- [121] L. Froideval, K. Pedoja, F. Garestier, P. M. C. Conessa, X. Pellerin le Bas, K. Traore, and L. Benoit, “A low cost open-source workflow to generate georeferenced 3D SfM photogrammetric models of rocky outcrops,” *The Photogrammetric Record*, vol. 34, no. 168, pp. 365–384, 2019.
- [122] R. Ferrari, D. McKinnon, H. He, R. Smith, P. Corke, M. González-Rivero, P. Mumby, and B. Upcroft, “Quantifying multiscale habitat structural complexity: A cost-effective framework for underwater 3d modelling,” *Remote Sensing*, vol. 8, no. 2, pp. 113–134, 2016.
- [123] P. Andono, E. Yuniaro, M. Hariadi, and V. Venus, “3d reconstruction of under water coral reef images using low cost multi-view cameras,” in *International Conference on Multimedia Computing and Systems*, 2012, pp. 803–808.
- [124] W. Figueira, R. Ferrari, E. Weatherby, A. Porter, S. Hawes, and M. Byrne, “Accuracy and precision of habitat structural complexity metrics derived from underwater photogrammetry,” *Remote Sensing*, vol. 7, pp. 16 883–16 900, 2015.
- [125] C. Storlazzi, P. Dartnell, G. Hatcher, and A. Gibbs, “End of the chain? Rugosity and fine-scale bathymetry from existing underwater digital imagery using structure-from-motion (sfm) technology,” *Coral Reefs*, vol. 35, no. 3, pp. 889–894, 2016.
- [126] H. He, R. Ferrari, D. McKinnon, G. Roff, R. Smith, P. Mumby, and B. Upcroft, “Measuring reef complexity and rugosity from monocular video bathymetric reconstruction,” in *Proceedings of the 12th International Coral Reef Symposium*, 2012, pp. 1–5.

- [127] J. Leon, C. Roelfsema, M. Saunders, and S. Phinn, “Measuring coral reef terrain roughness using ‘structure-from-motion’ close-range photogrammetry,” *Geomorphology*, vol. 242, pp. 21–28, 2015.
- [128] S. Harwin, A. Lucieer, and J. Osborn, “The impact of the calibration method on the accuracy of point clouds derived using unmanned aerial vehicle multi-view stereopsis,” *Remote Sensing*, vol. 7, pp. 11 933–11 953, 2015.
- [129] D. Price, K. Robert, A. Callaway, C. Lo Iacono, R. Hall, and V. Huvenne, “Using 3D photogrammetry from ROV video to quantify cold-water coral reef structural complexity and investigate its influence on biodiversity and community assemblage,” *Coral Reefs*, vol. 38, pp. 1007–1021, 2019.
- [130] T. Hughes, N. Graham, J. Jackson, P. Mumby, and R. Steneck, “Rising to the challenge of sustaining coral reef resilience,” *Trends in Ecology & Evolution*, vol. 25, no. 11, pp. 633–642, 2010.
- [131] J. Rooker, Q. Dokken, C. Pattengill, and G. Holt, “Fish assemblages on artificial and natural reefs in the flower garden banks national marine sanctuary, usa,” *Coral Reefs*, vol. 16, pp. 83–92, 1997.
- [132] T. Wilding, E. Palmer, and N. Polunin, “Comparison of three methods for quantifying topographic complexity on rocky shores,” *Marine Environmental Research*, vol. 69, pp. 143–151, 2010.
- [133] D. Pygas, R. Ferrari, and W. Figueira, “Review and meta-analysis of the importance of remotely sensed habitat structural complexity,” *Estuarine, Coastal and Shelf Science*, vol. 235, p. 106468, 2020.
- [134] A. Fukunaga and J. Burns, “Metrics of coral reef structural complexity extracted from 3d mesh models and digital elevation models,” *Remote Sensing*, vol. 12, no. 17, p. 2676, 2020.
- [135] J. Carleton and P. Sammarco, “Effects of substratum irregularity on success of coral settlement: Quantification by comparative geomorphological techniques,” *Bulletin of Marine Science*, vol. 40, no. 1, pp. 85–98, 1987.
- [136] M. González-Rivero, A. Harborne, A. Herrera-Reveles, Y.-M. Bozec, A. Rogers, A. Friedman, A. Ganase, and O. Hoegh-Guldberg, “Linking fishes to multiple metrics of coral reef structural complexity using three-dimensional technology,” *Scientific Reports*, vol. 7, no. 13965, 2017.
- [137] A. Friedman, O. Pizarro, S. Williams, and M. Johnson-Roberson, “Multi-scale measures of rugosity, slope and aspect from benthic stereo image reconstructions,” *PLoS ONE*, vol. 7, no. 12, 2012.
- [138] J. Gardiner, J. Behnsen, and C. Brassey, “Alpha shapes: determining 3d shape complexity across morphologically diverse structures,” *BMC Evolutionary Biology*, vol. 18, no. 184, 2018.
- [139] R. Fisher, “Dispersion on a sphere,” in *Proceedings of the Royal Society of London. Series A, Mathematical and Physical Sciences*, vol. 217, no. 1130, 1953, pp. 295–305.
- [140] J. Sappington, K. Longshore, and D. Thompson, “Quantifying landscape ruggedness for animal habitat analysis: A case study using bighorn sheep in the Mojave Desert,” *The Journal of Wildlife Management*, vol. 71, no. 5, pp. 1419–1426, 2007.

- [141] G. Lambert, S. Jennings, H. Hinz, L. Murray, L. Parrott, M. Kaiser, and J. Hiddink, “A comparison of two techniques for the rapid assessment of marine habitat complexity,” *Methods in Ecology and Evolution*, vol. 4, pp. 226–235, 2013.
- [142] L. Zevenbergen and C. Thorne, “Quantitative analysis of land surface topography,” *Earth Surface Processes and Landforms*, vol. 12, pp. 47–56, 1987.
- [143] M. Beck, “Comparison of the measurement and effects of habitat structure on gastropods in rocky intertidal and mangrove habitats,” *Marine Ecology Progress Series*, vol. 169, pp. 165–178, 1998.
- [144] B. Mandelbrot, *The Fractal Geometry of Nature*, 1st ed. New York, USA: W. H. Freeman and Co., 1982.
- [145] R. Bradbury and R. Reichelt, “Fractal dimension of a coral reef at ecological scales,” *Marine Ecology Progress Series*, vol. 10, pp. 169–171, 1983.
- [146] D. Mark, “Fractal dimension of a coral reef at ecological scales: a discussion,” *Marine Ecology Progress Series*, vol. 14, pp. 293–294, 1984.
- [147] H. Gu, H. Li, L. Yan, Z. Liu, R. Blaschke, and U. Soergel, “An object-based semantic classification method for high resolution remote sensing imagery using ontology,” *Remote Sensing*, vol. 9, no. 4, pp. 329–350, 2017.
- [148] A. Knudby and E. LeDrew, “Measuring structural complexity on coral reefs,” in *Proceedings of the American Academy of Underwater Sciences*, 2007.
- [149] S. Newman, E. Meesters, C. Dryden, S. Williams, C. Sanchez, P. Mumby, and N. Polunin, “Reef flattening effects on total richness and species responses in the caribbean,” *Journal of Animal Ecology*, 2015.
- [150] T. Sumathi, C. Lakshmi Devasena, and M. Hemalatha, “An overview of automated image annotation approaches,” *International Journal of Research and Reviews in Information Sciences*, vol. 1, no. 1, pp. 1–5, 2011.
- [151] A. Olaode and G. Naghdy, “Review of the application of machine learning to the automatic semantic annotation of images,” *IET Image Processing*, vol. 13, no. 8, pp. 1232–1245, 2019.
- [152] R. Heckel and F. Yilmaz, “Early stopping in deep networks: Double descent and how to eliminate it,” *arXiv preprint 2007.10099*, 2020.
- [153] M. Marcos, M. Soriano, and C. Saloma, “Classification of coral reef images from underwater video using neural networks,” *Optics Express*, vol. 13, no. 22, pp. 8766–8771, 2005.
- [154] O. Beijbom, P. Edmunds, D. Kline, B. Mitchell, and D. Kriegman, “Automated annotation of coral reef survey images,” in *Proceedings of the IEEE Conference on Computer Vision and Pattern Recognition*, 2012.
- [155] O. Beijbom, P. Edmunds, C. Roelfsema, J. Smith, D. Kline, B. Neal, M. Dunlap, C. Moriarty, T.-Y. Fan, C.-J. Tan, S. Chan, T. Treibitz, A. Gamst, B. Mitchell, and D. Kriegman, “Towards automated annotation of benthic survey images: Variability of human experts and operational modes of automation,” *PLoS ONE*, vol. 10, no. 7, 2015.

- [156] B. Hopkinson, A. King, D. Owen, M. Johson-Roberson, M. Long, and S. Bhandarkar, “Automated classification of three-dimensional reconstructions of coral reefs using convolutional neural networks,” *PLoS ONE*, vol. 15, no. 3, 2020.
- [157] R. Morais, M. Depczynski, C. Fulton, M. Marnane, P. Narvaez, V. Huertas, S. Brandl, and D. Bellwood, “Severe coral loss shifts energetic dynamics on a coral reef,” *Functional Ecology*, vol. 34, pp. 1501–1515, 2020.
- [158] J. Veron, M. Stafford-Smith, L. DeVantier, and E. Turak, “Overview of the distribution patterns of zooxanthellate Scleractinia,” *Frontiers in Marine Science*, vol. 1, p. 81, 2015.
- [159] J. Clifton, R. Unsworth, and D. Smith, *Marine Research and Conservation in the Coral Triangle*, 1st ed. New Youkr, USA: Nova Science Publishers, 2010.
- [160] B. Lin, “Close encounters of the worst kind: reforms needed to curb coral reef damage by recreational divers,” *Coral Reefs*, vol. 40, no. 5, pp. 1429–1435, 2021.
- [161] A. Gouraguine, J. Moranta, A. Ruiz-Frau, H. Hinz, O. R. nones, S. Ferse, J. Jompa, and D. Smith, “Citizen science in data and resource-limited areas: A tool to detect long-term ecosystem changes,” *PLoS ONE*, vol. 14, no. 1, p. e0210007, 2019.
- [162] A. Powell, D. Smith, L. Hepburn, T. Jones, J. Berman, J. Jompa, and J. Bell, “Reduced diversity and high sponge abundance on a sedimented Indo-Pacific reef system: Implications for future changes in environmental quality,” *PLoS ONE*, vol. 9, no. 1, 2014.
- [163] O. Wallacea, “Coral reef monitoring data,” 2016.
- [164] M. Crabbe and D. Smith, “Sediment impacts on growth rates of *acropora* and *porites* corals from fringing reefs of Sulawesi, Indonesia,” *Coral Reefs*, vol. 24, pp. 437–441, 2005.
- [165] Agisoft LLC, *Agisoft Metashape User Manual: Standard Edition, Version 1.8*, 2022.
- [166] C. Savrda, “Chalk and related deep-marine carbonates,” *Developments in Sedimentology*, vol. 64, pp. 777–806, 2012.
- [167] L. Buatois, R. Bromley, M. Mángano, E. Bellosi, and N. Carmona, “Ichnology of shallow marine deposits in the miocene chenque formation of patagonia: complex ecologic structure and niche partitioning in neogene ecosystems,” *Publicación Especial de la Asociación Paleontológica Argentina*, vol. 9, pp. 85–95, 2003.
- [168] R. Mortimore, “A chalk revolution: what have we done to the Chalk of England,” *Proceesings of the Geologists’ Association*, vol. 122, pp. 232–297, 2011.
- [169] A. Rees, E. Sheehan, and M. Attrill, “The lyme bay experimental potting study: A collaborative programme to assess the ecological effects of increasing potting density in the lyme bay marine protected area,” University of Plymouth Marine Institute and the Blue Marine Foundation, Tech. Rep., 2019.
- [170] F. Stephenson, A. Mill, C. Scott, N. Polunin, and C. Fitzsimmons, “Experimental potting impacts on common uk reef habitats in areas of high and low fishing pressure,” *ICES Journal of Marine Science*, vol. 74, no. 6, pp. 1648–1659, 2017.
- [171] UK Ministerial Orders, “The Cromer Shoal Chalk Beds Marine Conservation Zone Designation Order,” 2016. [Online]. Available: <https://www.legislation.gov.uk/ukmo/2016/4/created>



- [172] F. Tibbitt, J. Love, J. Wright, and J. Chamberlain, “Human impacts on Cromer Shoal Chalk Beds MCZ: Chalk complexity and population dynamics of commercial crustaceans,” Natural England, Tech. Rep., 2020.
- [173] Eastern Inshore Fisheries and Conservation Authority, “Marine and coastal access act 2009 (c.23),” 2019. [Online]. Available: <https://www.eastern-ifca.gov.uk/wp-content/uploads/2021/03/EIFCA-Minimum-Sizes-Byelaw-approved.pdf>
- [174] C. White, “Social resilience, place and identity in the small-scale North Norfolk “Cromer Crab” fishery, UK,” A thesis submitted for the degree of Doctor of Philosophy, University of East Anglia, 2015.
- [175] R. Spray. Sheringham lost pots Sept 19. [Online]. Available: <https://www.youtube.com/watch?v=SwyNkirXsHw/>
- [176] R. Hartnoll, “Circalittoral faunal turf biotopes: An overview of dynamics and sensitivity characteristics for conservation management of marine SACs,” Scottish Association of Marine Science (UK Marine SAC Project), Oban, Scotland, Tech. Rep., 1998.
- [177] F. Stephenson, C. Fitzsimmons, A. Polunin, A. Mill, and C. Scott, “Assessing long term benthic impacts of potting in Northumberland,” Natural England, Tech. Rep., Unpublished.
- [178] Ropeless Consortium. Rope-less fishing: A vision for how it can work. [Online]. Available: <https://ropeless.org/background/>
- [179] Scottish Entanglement Alliance. Ropeless technologies and virtual gear marking. [Online]. Available: <https://www.scottishentanglement.org/guest-blog-ropeless-technologies-and-virtual-gear-marking/>
- [180] N. Mieszkowska, L. Firth, and M. Bentley, “Impacts of climate change on intertidal habitats,” *Marine Climate Change Impacts Partnership: Science Review*, pp. 180–192, 2013.
- [181] M. Kaiser, J. Collie, S. Hall, S. Jennings, and I. Poiner, “12 impacts of fishing gear on marine benthic habitats,” *Responsible fisheries in the marine ecosystem*, vol. 57, no. 3, pp. 197–217, 2003.
- [182] P. Lawton, “Predatory interaction between the brachyuran crab *Cancer pagurus* and decapod crustacean prey,” *Marine Ecology Progress Series*, vol. 52, pp. 169–179, 1989.
- [183] W. Hunter and M. Sayer, “The comparative effects of habitat complexity on faunal assemblages of northern temperate artificial and natural reefs,” *ICES Journal of Marine Science*, vol. 66, no. 4, pp. 691–698, 2009.
- [184] D. Wilhelmsson, S. Yahya, and M. Öhman, “Effects of high-relief structures on cold temperate fish assemblages: A field experiment,” *Marine Biology Research*, vol. 2, pp. 136–147, 2006.
- [185] C. Vogan, P. Llewellyn, and A. Rowley, “Epidemiology and dynamics of shell disease in the edible crab *Cancer pagurus*: a preliminary study of Langland Bay, Swansea, UK,” *Diseases of Aquatic Organisms*, vol. 35, pp. 81–87, 1999.
- [186] J. Hill and C. Wilkinson, *Methods for Ecological Monitoring of Coral Reefs*, 1st ed. Townsville, Australia: Australian Institute of Marine Science, 2004.

- [187] P. Rubbens, S. Brodie, T. Cordier, D. Destro Barcellos, P. Devos, J. Fernandes-Salvador, J. Fincham, A. Gomes, N. Handegard, K. Howell, C. Jamet, K. Kartveit, H. Moustahfid, C. Parcerisas, D. P. R. Sauzède, M. Sokolova, L. Uusitalo, L. Van den Bulcke, A. van Helmond, J. Watson, H. Welch, O. Beltran-Perez, S. Chaffron, D. Greenberg, B. Kühn, R. Kiko, M. Lo, R. Lopes, K. Möller, W. Michaels, A. Pala, J. Romagnan, P. Schuchert, V. Seydi, S. V. K. Malde, and J. Irisson, “Machine learning in marine ecology: an overview of techniques and applications,” *ICES Journal of Marine Science*, vol. 80, pp. 1829–1853, 2023.
- [188] J. Chamberlain, A. Campello, J. P. Wright, L. G. Clift, A. Clark, and A. García Seco de Herrera, “Overview of ImageCLEFcoral 2019 task,” in *CLEF2019 Working Notes*, ser. CEUR Workshop Proceedings, vol. 2380. CEUR-WS.org, 2019.
- [189] —, “Overview of the ImageCLEFcoral 2020 task: Automated coral reef image annotation,” in *CLEF2020 Working Notes*, ser. CEUR Workshop Proceedings, vol. 2696. CEUR-WS.org, 2020.
- [190] J. Chamberlain, A. García Seco de Herrera, A. Campello, A. Clark, T. A. Oliver, and H. Moustahfid, “Overview of the ImageCLEFcoral 2021 task: Coral reef image annotation of a 3D environment,” in *CLEF2021 Working Notes*, ser. CEUR Workshop Proceedings, vol. 2936. LNCS Lecture Notes in Computer Science, Springer, 2021.
- [191] J. Chamberlain, A. García Seco de Herrera, A. Campello, and A. Clark, “ImageCLEFcoral task: Coral reef image annotation and localisation,” in *CLEF2022 Working Notes*, ser. CEUR Workshop Proceedings, vol. 3180. CEUR-WS.org, 2022.
- [192] G. Roff and P. Mumby, “Global disparity in the resilience of coral reefs,” *Trends in ecology and evolution*, vol. 27, no. 7, pp. 404–413, 2012.
- [193] G. Roff, “Evolutionary history drives biogeographic patterns of coral reef resilience,” *BioScience*, vol. 71, no. 1, pp. 26–39, 2021.
- [194] G. Pavoni, M. Corsini, M. Callieri, G. Fiameni, C. Edwards, and P. Cignoni, “On improving the training of models for the semantic segmentation of benthic communities from orthographic imagery,” *Remote Sensing*, vol. 12, no. 18, p. 3106, 2020.
- [195] W. Xiang, P. Yang, S. Wang, B. Xu, and H. Liu, “Underwater image enhancement based on red channel weighted compensation and gamma correction model,” *Opto-Electronic Advances*, vol. 1, no. 10, p. 180024, 2018.
- [196] C. Caridade and A. Marcal, “Automatic classification of coral images using color and textures,” in *CLEF2019 Working Notes*, ser. CEUR Workshop Proceedings, vol. 2380. CEUR-WS.org, 2019.
- [197] S. Jaisakthi, P. Mirunalini, and C. Aravindan, “Coral reef annotation and localization using faster r-cnns,” in *CLEF2019 Working Notes*, ser. CEUR Workshop Proceedings, vol. 2380. CEUR-WS.org, 2019.
- [198] K. Bogomasov, P. Grawe, and S. Conrad, “A two-stage approach for localization and classification of coral reef structures,” in *CLEF2019 Working Notes*, ser. CEUR Workshop Proceedings, vol. 2380. CEUR-WS.org, 2019.
- [199] A. Steffens, A. Campello, J. Ravenscroft, A. Clark, and H. Hagraas, “Deep segmentation: Using deep convolutional networks for coral reef pixel-wise parsing,” in *CLEF2019 Working Notes*, ser. CEUR Workshop Proceedings, vol. 2380. CEUR-WS.org, 2019.

- [200] L. Pícek, A. Říha, and A. Zita, “Coral reef annotation, localisation and pixel-wise classification using Mask R-CNN and Bag of Tricks,” in *CLEF2020 Working Notes*, ser. CEUR Workshop Proceedings, vol. 2696. CEUR-WS.org, 2020.
- [201] I. Gruber and Straka, “Automatic coral detection using neural networks,” in *CLEF2020 Working Notes*, ser. CEUR Workshop Proceedings, vol. 2696. CEUR-WS.org, 2020.
- [202] K. Bogomasov, P. Grawe, and S. Conrad, “Enhanced localization and classification of coral reef structures and compositions,” in *CLEF2020 Working Notes*, ser. CEUR Workshop Proceedings, vol. 2696. CEUR-WS.org, 2020.
- [203] M. Arendt, J. Rückert, R. Brüngel, C. Brumann, and C. Friedrich, “The effects of colour enhancement and IoU optimisation on object detection and segmentation of coral reef structures,” in *CLEF2020 Working Notes*, ser. CEUR Workshop Proceedings, vol. 2696. CEUR-WS.org, 2020.
- [204] L. Soukup, “Automatic coral reef annotation, localization and pixel-wise parsing using Mask R-CNN,” in *CLEF2021 Working Notes*, ser. CEUR Workshop Proceedings, vol. 2936. CEUR-WS.org, 2021.
- [205] R. Gunti and A. Rorissa, “A convolutional neural networks based coral reef annotation and localization,” in *CLEF2021 Working Notes*, ser. CEUR Workshop Proceedings, vol. 2936. CEUR-WS.org, 2021.
- [206] J. Wright, I.-L. Palosanu, L. Clift, A. García Seco de Herrera, and J. Chamberlain, “Pixelwise annotation of coral reef substrates,” in *CLEF2021 Working Notes*, ser. CEUR Workshop Proceedings, vol. 2936. CEUR-WS.org, 2021.
- [207] K. Zawada, M. Dornelas, and J. Madin, “Quantifying coral morphology,” *Coral Reefs*, vol. 38, pp. 1281–1292, 2019.
- [208] A. Abdul Ghani and N. Mat Isa, “Underwater image quality enhancement through composition of dual-intensity images and rayleigh-stretching,” *SpringerPlus*, vol. 3, no. 7, pp. 1–14, 2014.
- [209] —, “Underwater image quality enhancement through integrated color model with rayleigh distribution,” *Applied Soft Computing*, vol. 27, pp. 219–230, 2014.
- [210] A. Galdran, D. Pardo, A. Picón, and A. Álvarez-Gila, “Automatic red-channel underwater image restoration,” *Journal of Visual Communication and Image Representation*, vol. 26, pp. 132–145, 2015.
- [211] E. Stathopoulou and F. Remondino, “Semantic photogrammetry: Boosting image-based 3D reconstruction with semantic labeling,” *International Archives of the Photogrammetry, Remotes Sensing and Spatial Information Sciences*, vol. 42, no. 2, p. W9, 2019.
- [212] K. O’Shea and R. Nash, “An introduction to convolutional neural networks,” *arXiv preprint 1511.08458*, 2015.
- [213] Y. Liu and S. Wang, “A quantitative detection algorithm based on improved faster R-CNN for marine benthos,” *Ecological Informatics*, vol. 61, p. 101228, 2021.
- [214] N. Piechaud, C. Hunt, P. Culverhouse, N. Foster, and K. Howell, “Automated identification of benthic epifauna with computer vision,” *Marine Ecology Progress Series*, vol. 615, pp. 15–30, 2019.

- [215] E. Prado, A. Rodríguez-Basalo, A. Cobo, P. Ríos, and F. Sánchez, “3D fine-scale terrain variables from underwater photogrammetry: A new approach to benthic microhabitat modeling in a circalittoral rocky shelf,” *Remote Sensing*, vol. 12, no. 15, p. 2466, 2020.
- [216] A. Li, V. Chirayath, M. Segal-Rozenhaimer, J. Torres-Pérez, and J. van der Bergh, “NASA NeMO-Net’s Convolutional Neural Network: Mapping marine habitats with spectrally heterogeneous remote sensing imagery,” *IEEE Journal of Selected Topics in Applied Earth Observations and Remote Sensing*, vol. 13, pp. 5115–5133, 2020.
- [217] A. Mahmood, M. Bennamoun, S. An, F. Sohel, F. Boussaid, R. Hovey, G. Kendrick, and R. Fisher, “Coral classification with hybrid feature representations,” in *IEEE International Conference on Image Processing*, 2016, pp. 519–523.
- [218] G. Pavoni, M. Corsini, N. Pedersen, V. Petrovic, and P. Cignoni, “Challenges in the deep learning-based semantic segmentation of benthic communities from ortho-images,” *Applied Geomatics*, vol. 13, pp. 131–146, 2021.
- [219] B. Wang, X. Luo, Y. Yang, W. Sun, M. Cane, W. Cai, S. Yeh, and J. Liu, “Historical change of El Niño properties sheds light on future changes of extreme El Niño,” *PNAS*, vol. 116, no. 45, pp. 22 512–22 517, 2019.
- [220] L. Chen, G. Papandreou, F. Schroff, and H. Adam, “Rethinking atrous convolution for semantic image segmentation,” *arXiv preprint 1706.05587*, 2017.
- [221] S. Gall, L. Rodwell, S. Clark, T. Robbins, M. Attrill, L. Holmes, and E. Sheehan, “The impact of potting for crustaceans on temperate rocky reef habitats: Implications for management,” *Marine Environmental Research*, vol. 162, p. 105134, 2020.
- [222] D. Vaughan, “Fishing effort displacement and the consequences of implementing Marine Protected Area management - An English perspective,” *Marine Policy*, vol. 84, pp. 228–234, 2017.
- [223] J. Pierce, M. Butler Iv, Y. Rzhanov, K. Lowell, and J. Dijkstra, “Classifying 3-d models of coral reefs using Structure-From-Motion and Multi-View Semantic Segmentation,” *Frontiers in Marine Science*, vol. 8, p. 706674, 2021.
- [224] M. Johnson-Roberson, M. Bryson, A. Friedman, O. Pizarro, G. Troni, P. Ozog, and J. Henderson, “High-resolution underwater robotic vision-based mapping and three-dimensional reconstruction for archaeology,” *Journal of Field Robotics*, vol. 34, no. 4, pp. 625–643, 2017.
- [225] H. Albalawi, Z. Khan, A. Valle-Pérez, K. Kahin, M. Hountondji, H. Alwazani, S. Schmidt-Roach, P. Bilalis, M. Aranda, C. Duarte, and C. Hauser, “Sustainable and eco-friendly coral restoration through 3d printing and fabrication,” *ACS Sustainable Chemistry Engineering*, vol. 9, no. 37, pp. 12 634–12 645, 2021.
- [226] O. Ly, A. Yoris-Nobile, N. Sebaibi, E. Blanco-Fernandez, M. Boutouil, D. Castro-Fresno, A. Hall, R. Herbert, W. Deboucha, B. Reis, J. Franco, M. Borges, I. Sousa-Pinto, P. van der Linden, and R. Stafford, “Optimisation of 3d printed concrete for artificial reefs: Biofouling and mechanical analysis,” *Construction and Building Materials*, vol. 272, p. 121649, 2021.
- [227] F. Cruz, E. Pereira, I. Valente, M. Tiago, D. Maslov, and M. Pinheiro, “Structural design of an innovative multifunctional artificial reef,” in *OCEANS 2018 MTS/IEEE Charleston*, 2018, pp. 1–7.

# I | Agisoft Metashape outline

## I.1 Processing 3D models in Agisoft Metashape

Imaging a reef is only the first step in creating a 3D reconstruction. The building of a model can utilise many varied techniques, but SfM is both common across marine monitoring and assessment [3, 17, 48, 122] and relatively inexpensive and simple to carry out compared to many other reconstruction methods. It relies on the extrapolation of camera position in 3D space through common points between adjacent images to build an accurately scaled and positioned model of the environment. Metashape has automated these steps into user-friendly software with customisable settings and interactive models. Each key step is outlined below with the adjustable settings (*italicised*) detailed.

### I.1.1 Step 1 - Photo alignment

The first stage of the SfM process is to align all images and orientate them in 3D space, looking for commonalities in photos to associate them together. A sparse cloud of common features is produced and extrapolated to determine the position of each image (and the associated position of the camera when it was captured) in relation to others. When selecting this process, several settings can be adjusted to customise the workflow. The images do not have to be in any particular order, which is an advantage of SfM, particularly when using multiple camera devices.

*Accuracy* alters the resolution of uploaded images within the workflow. It can be set to either “lowest,” “low,” “medium,” “high,” or “highest” to, in turn, downscale the image by a factor of 64, 16, or 4; use the original image; or upscale by a factor of 4. Downscaling occurs when an image is used with a reduced pixel count and subsequent smaller storage size but the same 2D scale, and upscaling is the reverse, to alter the resolution of the images. Lower accuracy reduces the processing time of the model but must be balanced with the desired output. A model that will have a lot of fine scale detail will be less tolerant of lower accuracy than a less detailed one.

*Generic preselection* determines whether all images will be compared as inputted from the start of processing, or if a pre-scan with lower accuracy versions of images will take place to find commonalities and extract camera positions. This setting is either on or off only. When selected, processing time is reduced as it negates the need for each image to be compared to all other images at their largest size (in terms of computer storage and pixel count); however, this can cause issues when lower image quality is used as the already poor texture of the image can be lost in downscaling, so some common points and image overlaps may not be detected.

*Reference preselection* and reset current alignment settings presume that an alignment has already taken place on the current image set and is being reattempted. When selected, they leverage the previous alignment to increase accuracy. This is useful if a lower quality alignment was required to get initial positioning, but a higher quality model is desired. Processing time is increased with every alignment iteration.

In photogrammetry, key points are distinct or interesting features within images (e.g. an area with high contrast). The *key point limit* setting subsequently caps the number

of key points to be found within an image. It has a default setting of 40,000, but can have any input, with a 0 setting meaning no limit is set. The number of key points within an image will not necessarily reach the set limit, particularly on poorer quality images such as with underwater scenes, as images with similar colours, textures, or other features throughout show fewer distinctions to be tagged as interesting. A higher limit, or no limit, will increase processing time, but also increases the number of points available to construct the 3D model. Finding more points may not be a benefit if the number of incorrect or irrelevant points increases more than the number of useful ones.

Tie points are the key points that occur in more than one image, i.e. they “tie” images together through common features. The *tie point limit* setting determines the number of key points taken from each image to connect it to other images, with a default setting of 4,000 points. If key point limit and tie point limit were set to default, up to 40,000 key points would be identified per image, of which up to 4,000 would be used to connect each image to others. These points combine into a sparse cloud - a reconstruction of all tie points in three-dimensional space. Upping the tie point limit will increase the number of points in the sparse cloud at the cost of greater processing time. Tie points can be thinned retroactively without affecting alignment, which could speed up later processing.

The *apply masks to* setting presumes that some part of an image or images have been masked off. Masks can be applied to “tie points,” “key points,” or “none.” If applied to key or tie points, masked areas will be ignored when those points are determined, or if set to none, masked areas will be ignored and treated as normal image areas.

Selecting for *guided image matching* increases key points per image without affecting the processing time greatly. It is used with particularly high resolution images, to minimise missed feature detection. The option for *adaptive camera model fitting* automatically selects camera parameters to be adjusted with calibrations and applies these to all images.

### I.1.2 Step 2 - The dense cloud

Once the sparse cloud has been generated through photo alignment, a dense cloud of the model points is constructed. This workflow uses combined depth maps (an intermediary step that maps the distance between connected images and the position of the camera(s) when they were taken) to create a small dense cloud for each image’s associated points before merging them into the final dense cloud. This stage has the fewest adjustable settings.

Dense cloud *quality* can be set to “lowest,” “low,” “medium,” “high,” or “ultra high.” This quality setting performs in the same manner to the quality options in photo alignment, but with “ultra high” as the original image, and each step down leading to a factor 4 downscale from the previous level. Adjusting this setting alters the number of points within the dense cloud, with higher quality clouds containing more points.

A *depth filtering* setting is provided at this stage to avoid points from poor quality images, which may be outliers to the model. Settings for this are “aggressive,” “moderate,” “mild,” or “disabled.” Aggressive filtering is useful for models without intricate details and will remove most of what it considers outlying points. Mild filtering acts in the opposite manner, filtering minimally to maintain features with fine scale detailing. Moderate filtering acts as a middle ground to these options. Though the option to disable filtering is present, every potential outlier will be present which would produce a dense cloud with excessive noise in most cases. The stronger the filter used, the less noise in the dense cloud, but the greater the chance of lost detail in the model. Selection is therefore specific to both model type and image quality.

Checkboxes can be selected or deselected, providing the options to *reuse depth maps*, *calculate point colours*, and *calculate point confidence*. Reuse depth maps can only be selected if “keep depth maps” was selected prior to processing and is useful if a model is

being generated of the same object from a replicated camera path at the same settings. Calculate point colours uses information from the original images to colourise each point. This is useful if a general colour view is required and a lower resolution is not an issue, but is unnecessary if adding texture, which will colour the model to the images original resolution. Point confidence uses the number of depth maps used per point to map confidence across the dense cloud, which allows the removal of low confidence points from the dense cloud, which can be helpful if the cloud has a lot of noise or outlying points.

### I.1.3 Step 3 - Meshing

The model mesh is a polygon layer connecting the dense cloud points into one cohesive layer. Each dense cloud point is connected to its adjacent points with edges, which form a loop to create each face within the mesh. There are many customisation options within this process.

To build the mesh, the *source data* must first be selected. This can be one of three options: “tie points,” “dense cloud,” or “depth maps.” Each has their own merits. Using tie points allows for rapid construction, but produces a lower quality mesh. Dense cloud based meshes take longer to generate but are of a higher quality. Depth map meshes are less intensive to create than dense cloud meshes but, unlike dense clouds, they cannot be edited, so noisy or low confidence data cannot be removed.

*Surface type* can be set to “arbitrary” or “height field.” An arbitrary surface can apply to models of any type as no assumptions are made about the modelled object/region. A height field surface is used for modelling flat surfaces, and is particularly designed for aerial imagery and other types of planar fields. Arbitrary surface type requires more processing power, but can be used on 3D structures and reconstructions. The *quality*, *depth filtering*, *use strict volume mask*, and *reuse depth maps* settings become available if depth maps are selected as the source type and follows the same settings as in the dense cloud settings.

*Face count* sets the number of polygons generated within the mesh. This can be set to “high,” “medium,” “low,” or “custom.” The preset values are determined by the software as  $\frac{1}{5}$ ,  $\frac{1}{15}$ , and  $\frac{1}{45}$  of the number of points in the cloud data supplied (dense cloud or tie points) for high, medium, and low settings. The higher the face count value, the more detailed the model to a certain degree, though too high a number will vastly increase processing time and can cause issues with mesh visualisation. Too low a number can also cause visualisation issues, this time because the mesh is too unspecific and not able to overlay features appropriately.

The *interpolation* setting can be “disabled,” “enabled,” or “extrapolated.” Disabling interpolation will only reconstruct the mesh per the source data, creating an accurate model useful for further analysis or for precise reconstruction. Enabled interpolation will connect meshes within a preset diameter around each point, which fills smaller gaps in the mesh. Extrapolated interpolation creates a solid mesh without any holes. The latter two options are more beneficial for purely visual models without the need for further analysis, though with enabled interpolation may not negatively impact post modelling results depending on the diameter used.

A setting can be selected to *calculate vertex colours*, which colours the mesh from either source data or original image data.

### I.1.4 Step 4 - Adding texture

To complete the 3D reconstruction within Metashape, texture is added to the model mesh. This utilises a data set to map colour onto mesh faces and has several customisable settings.

Firstly, the *texture type* is selected. A “diffuse map” adds colour to the surface. A “normal map” leverages the surface normal (or the direction that light would reflect from the surface) of each pixel within the texture layer, modifying them to deviate from their native direction to give the illusion of further 3D structure from apparent convex or concave areas of the model texture. Normal maps are represented as RGB values (normalised on a 0-1 scale) which translate to XYZ coordinates of the difference in actual to modified surface normal. An “occlusion map” adds shading to the model by determining each face’s exposure to ambient lighting, producing a monochrome model.

*Source data* can be selected as “images” or a “3D model.” Using images as a source builds a diffuse map texture using either the images from the align input stage or from another model’s texture map. Using a 3D model enables normal and occlusion maps to be created, with the source 3D model being more detailed than the target one.

*Mapping mode* determines how the texture will be projected onto the mesh surface. The default “generic” mode which allows Metashape to determine the way in which images are connected into a texture atlas as uniformly as possible. “Orthophoto” mode uses a orthomosaic to provide texture through orthographic projection of the horizontal view of the model, without providing texture to the vertical. “Adaptive orthophoto” mapping mode textures in the same manner as orthophoto mode, but also textures the vertical sections of model separately. “Spherical” mapping mode is used for spherically structured models and applies texture through a specially designed texture atlas. “Single camera” mapping mode allows an image to be selected for use in texturing. “Keep UV” mode can be used with texture maps from other software.

*Blending mode* determines how the different colours from each image associated with a pixel will be combined and is not available with single camera mapping mode. When set to the default “mosaic” mode, the closest image to the pixel is used to determine its colour. “Average” blending mode takes the weighted average of the pixels colour values in all associated images. “Max intensity” and “min intensity” take the maximum or minimum bright pixel (i.e. the brightest or darkest) from all images for the pixel value. “Disabled” blending mode is used with imported models that already have an associated texture.

Entering a *texture size/count* sets the pixel dimensions of the texture atlas. Greater pixel dimensions and therefore higher texture resolution is enabled by using multiple texture files, the number of which is also specified in this setting.

Selecting to *enable hole filling* smooths the texture of surfaces where many small features impact other regions, while selecting to *enable ghosting filter* removes the impact of moving objects that were in images but not reconstructed from the model texture.



## II | Method testing data

Table II.1: Linear captured distance (cm) vertically and horizontally when holding an SJCam action camera in portrait or landscape orientation, at each field of view (FoV) setting and set distances from an imagined substrate.

Distance from substrate (m)	FoV setting			
	70°		170°	
	Portrait	Landscape	Portrait	Landscape
1	78.6	132.2	178.4	331.2
2	161.8	242.2	331.2	505.8
3	242.2	338.4	436.6	696.8
4	338.4	390.6	578.8	906.4
5	390.6	591.4	713.4	1116.2
7	591.4	857.2	1116.2	1622.6
10	857.2	1221.2	1622.6	2284.8

Table II.2: Linear captured distance (cm) vertically and horizontally when holding a GoPro action camera in portrait or landscape orientation, at each field of view (FoV) setting and set distances from an imagined substrate.

Distance from substrate (m)	FoV setting			
	Medium		Wide	
	Portrait	Landscape	Portrait	Landscape
1	132.0	220.2	227.0	356.2
2	283.4	512.2	440.6	740.4
3	398.4	671.2	645.0	1025.4
4	570.8	839.4	999.0	1335.0
5	726.2	1039.2	1036.0	1671.8
7	900.6	1405.4	1223.4	2087.8
10	1258.6	2016.6	1849.2	3177.6

Table II.3: Rugosity values extracted from models generated at the Pak Kasims reef site on Pulau Hoga using a single camera lawnmower method and a 5-camera array. Rugosity 1-6 corresponds to a “chain” within the model.

Quadrat		Rugosity						Multi camera							
		Single camera			Mean			SD			Mean			SD	
1	2	3	4	5	6	Mean	SD	1	2	3	4	5	6	Mean	SD
1.1	0.75	0.62	0.60	0.66	0.68	0.61	0.65	0.06	0.64	0.72	0.80	0.59	0.84	0.70	0.11
1.2	0.58	0.65	0.52	0.54	0.71	0.57	0.60	0.07	0.81	0.62	0.56	0.64	0.70	0.67	0.08
1.3	0.45	0.61	0.62	0.57	0.75	0.64	0.60	0.10	0.68	0.71	0.65	0.70	0.75	0.68	0.05
1.4	0.69	0.44	0.36	0.57	0.44	0.64	0.52	0.13	0.59	0.74	0.76	0.58	0.77	0.71	0.09
1.5	0.55	0.50	0.53	0.65	0.51	0.56	0.55	0.05	0.79	0.57	0.69	0.77	0.82	0.72	0.10
1.6	0.64	0.73	0.63	0.56	0.70	0.53	0.63	0.08	0.73	0.71	0.63	0.66	0.70	0.69	0.04
2.1	0.37	0.79	0.59	0.50	0.62	0.42	0.55	0.15	0.57	0.53	0.42	0.48	0.32	0.43	0.09
2.2	0.53	0.58	0.50	0.47	0.54	0.59	0.53	0.04	0.61	0.54	0.71	0.54	0.86	0.70	0.12
2.3	0.46	0.52	0.50	0.52	0.46	0.43	0.48	0.04	0.61	0.56	0.56	0.71	0.70	0.75	0.08
2.4	0.57	0.62	0.76	0.60	0.62	0.57	0.63	0.07	0.43	0.56	0.64	0.66	0.64	0.70	0.10
2.5	0.61	0.46	0.40	0.52	0.42	0.55	0.49	0.08	0.71	0.70	0.51	0.73	0.67	0.48	0.11
2.6	0.56	0.58	0.71	0.59	0.54	0.67	0.61	0.07	0.69	0.71	0.50	0.62	0.73	0.70	0.08
3.1	0.70	0.75	0.72	0.64	0.70	0.81	0.72	0.06	0.52	0.62	0.63	0.47	0.79	0.70	0.12
3.2	0.64	0.61	0.78	0.64	0.81	0.61	0.68	0.09	0.62	0.68	0.58	0.52	0.63	0.66	0.06
3.3	0.81	0.75	0.72	0.71	0.81	0.69	0.75	0.05	0.47	0.58	0.74	0.59	0.64	0.91	0.15
3.4	0.61	0.49	0.57	0.54	0.55	0.71	0.58	0.08	0.47	0.47	0.45	0.59	0.63	0.59	0.08
3.5	0.53	0.80	0.80	0.60	0.57	0.63	0.66	0.12	0.40	0.43	0.40	0.44	0.61	0.63	0.10
3.6	0.72	0.47	0.53	0.59	0.59	0.62	0.59	0.08	0.56	0.54	0.62	0.84	0.79	0.69	0.12
4.1	0.81	0.84	0.85	0.85	0.85	0.68	0.81	0.07	0.95	0.84	0.82	0.80	0.90	0.87	0.05
4.2	0.92	0.83	0.75	0.66	0.90	0.81	0.81	0.10	0.95	0.93	0.88	0.87	0.85	0.86	0.04
4.3	0.62	0.76	0.69	0.69	0.63	0.75	0.69	0.06	0.72	0.56	0.78	0.87	0.61	0.58	0.12
4.4	0.72	0.79	0.64	0.92	0.68	0.64	0.73	0.11	0.62	0.57	0.79	0.71	0.67	0.77	0.09
4.5	0.62	0.59	0.82	0.48	0.56	0.79	0.64	0.13	0.68	0.73	0.79	0.72	0.82	0.68	0.06
4.6	0.63	0.57	0.68	0.59	0.55	0.49	0.59	0.07	0.63	0.58	0.72	0.60	0.61	0.66	0.05

Table II.4: Vector dispersion and fractal dimension extracted from models generated at the Pak Kasims reef site on Pulau Hoga using a single camera lawnmower method. Vector dispersion is shown as a mean of 64 values per quadrat.

Quadrat	Vector dispersion						Fractal dimension					
	Single camera		Multi camera		Fractal camera		Single camera		Multi camera		Fractal camera	
	Mean	SD	Mean	SD	1-5 cm	5-15 cm	15-30 cm	30-60 cm	1-5 cm	5-15 cm	15-30 cm	30-60 cm
1.1	0.28	0.07	0.16	0.07	2.16	2.28	2.10	2.01	2.10	2.14	2.16	1.98
1.2	0.25	0.07	0.19	0.08	2.24	2.29	2.13	2.00	2.18	2.11	2.15	2.16
1.3	0.26	0.07	0.19	0.08	2.16	2.15	2.26	2.06	2.13	2.18	2.08	2.10
1.4	0.30	0.09	0.18	0.06	2.24	2.21	2.19	2.17	2.15	2.24	2.17	2.02
1.5	0.30	0.07	0.21	0.06	2.20	2.21	2.27	2.14	2.16	2.16	2.09	1.96
1.6	0.27	0.07	0.23	0.06	2.22	2.25	2.21	2.06	2.15	2.26	2.09	2.05
2.1	0.26	0.10	0.23	0.10	2.24	2.16	2.10	2.02	2.11	2.08	2.21	2.26
2.2	0.28	0.08	0.16	0.10	2.23	2.23	2.21	2.09	2.07	2.14	2.26	2.16
2.3	0.27	0.08	0.14	0.10	2.21	2.16	2.21	1.98	2.10	2.12	2.07	2.58
2.4	0.21	0.08	0.22	0.08	2.14	2.31	2.13	2.11	2.15	2.21	2.07	2.18
2.5	0.31	0.08	0.20	0.07	2.24	2.20	2.23	2.22	2.15	2.19	2.16	2.08
2.6	0.24	0.07	0.15	0.09	2.19	2.16	2.17	2.28	2.14	2.21	2.21	1.95
3.1	0.21	0.09	0.22	0.08	2.12	2.13	2.08	2.03	2.16	2.17	2.17	2.05
3.2	0.21	0.07	0.20	0.09	2.16	2.17	2.10	2.06	2.20	2.19	2.06	2.21
3.3	0.17	0.09	0.15	0.11	2.17	2.13	2.07	2.04	2.16	2.12	2.25	2.12
3.4	0.22	0.09	0.21	0.08	2.18	2.11	2.20	2.25	2.15	2.26	2.07	2.88
3.5	0.21	0.08	0.21	0.11	2.16	2.29	2.04	2.03	2.26	2.19	2.21	2.93
3.6	0.27	0.07	0.15	0.08	2.22	2.32	2.10	2.22	2.11	2.10	2.13	2.08
4.1	0.21	0.07	0.14	0.07	2.09	2.07	2.06	2.05	2.01	2.01	2.02	2.04
4.2	0.12	0.09	0.08	0.07	2.03	2.02	2.03	2.01	2.03	2.03	2.07	2.03
4.3	0.22	0.09	0.19	0.09	2.15	2.14	2.13	2.21	2.12	2.26	2.22	2.01
4.4	0.21	0.07	0.21	0.10	2.14	2.13	2.07	2.13	2.11	2.06	2.09	2.09
4.5	0.21	0.10	0.16	0.08	2.20	2.21	2.14	2.01	2.12	2.10	2.05	2.02
4.6	0.22	0.09	0.22	0.09	2.15	2.16	2.10	2.12	2.15	2.16	2.14	2.13

Table II.5: Percentage of aligned photos from coral reef quadrats using different quality settings in Agisoft Metashape.

Site	Quadrat	Setting	Alignment (%)
PK	1	Lowest	13.6
		Low	89.8
		Medium	100
		High	100
		Highest	100
	2	Lowest	53.4
		Low	61.0
		Medium	100
		High	100
		Highest	100
	3	Lowest	72.0
		Low	100
		Medium	100
		High	100
		Highest	100
	4	Lowest	12.5
		Low	100
		Medium	100
		High	100
		Highest	100
SAM	1	Lowest	7.1
		Low	100
		Medium	100
		High	100
		Highest	100
	2	Lowest	94.9
		Low	100
		Medium	100
		High	100
		Highest	100
	3	Lowest	65.6
		Low	100
		Medium	100
		High	100
		Highest	100
	4	Lowest	16.7
		Low	100
		Medium	100
		High	100
		Highest	100

Table II.6: Mean and standard deviation of cloud-to-cloud distance between dense clouds built at varying qualities after medium quality photo alignment (to 3 d.p.).

Site	Quadrat	Cloud quality setting		Mean	SD
		Reference	Comparison		
PK	1	Lowest	Low	0.055	0.060
		Low	Medium	0.030	0.042
		Medium	High	0.016	0.023
		High	Ultra high	0.001	0.016
	2	Lowest	Low	0.187	0.166
		Low	Medium	0.095	0.124
		Medium	High	0.060	0.075
		High	Ultra high	0.042	0.065
	3	Lowest	Low	0.047	0.063
		Low	Medium	0.024	0.040
		Medium	High	0.127	0.015
		High	Ultra high	0.008	0.011
	4	Lowest	Low	0.055	0.071
		Low	Medium	0.034	0.060
		Medium	High	0.018	0.031
		High	Ultra high	0.011	0.019
SAM	1	Lowest	Low	0.049	0.045
		Low	Medium	0.030	0.037
		Medium	High	0.016	0.018
		High	Ultra high	0.010	0.016
	2	Lowest	Low	0.059	0.047
		Low	Medium	0.033	0.035
		Medium	High	0.020	0.020
		High	Ultra high	0.014	0.022
	3	Lowest	Low	0.071	0.077
		Low	Medium	0.039	0.043
		Medium	High	0.023	0.025
		High	Ultra high	0.016	0.025
	4	Lowest	Low	0.030	0.036
		Low	Medium	0.017	0.025
		Medium	High	0.010	0.011
		High	Ultra high	0.006	0.112

# III | Cromer MCZ data

Table III.1: *Cancer pagurus* and *Homarus gammarus* abundance in the Cromer MCZ.

Site		Crustacean Abundance					
		<i>C. pagurus</i>			<i>H. gammarus</i>		
Location	Type	Juvenile	Mature	Total	Juvenile	Mature	Total
WS1	Pot	0	0	0	0	0	0
	Marker	0	1	1	0	0	0
	Pot	0	0	0	0	0	0
	Marker	0	0	0	0	0	0
WS2	Pot	0	0	0	0	0	0
	Marker	0	1	1	0	0	0
	Pot	0	1	1	0	1	1
	Marker	1	0	1	0	0	0
	Pot	0	0	0	0	0	0
	Marker	3	0	3	0	0	0
	Pot	1	1	2	0	0	0
	Marker	1	0	1	0	0	0
	Pot	14	0	14	0	0	0
	Marker	4	0	4	0	0	0
WR	Pot	0	0	0	2	0	2
	Marker	1	0	1	0	0	0
	Pot	1	0	1	0	0	0
	Marker	0	0	0	0	0	0
	Pot	1	0	1	0	0	0
	Marker	2	0	2	0	0	0
	Pot	1	2	3	0	0	0
	Marker	3	0	3	0	0	0
	Pot	3	0	3	0	0	0
	Marker	1	0	1	0	0	0
ER	Pot	15	0	15	0	1	1
	Marker	15	0	15	0	0	0
	Pot	5	2	7	0	0	0
	Marker	5	2	7	0	0	0
	Pot	15	10	25	1	1	2
	Marker	15	10	25	1	0	1

Table III.2: Rugosity values extracted from models generated at pot and marker sites on the Cromer Shoal Chalk Bed. Rugosity 1-6 corresponds to a “chain” within the model.

Site		Rugosity						Mean	SD
		1	2	3	4	5	6		
WS1	Pot	0.036	0.044	0.018	0.039	0.025	0.029	0.032	0.010
	Marker	0.055	0.049	0.072	0.035	0.050	0.091	0.059	0.020
	Pot	0.041	0.045	0.040	0.047	0.033	0.053	0.043	0.007
	Marker	0.049	0.041	0.031	0.042	0.068	0.081	0.052	0.019
WS2	Pot	0.161	0.085	0.030	0.079	0.147	0.105	0.101	0.048
	Marker	0.069	0.072	0.026	0.155	0.183	0.161	0.111	0.063
	Pot	0.095	0.195	0.036	0.195	0.240	0.179	0.157	0.076
	Marker	0.060	0.051	0.038	0.076	0.071	0.126	0.071	0.031
	Pot	0.043	0.028	0.012	0.077	0.083	0.042	0.048	0.028
	Marker	0.107	0.106	0.103	0.096	0.092	0.090	0.099	0.007
	Pot	0.060	0.039	0.033	0.032	0.054	0.056	0.046	0.013
	Marker	0.069	0.185	0.154	0.171	0.137	0.123	0.140	0.042
	Pot	0.056	0.035	0.051	0.041	0.051	0.094	0.055	0.021
	Marker	0.043	0.036	0.082	0.114	0.050	0.073	0.066	0.029
WR	Pot	0.151	0.136	0.176	0.192	0.151	0.089	0.149	0.036
	Marker	0.065	0.097	0.102	0.036	0.078	0.099	0.079	0.026
	Pot	0.112	0.131	0.114	0.105	0.099	0.055	0.103	0.026
	Marker	0.086	0.055	0.063	0.117	0.043	0.030	0.066	0.031
	Pot	0.094	0.086	0.080	0.057	0.044	0.046	0.068	0.021
	Marker	0.043	0.039	0.085	0.082	0.089	0.088	0.071	0.024
	Pot	0.328	0.347	0.395	0.052	0.228	0.425	0.296	0.137
	Marker	0.050	0.079	0.043	0.052	0.045	0.102	0.062	0.024
	Pot	0.032	0.022	0.056	0.042	0.107	0.151	0.068	0.050
	Marker	0.023	0.037	0.040	0.103	0.034	0.031	0.045	0.029
ER	Pot	0.135	0.044	0.037	0.215	0.187	0.169	0.131	0.075
	Marker	0.043	0.046	0.120	0.076	0.156	0.091	0.089	0.044
	Pot	0.157	0.107	0.159	0.074	0.166	0.179	0.140	0.041
	Marker	0.038	0.052	0.061	0.085	0.053	0.066	0.059	0.016
	Pot	0.063	0.118	0.087	0.105	0.076	0.082	0.089	0.020
	Marker	0.098	0.075	0.089	0.000	0.032	0.056	0.058	0.037
	Pot	0.089	0.074	0.074	0.090	0.152	0.108	0.098	0.029
	Marker	0.030	0.092	0.182	0.087	0.113	0.081	0.098	0.050
	Pot	0.090	0.056	0.094	0.105	0.091	0.078	0.086	0.017
	Marker	0.047	0.031	0.054	0.068	0.102	0.103	0.067	0.030

Table III.3: Vector dispersion and fractal dimension extracted from models generated at pot and marker sites on the Cromer Shoal Chalk Bed. Vector dispersion is shown as a mean of 64 values per quadrat.

Site		Vector dispersion	Fractal Dimension			
			1-5 cm	5-15 cm	15-30 cm	30-60 cm
WS1	Pot	0.0502	2.018	2.008	2.001	2.001
	Marker	0.0759	2.044	2.009	2.004	2.000
	Pot	0.0649	2.042	2.014	2.007	2.002
	Marker	0.1008	2.040	2.009	2.003	2.001
WS2	Pot	0.0816	2.036	2.051	2.012	2.027
	Marker	0.1070	2.028	2.033	2.043	2.032
	Pot	0.0405	2.049	2.025	2.029	2.027
	Marker	0.0855	2.055	2.038	2.035	2.027
	Pot	0.0632	2.049	2.025	2.029	2.027
	Marker	0.0597	2.053	2.041	2.055	2.029
	Pot	0.0776	2.029	2.010	2.015	2.007
	Marker	0.0945	2.068	2.115	2.033	2.086
	Pot	0.1105	2.031	2.025	2.014	2.019
	Marker	0.0716	2.047	2.043	2.016	2.005
WR	Pot	0.1473	2.053	2.043	2.032	2.008
	Marker	0.1185	2.056	2.031	2.021	2.023
	Pot	0.0811	2.064	2.059	2.037	2.022
	Marker	0.1360	2.035	2.032	2.036	2.015
	Pot	0.0680	2.024	2.024	2.019	2.020
	Marker	0.0879	2.048	2.055	2.035	2.048
	Pot	0.0724	2.061	2.095	2.120	2.150
	Marker	0.0936	2.037	2.031	2.020	2.010
	Pot	0.0553	2.022	2.038	2.030	2.036
	Marker	0.0506	2.025	2.020	2.028	2.006
ER	Pot	0.0646	2.035	2.025	2.011	1.998
	Marker	0.1282	2.052	2.056	2.020	2.022
	Pot	0.1124	2.078	2.037	2.028	2.007
	Marker	0.1295	2.039	2.029	2.025	2.011
	Pot	0.0827	2.049	2.050	2.038	2.008
	Marker	0.0805	2.045	2.046	2.009	1.960
	Pot	0.0678	2.068	2.050	2.009	2.006
	Marker	0.0756	2.059	2.032	2.018	2.013
	Pot	0.0957	2.048	2.037	2.015	2.022
	Marker	0.0842	2.038	2.019	2.018	2.007



## IV | Relief script

The script developed and used here can be found on [GitHub](#).

**The script below can be used to find the relief of a 3D model in Rhino:**

```
1 import rhinoscriptsyntax as rs
2
3 ### Split cube into concave and convex halves ###
4
5 box = rs.GetObject("Select cube to be split", rs.filter.mesh)
6 if box:
7     model = rs.GetObject("Select model to be cut along", rs.
8         filter.mesh)
9     if model: rs.MeshBooleanSplit(box, model)
10
11 ### Create bounding box around each half of split cube to get
12     relief ###
13
14 object_1 = rs.GetObject("Select top half of cube in front
15     view")
16 object_2 = rs.GetObject("Select bottom cube half in front
17     view")
18
19 bb_1 = rs.BoundingBox(object_1, view_or_plane=None,
20     in_world_coords=True)
21 bb_1_height = bb_1[4].Z - bb_1[0].Z
22
23 bb_2 = rs.BoundingBox(object_2, view_or_plane=None,
24     in_world_coords=True)
25 bb_2_height = bb_2[4].Z - bb_2[0].Z
26
27 relief_1 = bb_1_height - bb_2_height
28
29 print "Model relief is:", abs(relief_1)
```

## V | ImageCLEFcoral data

Table V.1: Results of ImageCLEFcoral 2019 subtask 1 per benthic substrate label using the intersection over union (IoU) metric, with the highest score in each substrate class shown in red.

Run ID	Team	Hard coral - Branching	Hard coral - Sub-Massive	Hard coral - Boulder	Hard coral - Encrusting	Hard coral - Table	Hard coral - Foliose	Hard coral - Mushroom	Soft Coral	Gorgonian	Sponge	Barrel Sponge	Fire coral	Algae
27497	ISEC	<b>0.080</b>	0.000	0.001	0.012	0.000	0.000	0.000	0.008	0.000	0.028	0.000	0.000	0.000
27115	VIT	0.044	0.000	0.081	0.017	0.000	0.013	0.066	0.072	0.000	0.035	0.053	0.000	0.000
27347	VIT	0.046	0.000	0.037	0.006	0.000	0.000	0.020	<b>0.092</b>	0.000	0.024	0.050	0.000	0.000
27348	VIT	0.055	0.000	0.096	0.017	0.000	<b>0.013</b>	0.119	0.078	0.000	<b>0.037</b>	0.058	0.000	0.000
27349	VIT	0.064	0.000	<b>0.101</b>	<b>0.020</b>	0.000	0.003	0.076	0.080	0.000	0.033	<b>0.062</b>	0.000	0.000
27350	VIT	0.060	0.000	0.031	0.014	0.000	0.000	0.042	0.081	0.000	0.030	0.060	0.000	0.000
27398	HHUD	0.001	0.000	0.017	0.000	0.000	0.000	0.000	0.070	0.000	0.002	0.000	0.000	0.000
27413	HHUD	0.007	<b>0.002</b>	0.006	0.001	0.000	0.002	0.000	0.052	0.000	0.006	0.000	0.000	0.000
27414	HHUD	0.009	0.000	0.016	0.002	0.000	0.000	0.000	0.056	0.000	0.010	0.005	0.000	0.000
27415	HHUD	0.000	0.000	0.000	0.000	0.000	0.000	0.000	0.073	0.000	0.000	0.000	0.000	0.000
27416	HHUD	0.035	0.000	0.034	0.006	0.000	0.000	<b>0.437</b>	0.055	<b>0.001</b>	0.009	0.022	0.000	<b>0.016</b>
27417	HHUD	0.036	0.000	0.033	0.007	0.000	0.000	0.041	0.051	<b>0.001</b>	0.009	0.021	0.000	0.016
27418	HHUD	0.025	0.000	0.032	0.004	0.000	0.000	0.027	0.045	0.001	0.009	0.032	0.000	0.001
27419	HHUD	0.026	0.000	0.032	0.004	0.000	0.002	0.023	0.042	0.001	0.009	0.030	0.000	0.001
27421	HHUD	0.001	0.000	0.017	0.005	0.000	0.001	0.011	0.057	0.000	0.007	0.000	0.000	0.000

Table V.2: Results of ImageCLEFcoral 2019 subtask 2 per benthic substrate label using the intersection over union (IoU) metric, with the highest score per substrate class shown in red.

Run ID	Team	Hard coral - Branching	Hard coral - Sub-Massive	Hard coral - Boulder	Hard coral - Encrusting	Hard coral - Table	Hard coral - Foliose	Hard coral - Mushroom	Soft Coral	Gorgonian	Sponge	Barrel Sponge	Fire coral	Algae
27505	HHUD	0.000	0.000	0.000	0.000	0.000	0.000	0.000	0.043	0.000	0.000	0.000	0.000	0.000
27343	SOTON	0.024	0.000	0.023	0.012	0.000	0.001	0.048	0.115	0.000	0.011	0.000	0.004	0.000
27324	SOTON	0.026	<b>0.030</b>	0.018	0.019	<b>0.014</b>	<b>0.014</b>	0.003	0.085	<b>0.025</b>	0.028	0.014	<b>0.021</b>	<b>0.017</b>
27212	SOTON	0.012	0.005	0.015	0.019	0.000	0.004	0.002	0.085	0.000	0.000	0.016	0.000	0.001
27500	MTRU	<b>0.096</b>	0.000	<b>0.166</b>	<b>0.045</b>	0.000	0.007	<b>0.219</b>	<b>0.130</b>	0.019	<b>0.057</b>	<b>0.089</b>	0.000	0.001

Table V.3: Results of ImageCLEFcoral 2020 subtask 1 per benthic substrate label, using the intersection over union (IoU) metric, with the highest score per substrate class shown in red.

Run ID	Team	Hard coral - Branching	Hard coral - Sub-Massive	Hard coral - Boulder	Hard coral - Encrusting	Hard coral - Table	Hard coral - Foliose	Hard coral - Mushroom	Soft Coral	Gorgonian	Sponge	Barrel Sponge	Fire coral	Algae
68213	HHUD	0.016	0.000	0.171	0.306	0.066	0.097	0.15	0.038	0.042	0.359	0.082	0.12	0.089
68212	HHUD	0.012	0.000	0.218	0.327	0.09	0.105	0.231	0.067	0.034	0.445	0.059	0.121	0.134
68205	HHUD	0.019	0.000	0.093	0.091	0.023	0.056	0.081	0.024	0.017	0.185	0.000	0.036	0.039
68202	HHUD	0.007	0.000	0.16	0.247	0.053	0.115	0.154	0.032	0.026	0.314	0.037	0.067	0.082
68201	HHUD	0.016	0.000	0.052	0.142	0.005	0.003	0.155	0.002	0.000	0.144	0.000	0.019	0.023
68198	HHUD	0.002	0.000	0.221	0.316	0.077	0.119	0.183	0.041	0.029	0.462	0.037	0.107	0.115
68182	FHD	0.000	0.000	0.199	0.35	0.005	0.012	0.187	0.000	0.000	0.484	0.000	0.104	0.064
68183	FHD	0.000	0.000	0.209	0.337	0.000	0.022	0.197	0.000	0.000	0.456	0.000	0.07	0.098
68197	HHUD	0.008	0.000	0.105	0.137	0.022	0.072	0.149	0.011	0.021	0.399	0.000	0.045	0.028
68196	HHUD	0.005	0.000	0.159	0.3	0.056	0.056	0.128	0.015	0.022	0.367	0.088	0.123	0.053
68188	FHD	0.006	0.000	0.249	0.301	0.032	0.182	0.397	0.004	0.035	0.453	0.057	0.088	0.135
68187	FHD	0.009	0.000	0.256	0.306	0.038	0.192	0.402	0.007	0.039	0.48	0.061	0.099	0.134
68186	FHD	0.008	0	0.257	0.322	0.03	0.195	0.42	0.000	0.031	0.485	0.076	0.097	0.142
68185	FHD	0.000	0.000	0.185	0.319	0.039	0.131	0.156	0.000	0.02	0.423	0.046	0.084	0.119
68184	FHD	0.006	0.000	0.246	0.323	0.052	0.122	0.25	0.003	0.041	0.467	0.067	0.109	0.102
68181	FHD	0.000	0.000	0.179	0.316	0.000	0.000	0.288	0.000	0.000	0.472	0.000	0.12	0.02
68179	HHUD	0.000	0.000	0.000	0.037	0.000	0.000	0.000	0.000	0.000	0.146	0.000	0.000	0
68178	HHUD	0.000	0.000	0.017	0.014	0.005	0.001	0.000	0.002	0.000	0.056	0.000	0.009	0
68146	FZ PiVa	0.000	0.000	0.133	0.181	0.046	0.13	0.182	0.011	0.000	0.452	0.000	0.103	0.049
68145	FZ PiVa	0.000	0.000	0.105	0.123	0.021	0.038	0.122	0.000	0.000	0.387	0.000	0.093	0.014
68143	FZ PiVa	0.000	0.000	0.054	0.089	0.008	0.009	0.109	0.002	0.000	0.29	0.000	0.065	0.01
68138	FZ PiVa	0.001	0.000	0.159	0.211	0.052	0.149	0.204	0.016	0.000	0.462	0.000	0.113	0.062
68094	FZ PiVa	0.000	0.000	0.108	0.127	0.02	0.038	0.121	0.001	0.000	0.393	0.000	0.087	0.004
68093	FZ PiVa	0.001	0.000	0.206	0.3	0.08	0.147	0.22	0.017	0.009	0.465	0.082	0.117	0.067
67919	FHD	0.000	0.000	0.222	0.243	0.049	0.000	0.000	0.000	0.000	0.45	0.000	0.118	0
67914	FHD	0.000	0.000	0.227	0.259	0.042	0.086	0.194	0.000	0.000	0.474	0	0.13	0.057
67863	FZ PiVa	0.000	0.000	0.103	0.104	0.01	0.001	0.134	0.002	0.000	0.338	0.000	0.07	0.004
67862	FZ PiVa	0.000	0.000	0.176	0.219	0.038	0.101	0.211	0.006	0.008	0.464	0.033	0.106	0.03
67858	FZ PiVa	0.000	0.000	0.22	0.297	0.057	0.1	0.315	0.032	0.012	0.508	0.047	0.11	0.089
67857	FZ PiVa	0.000	0.000	0.221	0.306	0.06	0.105	0.32	0.034	0.015	0.512	0.044	0.111	0.09
67558	FZ CV	0.000	0.000	0.216	0.228	0.048	0.031	0.139	0.000	0.000	0.413	0.026	0.097	0.064
67539	FZ CV	0.000	0.000	0.155	0.259	0.047	0.094	0.096	0.000	0.015	0.475	0.028	0.057	0.085

Table V.4: Results of ImageCLEFcoral 2020 subtask 1 per location per benthic substrate, using the intersection over union (IoU) metric, with the highest score per substrate class shown in red.

Location	Team	Hard coral - Branching	Hard coral - Sub-Massive	Hard coral - Boulder	Hard coral - Encrusting	Hard coral - Table	Hard coral - Foliose	Hard coral - Mushroom	Soft Coral	Gorgonian	Sponge	Barrel Sponge	Fire coral	Algae
Wakatobi	FZ PiVA	0.061	0.000	<b>0.448</b>	0.316	<b>0.146</b>	0.361	0.308	<b>0.113</b>	0.146	<b>0.512</b>	<b>0.208</b>	0.222	0.272
	FZ CV	0.000	0.000	0.443	0.380	0.144	0.293	0.143	0.000	0.131	0.490	0.177	0.146	0.168
	FHD	<b>0.249</b>	0.000	0.429	0.387	0.114	<b>0.398</b>	<b>0.406</b>	0.002	0.292	0.500	0.149	<b>0.225</b>	<b>0.488</b>
Spermonde	HHUD	0.078	0.000	0.434	0.312	0.121	0.210	0.207	0.084	<b>0.309</b>	0.453	0.133	0.205	0.281
	FZ PiVA	0.000	0.000	0.163	0.163	0.101	0.012	0.000	0.039	0.010	0.000	0.000	0.036	0.000
	FZ CV	0.000	0.000	0.066	0.146	0.011	0.000	0.000	0.000	0.005	0.000	0.000	0.029	0.000
Seychelles	FHD	0.000	0.000	0.191	0.312	0.039	0.015	0.000	0.010	0.029	0.002	0.000	0.081	0.000
	HHUD	0.008	0.000	0.089	0.260	0.024	0.000	0.000	0.056	0.004	0.001	0.000	0.023	0.000
	FZ PiVA	0.000	0.000	0.250	0.515	0.000	0.018	0.000	0.000	0.000	0.000	0.000	0.007	0.000
Seychelles	FZ CV	0.000	0.000	0.264	0.590	0.000	0.033	0.000	0.000	0.000	0.001	0.000	0.002	0.000
	FHD	0.000	0.000	<b>0.272</b>	<b>0.593</b>	0.000	0.016	0.000	0.000	0.000	0.002	0.000	0.010	0.000
	HHUD	0.002	0.000	0.237	0.489	0.004	0.003	0.000	0.000	0.000	0.000	0.000	0.000	0.000
Dominica	FZ PiVA	0.000	0.000	0.056	0.000	0.018	0.000	0.000	0.000	0.000	0.000	0.000	0.088	0.045
	FZ CV	0.000	0.000	0.172	0.000	0.035	0.000	0.000	0.000	0.000	0.000	0.000	0.073	0.043
	FHD	0.003	0.000	0.190	0.000	0.014	0.000	0.000	0.000	0.000	0.000	0.000	0.072	0.091
HHUD	0.042	0.000	0.154	0.000	0.047	0.000	0.000	0.000	0.000	0.000	0.000	0.168	0.065	

Table V.5: Results of ImageCLEFcoral 2020 subtask 2 per benthic substrate label using the intersection over union (IoU) metric, with the highest score per substrate class shown in red.

Run ID	Team	Hard coral - Branching	Hard coral - Sub-Massive	Hard coral - Boulder	Hard coral - Encrusting	Hard coral - Table	Hard coral - Foliose	Hard coral - Mushroom	Soft Coral	Gorgonian	Sponge	Barrel Sponge	Fire coral	Algae
68192	FHD	0.010	0.000	0.305	0.387	0.092	0.223	<b>0.505</b>	0.009	0.075	<b>0.545</b>	0.023	0.130	0.175
68191	FHD	0.000	0.000	0.222	0.333	0.009	0.132	0.255	0.000	0.021	0.490	0.000	0.085	0.116
68190	FHD	0.000	0.000	0.296	0.362	0.009	0.110	0.456	0.000	0.051	0.520	0.018	0.086	0.147
68189	FHD	0.010	0.000	0.294	0.338	0.072	0.124	0.245	0.003	0.059	0.522	0.061	0.133	<b>0.177</b>
68147	FZ PIVA	0.000	0.000	0.135	0.184	0.044	0.129	0.184	0.009	0.000	0.453	0.000	0.095	0.049
68144	FZ PIVA	0.000	0.000	0.109	0.125	0.020	0.041	0.122	0.000	0.000	0.394	0.000	0.092	0.014
68142	FZ PIVA	0.000	0.000	0.106	0.123	0.019	0.040	0.139	0.000	0.000	0.403	0.000	0.087	0.014
68140	FZ PIVA	0.001	0.000	0.203	0.283	0.075	0.148	0.226	0.012	0.010	0.443	0.055	0.113	0.079
68139	FZ PIVA	0.000	0.000	0.057	0.091	0.007	0.007	0.108	0.001	0.000	0.305	0.000	0.060	0.010
68137	FZ PIVA	0.001	0.000	0.162	0.213	0.050	0.148	0.199	0.013	0.000	0.456	0.000	0.102	0.064
68095	FZ PIVA	0.000	0.000	0.113	0.128	0.019	0.041	0.121	0.000	0.000	0.403	0.000	0.085	0.004
68092	FZ PIVA	0.001	0.000	0.210	0.293	0.077	0.128	0.225	0.013	0.010	0.462	0.055	0.109	0.071
67969	FHD	0.008	0.000	<b>0.321</b>	0.382	<b>0.093</b>	<b>0.275</b>	0.450	0.019	<b>0.087</b>	0.527	<b>0.074</b>	0.140	0.171
67968	FHD	<b>0.009</b>	0.000	0.307	0.342	0.043	0.213	0.435	0.006	0.048	0.544	0.047	0.113	0.158
67967	FHD	0.000	0.000	0.249	0.311	0.018	0.073	0.177	0.000	0.000	0.517	0.000	0.111	0.104
67965	FHD	0.000	0.000	0.286	0.296	0.014	0.102	0.226	0.000	0.000	0.522	0.000	0.105	0.110
67964	FHD	0.000	0.000	0.297	<b>0.398</b>	0.011	0.073	0.318	0.000	0.000	0.533	0.000	0.125	0.071
67963	FHD	0.000	0.000	0.276	0.303	0.058	0.149	0.190	0.000	0.000	0.538	0.050	<b>0.160</b>	0.018
67864	FZ PIVA	0.000	0.000	0.105	0.108	0.01	0.001	0.137	0.000	0.000	0.349	0.000	0.067	0.004
67856	FZ PIVA	0.000	0.000	0.228	0.287	0.055	0.104	0.318	<b>0.026</b>	0.014	0.498	0.051	0.099	0.091
67620	FZ CV	0.000	0.000	0.212	0.222	0.046	0.033	0.138	0.000	0.000	0.434	0.023	0.094	0.064

Table V.6: Results of ImageCLEFcoral 2020 subtask 2 per location per benthic substrate, using the intersection over union (IoU) metric, with the highest score per substrate class shown in red.

Location	Team	Hard coral - Branching	Hard coral - Sub-Massive	Hard coral - Boulder	Hard coral - Encrusting	Hard coral - Table	Hard coral - Foliose	Hard coral - Mushroom	Soft Coral	Gorgonian	Sponge	Barrel Sponge	Fire coral	Algae
Wakatobi	FZ PiVA	0.042	0.000	0.500	0.338	0.156	0.358	0.341	0.099	0.132	0.502	0.273	0.203	0.291
	FHD	0.251	0.000	0.547	0.409	0.192	0.420	0.496	0.071	0.417	0.556	0.422	0.242	0.562
Spermonde	FZ CV	0.000	0.000	0.427	0.264	0.113	0.068	0.107	0.000	0.000	0.460	0.191	0.078	0.115
	FZ PiVA	0.000	0.000	0.228	0.202	0.096	0.013	0.000	0.024	0.010	0.000	0.000	0.048	0.000
Seychelles	FHD	0.000	0.000	0.319	0.440	0.145	0.014	0.000	0.023	0.087	0.003	0.000	0.119	0.000
	FZ CV	0.000	0.000	0.097	0.160	0.006	0.000	0.000	0.000	0.000	0.000	0.000	0.015	0.000
Dominica	FZ PiVA	0.000	0.000	0.297	0.543	0.000	0.020	0.000	0.000	0.000	0.000	0.000	0.004	0.000
	FHD	0.000	0.000	0.407	0.718	0.000	0.010	0.000	0.000	0.000	0.003	0.000	0.014	0.000
Dominica	FZ CV	0.000	0.000	0.267	0.192	0.000	0.000	0.000	0.000	0.000	0.000	0.000	0.002	0.000
	FZ PiVA	0.000	0.000	0.057	0.000	0.013	0.000	0.000	0.000	0.000	0.000	0.000	0.088	0.049
Dominica	FHD	0.000	0.000	0.244	0.000	0.030	0.000	0.000	0.000	0.000	0.000	0.000	0.103	0.099
	FZ CV	0.000	0.000	0.237	0.000	0.014	0.000	0.000	0.000	0.000	0.000	0.000	0.070	0.046